The distribution of the coarse fraction in QRNR deposits is mapped for the depth intervals associated with each of the top three model layers from hundreds of thousands of well logs assembled in support of the LMB model (Arihood, 2009). The texture of glacial deposits was mapped in Michigan, Indiana, and Wisconsin but not in Ohio or Illinois.

The pattern of the coarse fraction in layer 1 (fig. 37*A*) correlates with the map of glacial categories (fig. 36*A*) except in outwash areas where drillers have encountered predominantly fine-grained deposits and areas of clayey till or fine stratified deposits where drillers encountered predominantly coarse-grained deposits. The pattern of the coarse fraction in layer 2 (fig. 37*B*) and especially layer 3 (fig. 37*C*) is more approximate than in layer 1, owing to the relative scarcity of boreholes (Arihood, 2009).

The initial hydraulic-conductivity assignment to the inland QRNR deposits is a function of not only the glacial category but also the coarse fraction attributed to an inland nearfield or farfield model cell in layers 1, 2, and 3. The two variables are combined by means of an empirical "power law" that uses an expected K_h value and an allowable range based on the glacial category and then computes K_h values within the allowable range based on the coarse fraction (appendix 3). The power law yields K_h values with assumed expected ranking of K_h (clayey till < fine stratified < loamy till and organic < sandy till < medium and coarse stratified). Where coarse-fraction information is missing (for example, in northeastern Illinois and northeastern Ohio), the expected value of K_h for the mapped glacial categories is assigned directly to all cells. Where the glacial category is unknown (parts of layer 2 and most of layer 3), parameters corresponding to fine stratified deposits are assumed (see appendix 3).

Plots of the power-law relations between the coarse fraction and the estimated K_h for different glacial materials (fig. 38*A*–*C*) show the expected K_h (based on the average coarse fraction encountered in QRNR cells), as well as the possible range of values. For example, the K_h that corresponds to the average coarse fraction for clayey till is around 1 ft/d, but the allowable range is from 0.1 to 10 ft/d. This procedure yields the nearfield distribution of initial K_h for layer 1 shown in figure 39.

The initial value of K_v for any given inland QRNR cell is derived from the computed K_h by means of a single vertical anisotropy factor set at 20 to 1. Accordingly, an initial K_h of 100 ft/d automatically yields an initial K_v of 5 ft/d, and an initial K_h of 1 ft/d yields an initial K_v of 0.05 ft/d.

The arrays of initial K_h and initial K_v are both subject to calibration and sensitivity analysis. The calibration is not performed individually for each cell; rather, a single K_h and a single K_v multiplier is estimated for each glacial category across all three QRNR layers as a way to improve the agreement between observed field conditions and the model simulation. The updated postcalibration values are discussed in section 5. In section 7, the sensitivity of the model results to the method for estimating QRNR *K* is evaluated by comparing the base model to a simplified simulation in which one average value for K_h and one average value for K_v represent all the cells belonging to a single glacial category.

4.8.2 QRNR Layers Below Lake Michigan and Farfield Lakes

The distribution and rate at which groundwater discharges directly to Lake Michigan is, in part, a function of the horizontal and, more especially, the vertical hydraulic conductivity of the glacial and recent sediments that underlie the lake. A number of resource-assessment, geomorphological, and geophysical investigations provide insight into the texture and permeability of the lakebed material. One set of studies identified mappable sand bodies in the lakebed sediment, which are assumed to be zones of relatively high hydraulic conductivity (Ayers and Chandler, 1967; Meisburger and others, 1979; Eadie and Lozano, 1999; Ayers, unpublished report for the NOAA Great Lakes Environmental Research Laboratory). Some of these investigations employed gravity and seismic methods along multiple transects (for example, Lineback and others, 1971). Other studies used geomorphological methods to identify the proximal (nearshore) sections of ancient deltas that prograded into the lake at low stage (Colgan and Principiato, 1998; Soller, 1998; National Oceanic and Atmospheric Administration, 2005). These deltas, which overlap with the distribution of sand bodies, are likely sites for the accumulation of sediment with enhanced coarse fraction. One delta extends about 12 mi into Lake Michigan northeast of Green Bay, Wis.; others are located where ancient rivers emptied into the lake north and south of Grand Rapids, Mich. The final source used to map the texture of lakebed sediments was results from geophysical studies along the Wisconsin shoreline (Cherkauer and others, 1990). The investigators converted measurements of electric conductance into estimates of hydraulic conductance terms, which, when paired with thickness estimates, allow the nearshore to be segmented into texture zones.

By combining the available data sources, it is possible to assemble a map for the nearshore that categorizes hydraulic conductivity into areas of low, middle, and high for the Lake Michigan lakebed (fig. 40). Nearshore sediments (corresponding to a lateral distance of three model cell widths, or about 3 mi) are assigned to the middle *K* zone unless evidence from sand-body studies, geomorphology, or the electric conductance records indicates that the sediments have coarser or finer texture. Most of the interior of the lakebed is assumed to be composed of fine-grained sediments, except where data suggest otherwise. The values applied to layer 1 are extended to layer 2 where the estimated unconsolidated thickness exceeds 100 ft and to layer 3 where it exceeds 300 ft. In terms of proportion, 73 percent of the lakebed area is assigned to the interior, 1 percent to the low, 24 percent to the middle, and only 2 percent to the high *K* zones. However, in some areas along the shoreline, the high *K* zone is notable.

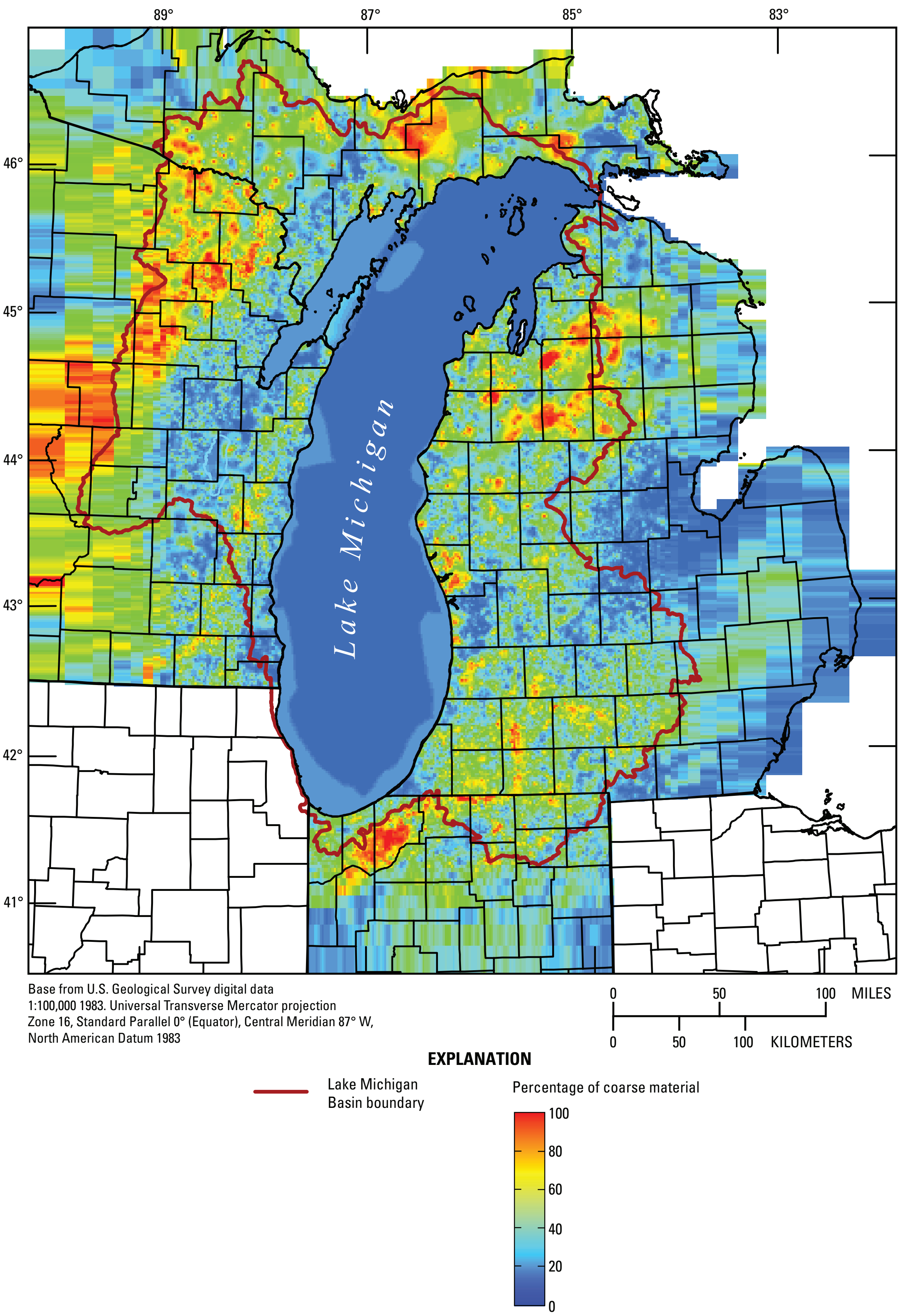

Figure 37*A*. Coarse fraction in model layer 1.

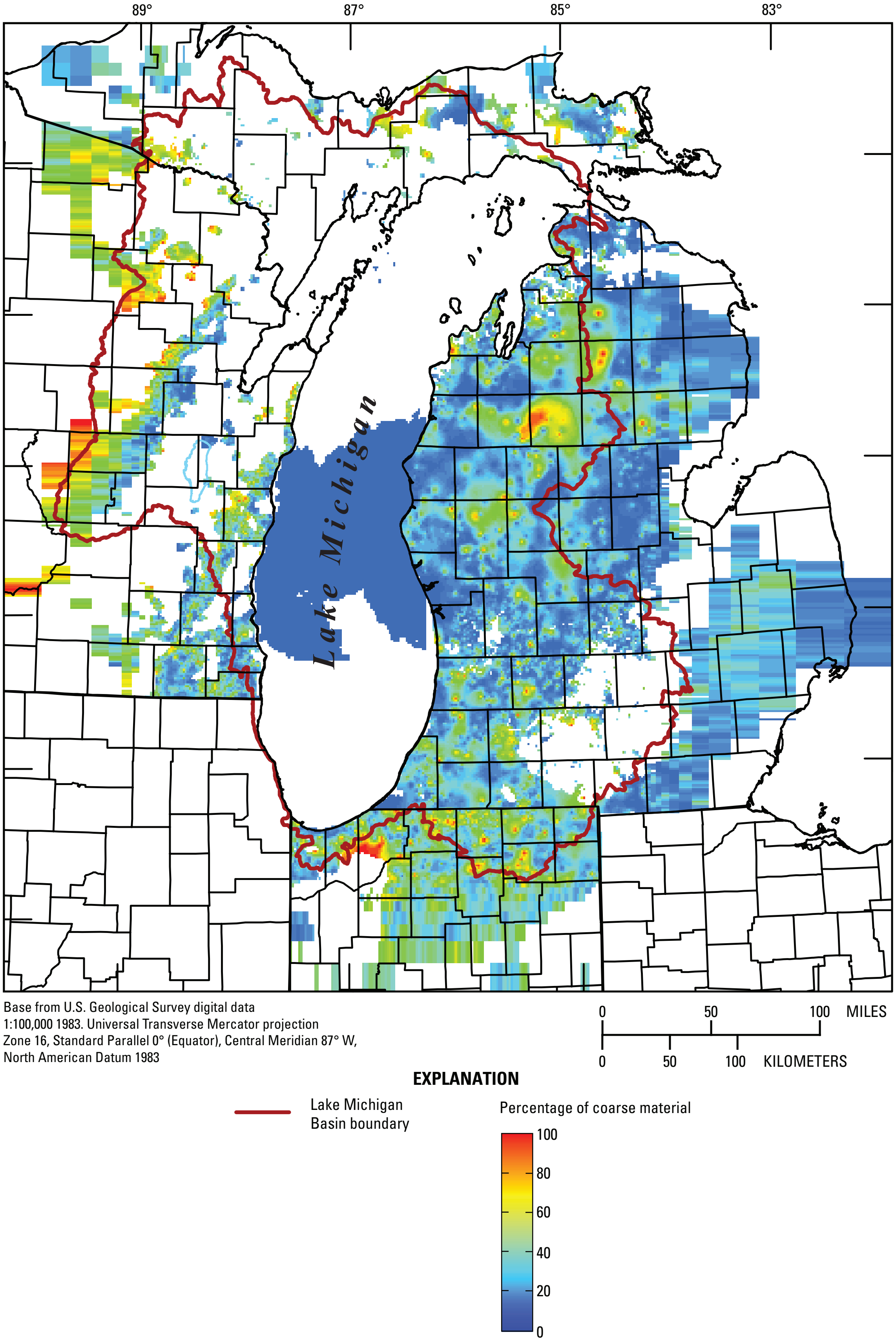

Figure 37*B*. Coarse fraction in model layer 2.

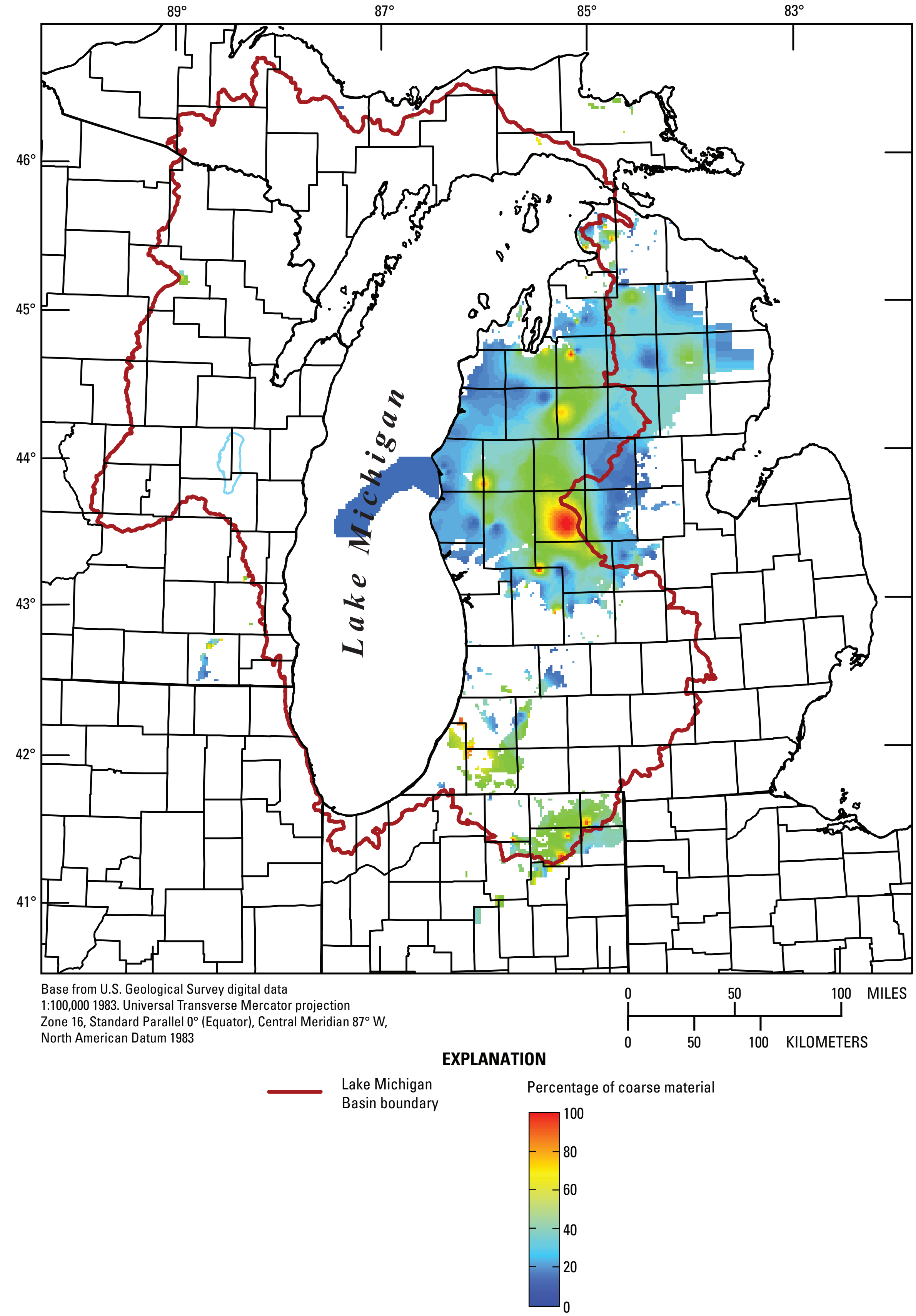

Figure 37*C*. Coarse fraction in model layer 3.

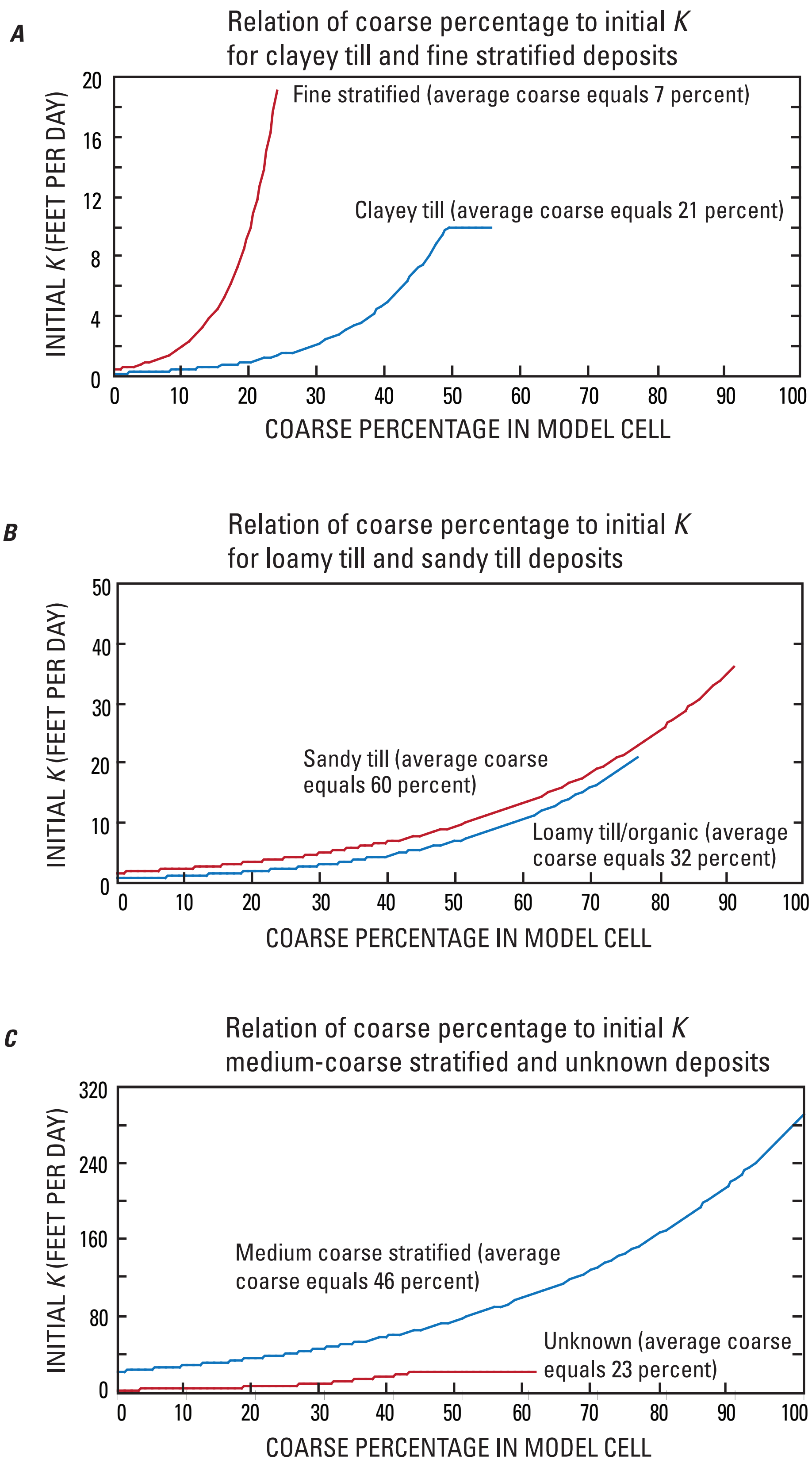

Figure 38. Relation of initial hydraulic conductivity values to coarse fraction, by glacial category.

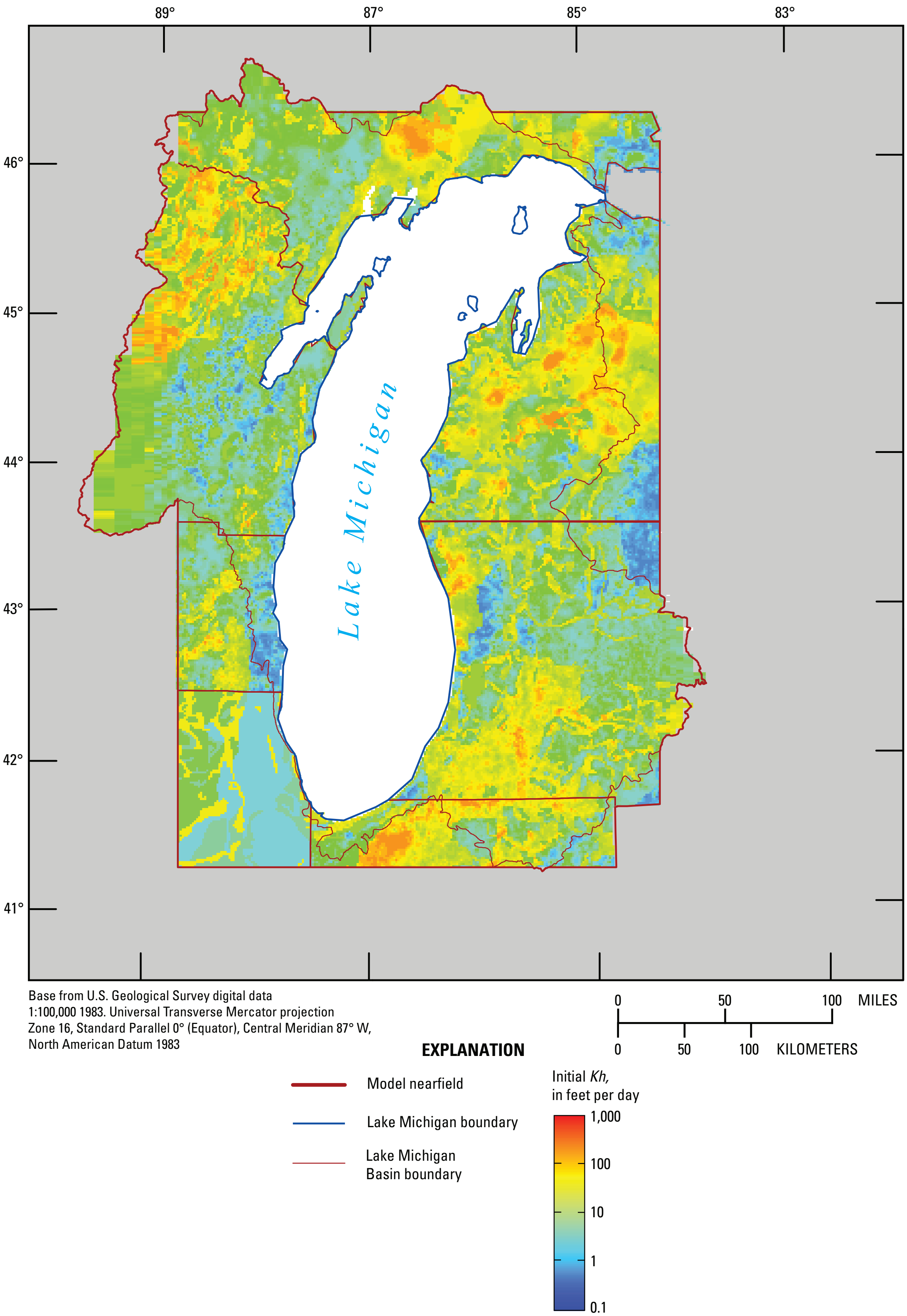

Figure 39. Initial horizontal hydraulic conductivity distribution in nearfield area of model layer 1.

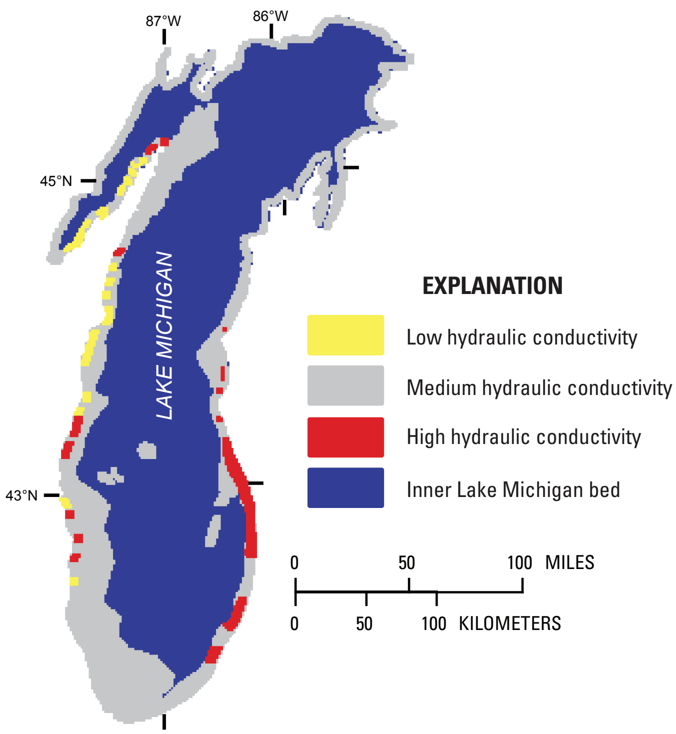

Figure 40. Hydraulic conductivity zones under Lake Michigan.

Because direct discharge of groundwater to Lake Michigan is controlled largely by the upward vertical component of the hydraulic gradient, the K_v values assigned the lakebed zones are of particular importance. Calculations based on the geophysical study along the Wisconsin shoreline (Cherkauer and others, 1990) suggest that values in the range of 0.001 to 0.1 ft/d are reasonable starting estimates. Accordingly, the high end of the expected range was assigned to the high *K* zones, the low end was assigned to the low and interior *K* zones, and an intermediate value was assigned to the middle *K* zone. The K_v zones were adjusted during model calibration (appendix 5, table A5–2). The K_h values for the same sediments range from 0.1 to 1 ft/d and were fixed during the calibration. Both K_h and K_v were modified during model sensitivity analysis (see section 7).

The K_v values specified for QRNR sediments in the model farfield under Lakes Superior, Huron, St. Clair, and Erie were based on the mapped glacial categories because no drilling logs were available. The glacial categories were not derived from the Fullerton compilation (which is limited to inland areas) but from a map of Quaternary sediments in the eastern United States prepared by Soller and Packard (1998).[17]

The resulting zonation of the QRNR sediments under the farfield lakes is shown in figure 36*A*. During the calibration process, their K_h and K_v values are subject to the same multiplier parameters as the inland cells grouped in the same glacial category.

4.8.3 Bedrock Hydraulic Conductivity and Transmissivity of Aquifer Systems

Horizontal and vertical hydraulic-conductivity values are assigned to the model bedrock layers (4 to 20) in *blocks* of cells. The increasing scarcity of hydraulic-conductivity data with depth make it unreasonable to vary bedrock K_h and K_v on a cell-by-cell basis; instead these parameters are varied in a piecewise constant manner (that is, by blocks).[18]

The assignment of K_h and K_v block values draws on four types of sources: results of aquifer tests, specific-capacity calculations based on water-well driller logs, published reports that analyze hydrogeology at the county or subregional scale, and interpretations from published groundwater-flow models. The mix of sources is presented by state in appendix 4*A*.

Appendix 4*B* contains a detailed description of the *initial* block K_h and K_v assignments to bedrock aquifer systems, organized by layer. The transmissivities of bedrock aquifer systems are calculated by multiplying the K_h values by the layer thickness (transmissivity units: ft^2/d). Pinched cells are excluded, as well as cells for which the head solution with the initial input falls below the bottom of the cell. The results for each of the five aquifer systems are displayed in figure 41 according to a log scale. For completeness, the initial transmissivities for the unconsolidated units in the QRNR aquifer system are compared to the distribution in the bedrock systems.

The initial transmissivity for the topmost QRNR aquifer system (fig. 41*A*) reflects the underlying geology of the deposits. The highest transmissivities are clustered where outwash deposits are thick in the NLP_MI subregion and to a lesser extent in N_IND, the western part of NE_WI, and the so-called kettle moraine area some distance inland in SE_WI. The lowest transmissivity is associated with the clayey tills commonly found along the Lake Michigan shoreline in the subregions of NE_WI, SE_WI, and NE_ILL. Values are also very low in parts of the UP_MI where glacial deposits are very thin and under Lake Michigan where the system is dominated by fine-grained deposits.

[17] This map employs only a few unconsolidated units, which are equated to the model glacial categories as follows:

Glacial Units in Soller and Packard map	Glacial categories in LMB model
Coarse stratified	Medium/Coarse stratified
Fine stratified	Fine stratified
Till	Loamy till
Patchy QRNR	Loamy till
Organic	Organic

[18] During the calibration process, a single multiplier is applied either to the value assigned to one block of cells or, alternatively, the multiplier is applied to the multiple values in multiple blocks. The cells in one or more blocks subject to a single calibration multiplier constitute a zone. In this section, only the block assignments are discussed; the calibration zones are described in section 5.

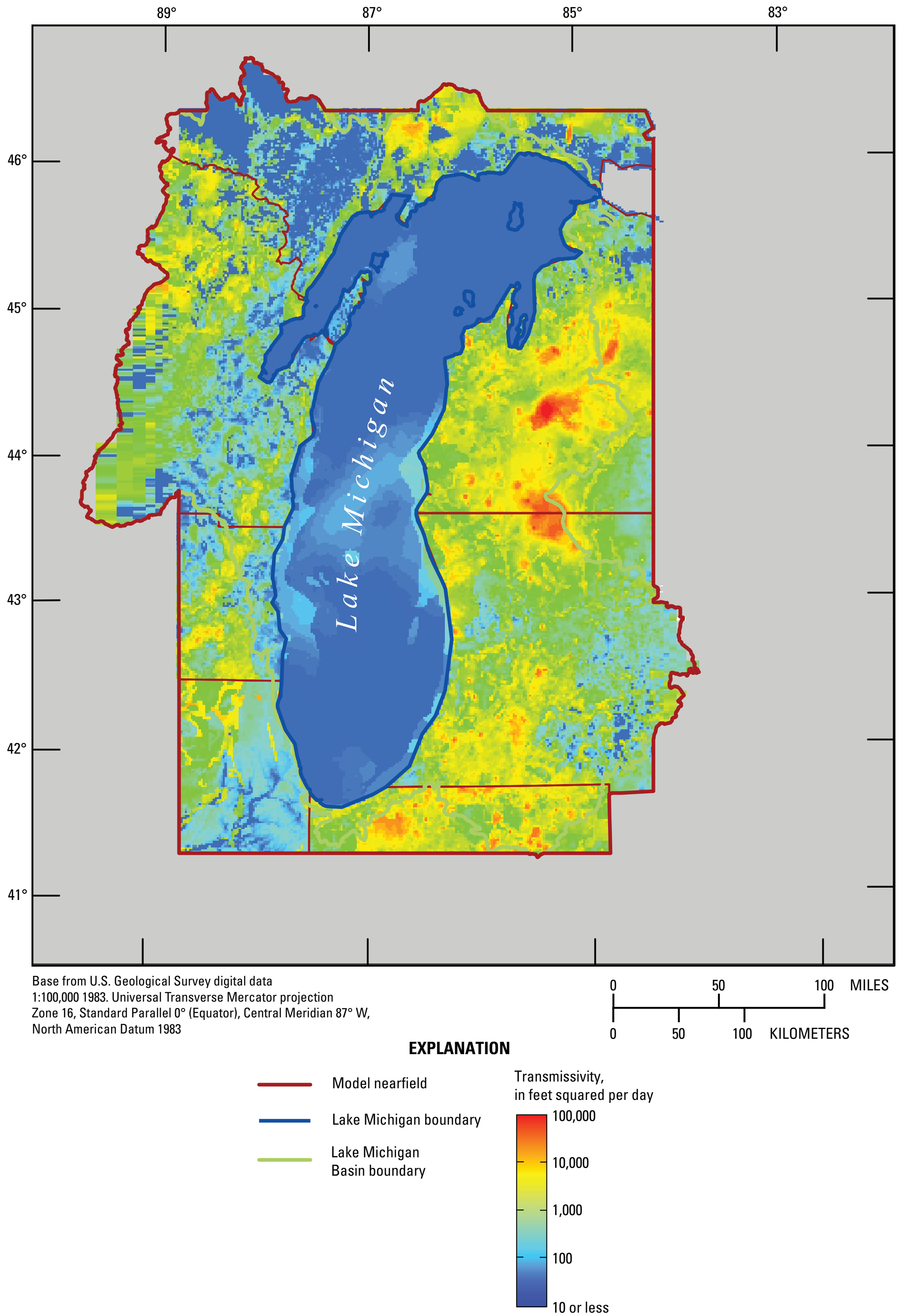

Figure 41*A*. Initial transmissivity distribution in aquifer system QRNR.

The two aquifer systems limited to the NLP_MI and SLP_MI subregions show small transmissivity trends. For the PENN aquifer system (fig. 41*B*), transmissivities tend to decrease from north to south with some local variations. For the MSHL aquifer system (fig. 41*C*), transmissivities tend to increase from north to south.

The SLDV aquifer system thickens appreciably in the center of the Michigan Basin, and this thickening influences the pattern of transmissivity (fig. 41*D*). The lowest transmissivities are found in areas to the west where the rocks subcrop beneath QRNR deposits.

Available data from well logs and pumping tests indicate that the transmissivity for the C-O aquifer decreases from north to south, owing to a greater fraction of fine-grained clastics (for example, siltstone) relative to sandstone (Feinstein, and others, 2005). However, increasing thickness of deposits causes transmissivity to increase for some hydrostratigrahic units toward the middle of the Michigan Basin (fig. 41*E*). Transmissivities are lowest in the northwest farfield part of the model domain, where the C-O rocks are thin and chiefly restricted to the MTSM unit.

The K_v assignments for confining units control the rate deep regional flow. Values generally range between 1.0 E−3 and 1.0 E−7 ft/d, as shown in a representative west/east section (fig. 42). The lowest values are associated with the evaporites in the SLDV aquifer system, followed by the shales in the DVMS system and at the top of the C-O system (the Maquoketa unit). Note that the K_v for SLDV aquifer increases as you move out of the Michigan Basin and away from the evaporite deposits in the Salina Group.

The K_h and K_v values assigned to bedrock aquifer systems for layers 4 to 20 produce a range of vertical anisotropy values. For layers defined as aquifers, the ratio of K_h to K_v varies between 50 to 1 and 2,000 to 1. For layers defined as confining units, the ratio varies between 1,000 to 1 and 20,000 to 1. The large ratios reflect the low K_v associated with confining shale beds and evaporites. The vertical anisotropy ratios reflect the presence of fractured or permeable beds inside the confining units (which increase the ease of horizontal flow) alternating with shale beds (which produce high resistance to vertical flow). This condition, for example, is well documented for shales in the Maquoketa hydrogeologic unit (Eaton, 2002). The biggest range in anisotropy is for layers defined as both aquifers and confining units, owing to the occurrence of high- and low-permeability material in the same unit. The vertical anisotropy ratios for these units vary between 50 to 1 and 10,000 to 1.

4.9 Storage

Storage parameters control the release or gain of water within the groundwater-flow system that accompany water-level changes in response to pumping and recharge. Different storage parameters are assigned for unconfined and confined aquifers. In confined aquifers, the specific storage (S_s, units of ft^{-1}) reflects both the elasticity of the aquifer material and the expansion or contraction of the groundwater. The specific storage is multiplied by thickness to yield the storage coefficient (*S*, dimensionless). In unconfined aquifers, the specific yield (S_y, dimensionless) reflects the draining or filling of pores and partings. A confined aquifer can be converted to an unconfined aquifer if the hydraulic head falls below the aquifer top elevation; in that case, changes in storage changes are controlled by the specific yield rather than the specific storage. The opposite can occur when the water table rises above the aquifer top.

There are limited sources of data that quantify storage parameters in the LMB model domain, so zonation of storage parameters is much simpler than the zonation for other parameters such as recharge and hydraulic conductivity. A single S_s value of 2.6 E−7 ft^{-1} is specified for all bedrock aquifers in the model. This value is based on pumping-test information from Wisconsin and Illinois and reflects conditions in the C-O aquifer system (Foley and others, 1953; Mandle and Kontis, 1992; Feinstein, Eaton, and others, 2005; Feinstein, Hart, and others, 2005). A larger S_s value of 5.7 E−6 ft^{-1} is assigned the QRNR system in the three top unconsolidated layers to account for their more compressible material. It is worth noting, however, that because the water table generally (although not always) resides in the top model layer, the parameter that more heavily influences storage change in layer 1 is typically the specific yield. The S_y values input to the model for unconfined cells are much higher than the product of S_s and thickness for confined cells; this imbalance indicates the powerful effect on storage release exercised by dewatering of pores compared to the weak storage effect produced by elastic responses for the same change in water level. Cells in layers 1 to 3 within the QRNR system are initially assigned a single S_y value equal to 0.15, a typical average (Anderson and Woessner, 1992) used in place of a possible range from below 0.05 to above 0.40, depending on grain-size distribution and resulting porosity and packing (Morris and Johnson, 1967). The S_y of layers in the PENN and MSHL aquifers systems are assumed equal to 0.05, which reflects the predominance of clastic material in these rocks and the limited availability of pore space between the grains of the matrix. The initial specific yield of layers in the SLDV aquifer system is set even lower, to 0.005, because the porosity in these carbonate rocks is largely derived from joints and fractures. Finally, S_y in the C-O aquifer system is assumed to be either 0.05 to reflect porosity in the units dominated by sandstone (STPT through MTSM units) or 0.005 to reflect predominant fracture porosity in shale and carbonate-dominated rocks (MAQU and SNNP units). The bedrock S_y values influence the simulated solution only when the water table fluctuates in bedrock layers, which can occur in isolated areas of bedrock highs or in places where deep withdrawals cause dewatering of a zone at the top of an aquifer and the presence of an underlying deep water table. The latter mechanism is documented in parts of the LMB model domain where deep pumping centers penetrate the C-O aquifer system (see section 7).

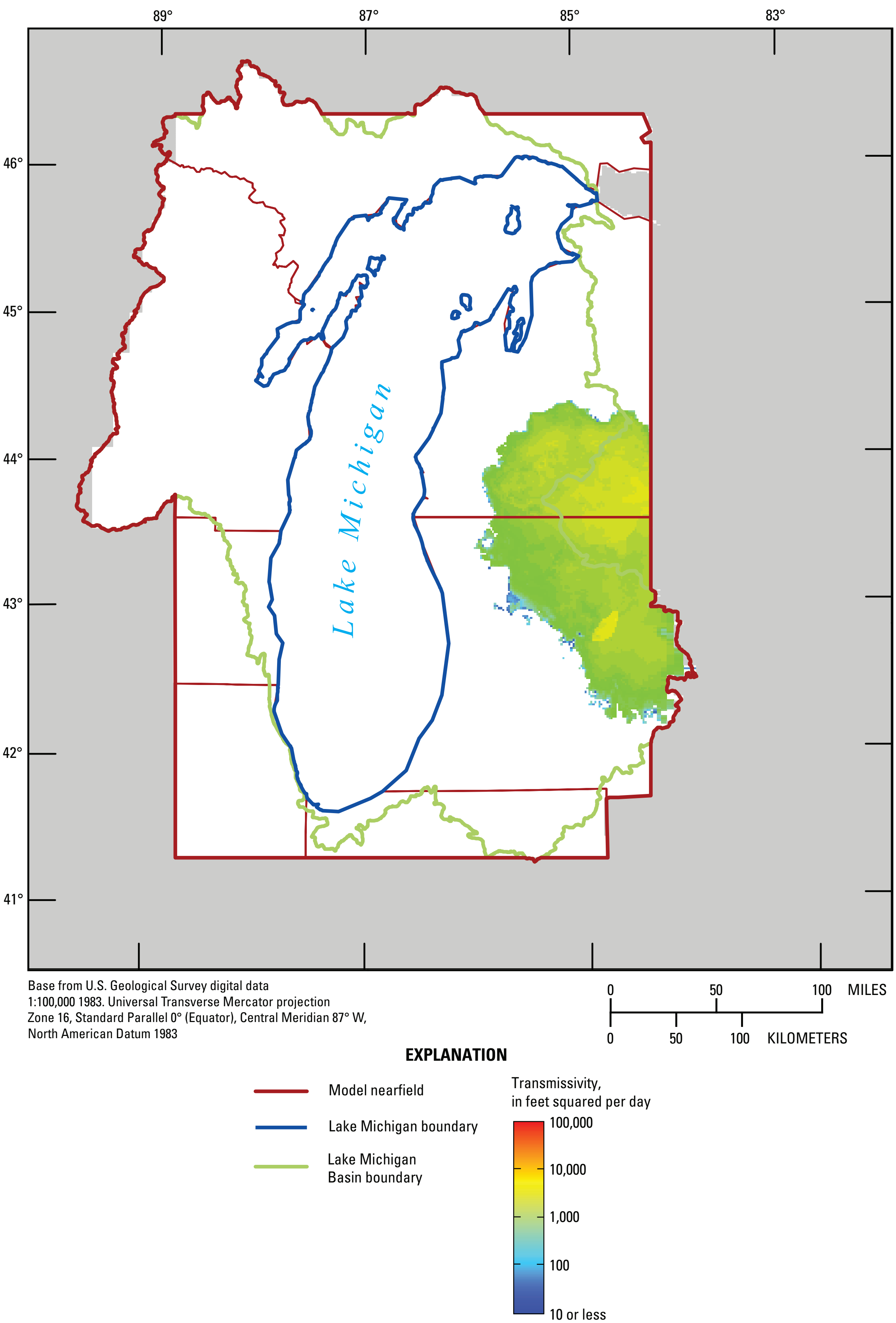

Figure 41*B*. Initial transmissivity distribution in aquifer system PENN.

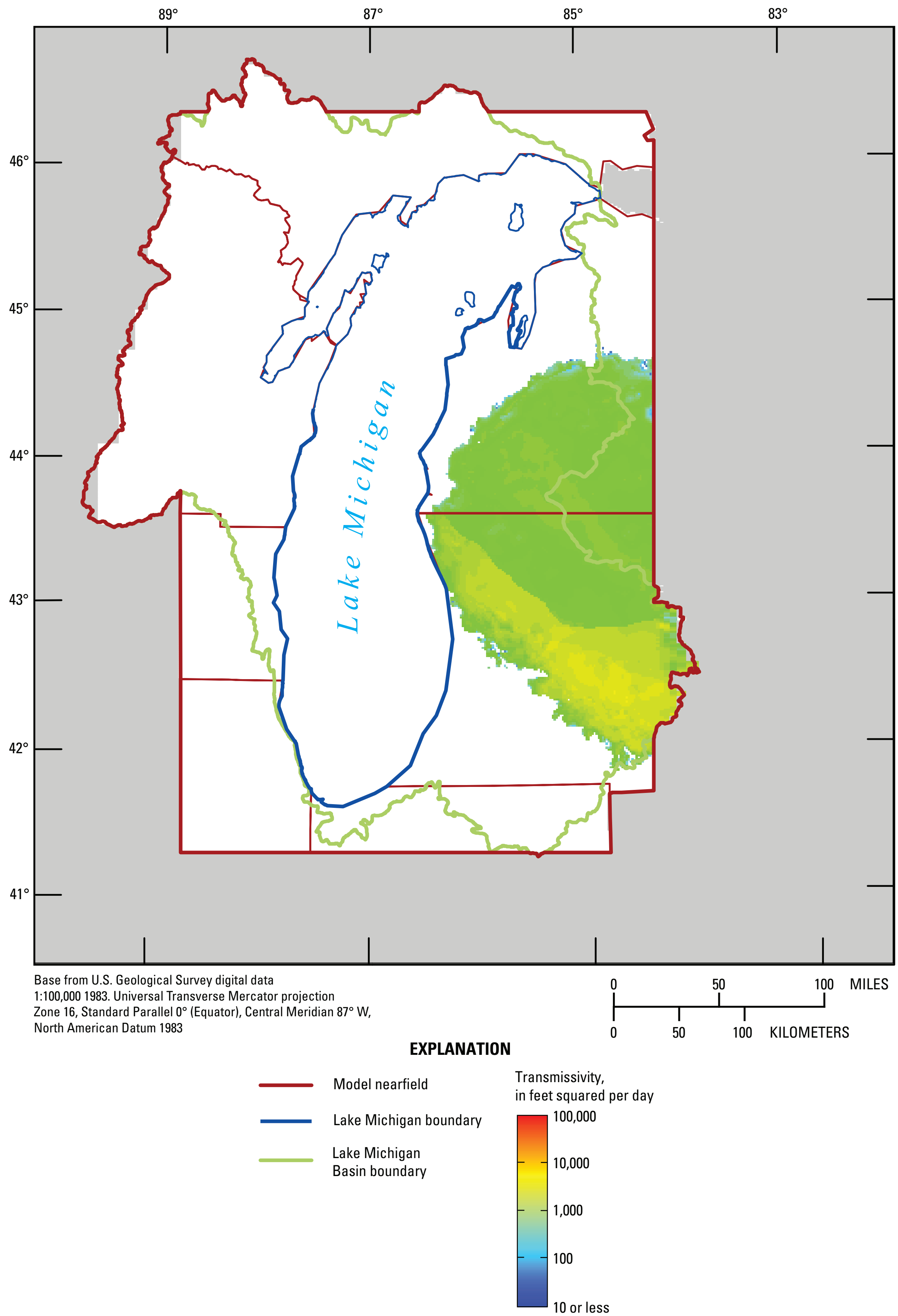

Figure 41*C*. Initial transmissivity distribution in aquifer system MSHL.

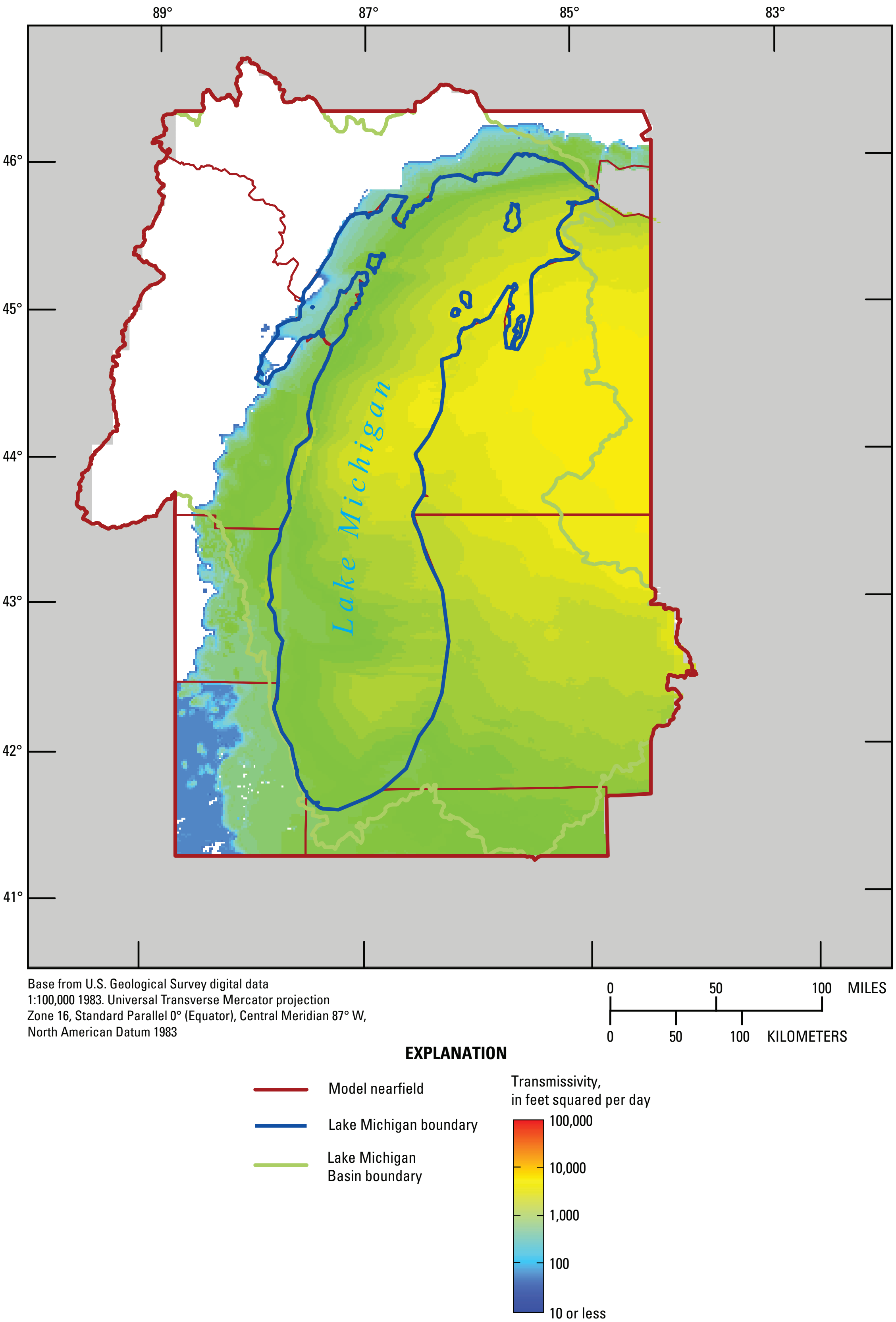

Figure 41*D*. Initial transmissivity distribution in aquifer system SLDV.

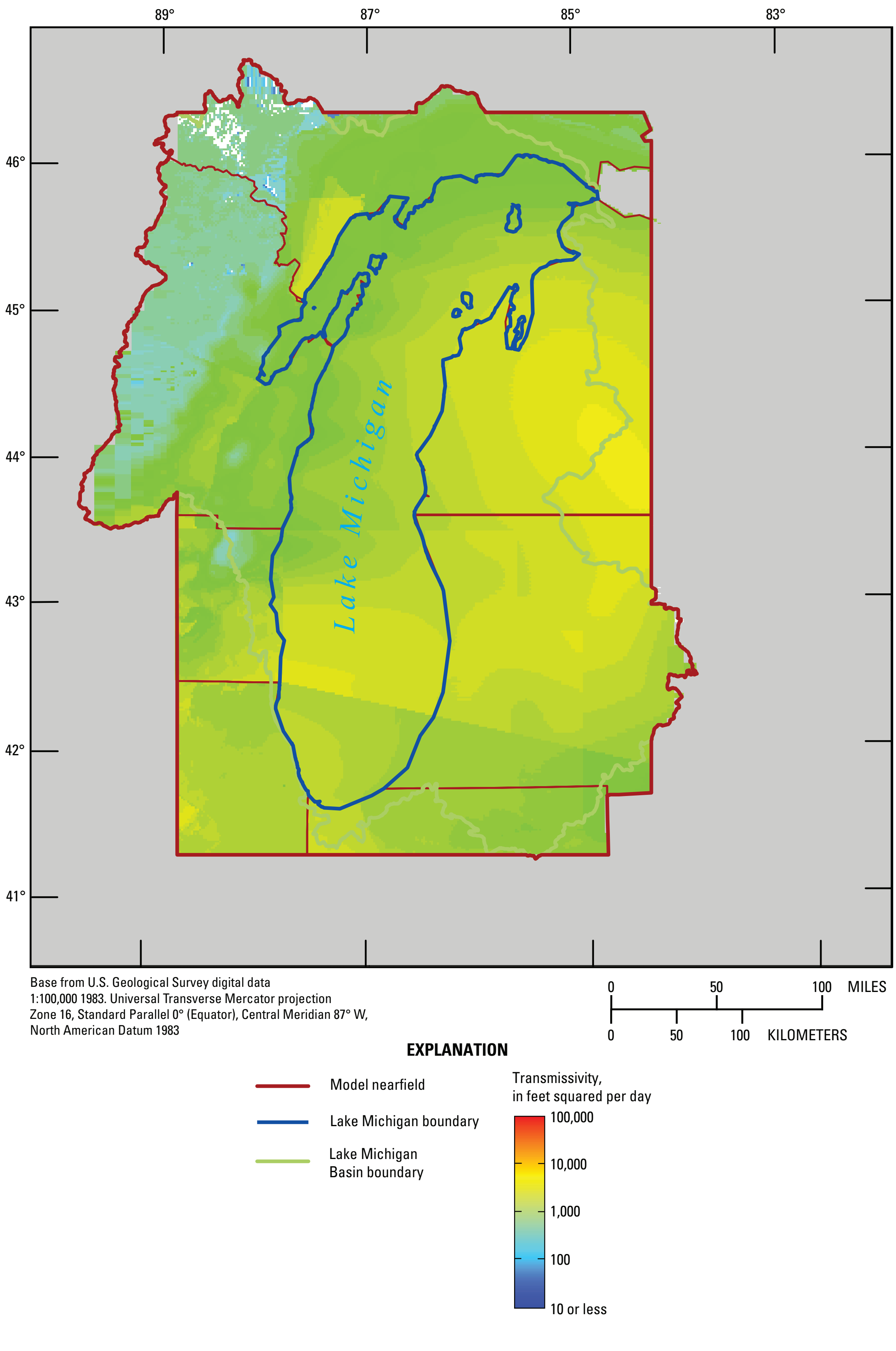

Figure 41*E*. Initial transmissivity distribution in aquifer system C-O.

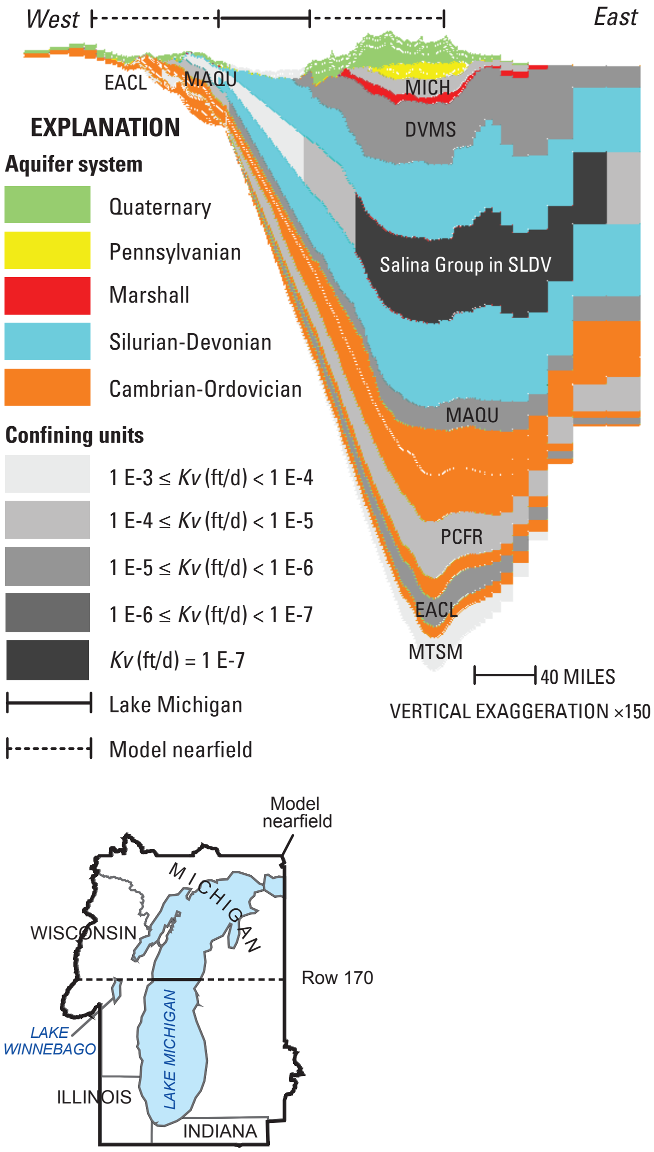

Figure 42. Initial vertical hydraulic conducitivities in major confining units, row 170.

4.10 Salinity

The presence of saline water (including brines with concentrations greater than 100,000 mg/L) in the Michigan Basin and the potential interaction of the drawdown cones of pumping centers in freshwater zones with surrounding saline water motivate the use of the variable-density groundwater-flow model SEAWAT (Guo and Langevin, 2002; Langevin and others, 2003). SEAWAT is an adaptation of the USGS groundwater-flow model MODFLOW; it incorporates extra terms in the governing groundwater-flow equation to account for variable density and utilizes the transport code MT3D to simulate the movement of salinity as a solute. SEAWAT-2000 version 4 (Langevin and others, 2007) allows density to be a function of multiple dissolved species and the groundwater-flow equation to respond to viscosity and temperature as well as density variations. The coupled flow and transport model invokes an equation of state that describes how fluid density varies with changes in solute concentration or fluid temperature.

For the Lake Michigan Basin model, the main interest from a water-availability viewpoint is the freshwater part of the system and its water levels, drawdown, and flow patterns. As a result, the saline water in other parts of the flow system can be viewed as boundary that influences the movement of groundwater toward surface-water features and pumping wells in the freshwater areas. Accordingly, the details of the circulation in the most saline part of the system are of secondary importance. The freshwater focus of the study leads to a simplification of SEAWAT whereby the water density in the system is fixed to always correspond to the salinity input to the model on the basis of available data. The density-dependent groundwater flow equation within SEAWAT is solved and the influence of saline water on the magnitude and direction of flow is simulated, but transport is not represented; thus, the density conditions within the saline water remain constant. The major assumptions implicit in this approximation are that pumping from deep wells does not significantly alter the salinity distribution and that the salinity distribution is stable during the 141-year transient simulations. These assumptions are tested and supported with an alternative fully coupled flow and transport model, which does simulate changes in density and concentration over time (presented in section 7). Additional work could be done to assess the effects of temperature and viscosity on the response of the system to pumping.[19] Despite these omissions, it is posited that the consideration of fixed saline conditions by itself improves the ability of the simulation to approximate real processes when compared to a model that considers only freshwater conditions, because the SEAWAT solution more accurately simulates the response of the variable-density system to stresses, particularly to deep pumping.

The estimated density of the groundwater in areas of saline water is based on both dissolved solids concentration and density information (Lampe, 2009). Concentration data representing salinity can be converted to density with a simple linear equation of state (Baxter and Wallace, 1916):

$$\rho = \rho_o + EC$$

where

- ρ_o is the reference density,
- E is the density-concentration slope, and
- C is the concentration of the fluid.

To compute density from concentration, a reference density, corresponding to freshwater conditions (62.44 lb/ft^3) is assumed, salinity is defined in dissolved solids concentration units of milligrams per liter (mg/L), and the density-concentration slope factor is set to 4.46 E−5 (lb/ft^3)/(mg/L).

[19] It also is unclear whether isostatic rebound induced by glacial unloading persists in the deep part of the Michigan Basin and whether it affects fluid movement in the saline waters of the Michigan Basin.

For example, a salinity of 10,000 mg/L corresponds to a fluid density of 62.78 lb/ft^3, and a salinity of 400,000 mg/L corresponds to a fluid density of 80.28 lb/ft^3. This linear equation is an approximation of the true relation between density and concentration, but it appears to hold even at brine concentrations close to halite saturation (Yager and others, 2007).

The distribution of dissolved solids concentrations for the LMB model domain presented by Lampe (2009) is interpolated from available data sources for the following units:

- QRNR in layer 1 (Waherer and others, 1996),
- PEN1 in layer 5 (Meissner and others, 1996),
- MSHL in layer 8 (Ging and others, 1996),
- SLDV in layer 11 (Gupta, 1993; Eberts and George, 2000; Schnoebelen and others, 1998),
- SNNP in layer 14 (Gupta, 1993; Visocky and others, 1985; Kammerer and others, 1998),
- PCFR in layer 16 (Gupta, 1993; Young, 1992; Kammerer and others, 1998), and
- MTSM in layer 19 (Gupta, 1993; Bond, 1972; Kammerer and others, 1998).

The concentrations in the remaining units are derived from layers presented above as follows:

- QRNR in layers 2 and 3 is equated with layer 1,
- JURA in layer 4 is the average of corresponding cells in layers 1 and 5,
- PEN2 in layer 6 is equated with layer 5,
- MICH in layer 7 is the average of corresponding cells in layers 5 and 8,
- DVMS in layer 9 and SLDV in layer 10 are the average of corresponding cells in layers 8 and 11,
- SLDV in layer 12 is equated with layer 11,
- MAQU in layer 13 is the average of corresponding cells in layers 11 and 14,
- STPT in layer 15 is the average of corresponding cells in layers 14 and 16,
- IRGA in layer 17 is equated with layer 16,
- EACL in layer 18 is the average of corresponding cells in layers 16 and 19,
- MTSM in layer 20 is equated with layer 19.

Sources of water in the model (recharge, the water induced from surface-water features and infiltrated water) are assigned salinities equal to zero. The only boundary that is potentially affected by salinity is the constant-flow boundary representing underflow through bedrock systems along the southwestern part of the model. Even though it is not correct, the salinity of this flow is also assumed to be zero. However, the effect on simulated water levels is likely to be very small and localized (Christian Langevin, U.S. Geological Survey, written commun., February 12, 2009).

In order to be certain that mapped concentration transitions from layer to layer are stable, a 100-year transport simulation was run with the initial parameter assignments and steady-state conditions assumed (that is, no pumping). Assumed values for dispersivities in this transport simulation were 10 ft (longitudinal), 1 ft (transverse horizontal), and 0.1 ft (transverse vertical); the assumed value for molecular diffusion was 1.0 E−5 ft^2/d; the assumed value for porosity and effective porosity was 0.2. The maximum transport time step was 1 year. After 100 years of coupled flow and transport simulation, less than 0.1 percent of the mass represented by the initial salinity distribution was lost by moving across the sides of the model. Within the domain, changes in concentration were extremely small, suggesting that the mapped concentrations are relatively stable. The transport simulation was eventually repeated by using calibrated parameter values (see section 5) with the same stable result. It is unlikely that changes in the initial concentration (density) distribution affect the results of the 141-year simulations described later in the report. For the final model runs, salinities were fixed to equal the results of the 100-year transport run with calibrated parameter values.

In general, salinity levels are much higher on the east side than the west side of Lake Michigan (table 10). There is also a striking vertical segmentation, with high salinity levels appearing only in the MSHL hydrogeologic unit and below (table 10). The spatial pattern is shown for four west/east hydrogeologic sections in figure 43. Dissolved solids concentrations in the Michigan Basin approach 500,000 mg/L in the evaporite-rich areas of the SLDV and in some underlying units, but concentrations are less than 10,000 mg/L west of Lake Michigan except in isolated parts of Wisconsin (see row 170) and in northeastern Illinois (see row 350). Concentrations in shallow units are highest to the east toward Lake Huron (row 170). The four sections also indicate saline conditions under Lake Michigan. Interpolation between available data points near the east and west shores of the lake indicates that concentrations can exceed 100,000 mg/L in bedrock units under the lake. The high density associated with such saline levels could affect the propagation of drawdown around deep pumping centers along the west shore of Lake Michigan, and, consequently, could distort the shape of source areas of water to these wells. One objective of the LMB model construction is to assess this possibility.

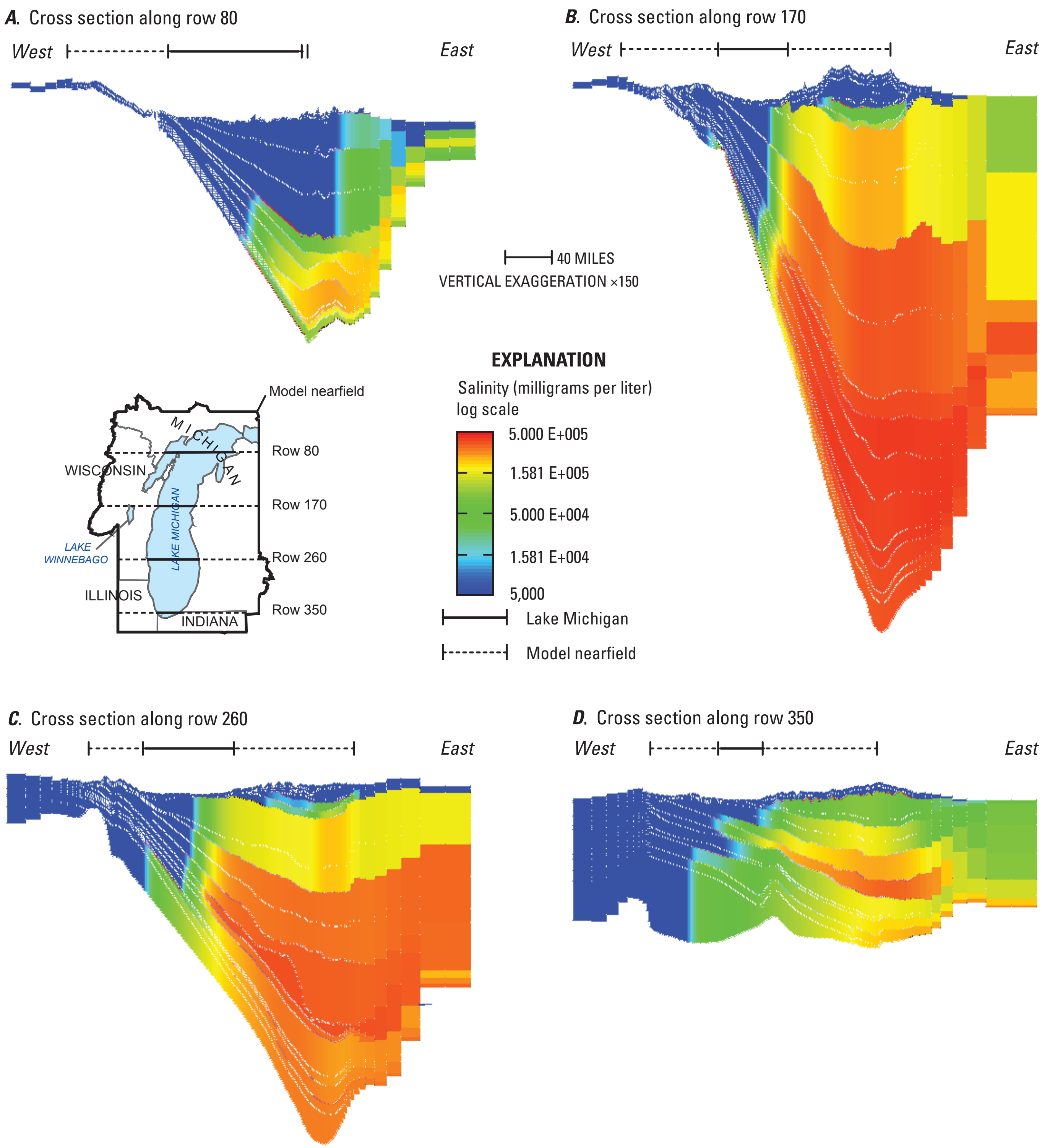

Figure 43. Fixed salinity distribution along selected model rows.

Table 10. Percentage of model nearfield that is saline west and east of Lake Michigan.

[Saline conditions correspond to model cells with concentrations greater than 10,000 milligrams per liter]

Layer	Aquifer system	Saline area west of Lake Michigan (percent)	Saline area east of Lake Michigan (percent)
1	QRNR	0.00	0.03
2	QRNR	.00	.05
3	QRNR	.00	.69
4	PENN	.00	.00
5	PENN	.00	.01
6	PENN	.00	.12
7	MSHL	.00	66.82
8	MSHL	.00	59.70
9	SLDV	.00	92.58
10	SLDV	.00	88.03
11	SLDV	.00	89.67
12	SLDV	.00	91.35
13	C-O	1.65	99.39
14	C-O	2.32	99.59
15	C-O	2.14	100.00
16	C-O	.46	99.15
17	C-O	.53	99.13
18	C-O	8.72	100.00
19	C-O	10.38	100.00
20	C-O	13.59	100.00

4.11 Model Input Packages, Program Executable, and Graphical Interface

The LMB model uses the following MODFLOW and MODFLOW-2000 packages:

- Basic (BAS6)
- Block-Centered Flow (BCF6)
- Recharge (RCH6)
- River (RIV6)
- General Head (GHB6)
- Well (WEL6)
- Multi-Node Well (MNW1)
- Discretization (DIS)
- Output Control (OC)
- Preconditioned Conjugate Gradient 2 (PCG2)

The Block-Centered Flow (BCF) package is used instead of the Layer Property Flow (LPF) package because with the BCF package the vertical conductance between layers is independent of the saturated thickness of each layer; this makes the numerical solution more stable, particularly in the case where deep layers dewater in response to pumping. The RIV package simulates exchange between the groundwater and surface-water systems. As explained above, in the case of water bodies (lakes and wetlands), the input to this package is adjusted so that it mimics the MODFLOW Drain package and only allows exchange to occur from the groundwater to the surface water. The WEL package is used for flux boundary conditions and for pumping wells (or for injection wells used to represent infiltration from surface impoundments) that penetrate a single layer. The MNW package is used for pumping wells that penetrate multiple layers. The MNW package is able to simulate flow through boreholes for both pumped and passive conditions, but it is invoked in the LMB model only for actively pumped wells. A special option in the OC package is invoked to reference simulated drawdown to the end of the first stress period; that is, to predevelopment conditions. The PCG2 solver package controls the path to convergence for each of the 61 model time steps. For example, it allows the user to dampen the maximum amount of head change allowed during iterations within a time step. Convergence is reached only when the maximum head change and flux change in all cells satisfy tolerance criteria. Discussion of the damping and tolerance criteria selected for this application is postponed to section 5 because these critera are important elements of the calibration process.

One package called by the LMB model is specific to SEAWAT—the Variable Density Flow (or VDF) package. It depends on a file that contains cell-by-cell fixed densities converted from salinity concentrations by using the linear constitutive equation discussed above. Simulations are executed with version 4 of SEAWAT-2000, compiled by the USGS in November 2007. The internal calculations of SEAWAT-2000 are in double precision, but the output is in single precision. The platform used to visualize input and output is Ground Water Vistas version 5 (Rumbaugh and Rumbaugh, 2004, 2007).

5. Model Calibration

The LMB model is very large (in excess of 2 million cells that cover parts of four states) and simulates the transient response of multiple aquifers to multiple pumping centers. It also simulates the exchange of groundwater between a dense surface-water network and notably heterogeneous glacial deposits underlain by a series of overlapping bedrock units dipping from the Wisconsin Arch into the saline Michigan Basin. These elements complicate the calibration process, which involves updating the initial estimates for a large number of input values in order to improve the match between simulated groundwater levels and flows and corresponding field observations, called *targets*. Multiple strategies are employed to enhance the calibration process and make it tractable for *parameter estimation* through the use of nonlinear regression techniques to adjust model inputs as a function of target outputs; in this study, parameter estimation was done by use of the code PEST (Doherty, 2008a). The strategies include linearization of the flow equation, grouping of input blocks into parameter zones subject to a single multiplier, assembly of diverse predevelopment and postdevelopment target types, filtering of targets, adjustment of target weights, special regression methods such as singular value decomposition, and focused use of pilot points to fully extract information from available targets and thereby allow more variation of crucial parameters. In the end, the calibration process not only improves the fit between measured and simulated targets but also adds insight into the major controls on the flow system through identification of parameter groups to which model results are most sensitive.

5.1 Linearization of Flow Equation

The original calibration strategy involved a version of the LMB model that included unconfined aquifers in areas where the water table is below the top of the model layer. Unconfined conditions typically occur in layer 1 but can also occur in layers 2 and below in areas where the stage elevations of surface-water features are below the bottom of the top layer. Finally, partially saturated conditions occur where drawdown from pumping deep wells creates unconfined conditions within deep confined aquifers. This pumping causes the upper part of the flow system to detach from the lower in the form of an unsaturated zone between the two and the formation of a second water table at depth.[20]

When the LMB model is simulated in confined mode, the original transmissivites and storage parameters (as well as pumping rates) assigned to cells still pertain even if dewatering has occurred and the head associated with the dewatered cell has fallen below the layer top (in which case the cell is implicitly a water-table cell) or below the layer bottom (in which case the cell is implicitly dry, although in confined mode it remains part of the model solution). The transmissivity is still calculated as a function of the total cell thickness, and the storage change is still calculated as a function of specific storage.

When the LMB model is simulated in unconfined mode, then, for unconfined aquifers, the transmissivity is calculated from the saturated thickness of the aquifer rather than the total thickness. In addition, storage is controlled by the specific yield rather than by specific storage. When transient simulations are run with the unconfined version of the LMB model, any changes from confined to unconfined conditions are accounted for by SEAWAT, which recomputes the transmissivity and storage parameters during the model-solution iteration. These changes have two effects: (1) the flow equation is no longer linear in the sense that model parameters (transmissivity and storage) are now dependent on simulated water levels, and (2) in areas where simulated water levels decline below the bottom of the unconfined aquifer, the model solution produces “dry cells” with zero saturated thickness. The latter phenomenon can be important because some of the wells in the dry cells are removed from the numerical solution and, as a result, pumping that is associated with these areas is not represented. The conversion from confined to unconfined conditions potentially poses several problems for automated calibration of the LMB model through nonlinear regresssion. A transient simulation can produce dry cells in any time step, which means that some cells containing calibration targets and pumping wells could be omitted from the numerical solution during the exploration of the parameter space. A second consideration is that the accuracy of the simulation of the vertical flow field is affected by the continuity of saturated conditions. It is possible for the MODFLOW-2000/SEAWAT-2000 codes in unconfined mode to simulate discontinuous saturated conditions at depth when a dewatered zone overlies a deep water table. The dewatered zone can be represented by a single *partially saturated* cell that contains a water table, or it can correspond to one or more inactive cells (that is, unsaturated or dry cells) stacked vertically above a deeper cell that is partially or fully saturated. Under partially saturated conditions, the code transfers water between the overlying cell and the saturated

[20] Field evidence for dewatering in deep aquifers west of Lake Michigan is provided below in section 7.1, along with modeling results in line with the field evidence.

part of a partially saturated cell by using a simplified algorithm that modifies the vertical gradient but does not take account of the unsaturated properties of the dewatered zone. When a cell is inactive, the code allows no exchange at all between the inactive cell and vertically or horizontally adjacent cells (McDonald and Harbaugh, 1988).[21] In the present study, areas with multiple water tables are present but limited in extent *and* concentrated around major deep pumping centers. (For fuller analysis of deep water-table conditions and the effect on confined and unconfined model results, see section 7.)

An additional disadvantage of an unconfined simulation is the tradeoff between runtimes (the time needed to solve the model across stress periods) and the solution-convergence criteria, which determine the number of iterations within the time step to obtain a solution deemed sufficiently accurate. The PCG2 solver applied to the LMB model applies two convergence criteria: one to limit the maximum head change that can occur in any cell between iterations within a time step, and one to impose a maximum change in the flux passing through the cell. The more restrictive these criteria are, the longer the runtime but the smaller the global water-budget error arising from an imbalance between flows into and out of the model domain for any time step. Criteria are normally set to insure that the global water-budget error (calculated for SEAWAT-2000 in terms of mass rather than volumetric flux) is less than 1 percent for any time step, and, preferably, less than 0.1 percent. For an unconfined solution, the criteria necessary to meet the 0.1-percent water-budget error yield a runtime on the order of 11 hours on a 2008 model IBM personal computer. A confined run with the same initial input solves in less than 2 hours. Finally, the most serious difficulty arising from using the unconfined solution for parameter estimation stems from relatively large degradation in the differentiability of the problem. Nonlinear regression methods commonly rely on tracking the effect of small perturbations of parameter values to changes in model outputs, in this case simulated head or flux values associated with calibration targets (Doherty, 2008a). The ratio of the latter to the former defines a matrix of observation to parameter derivatives (called the “Jacobian” or sensitivity matrix), a matrix whose size is the number of parameters multipled by the number of observations. Sensitivity information contained in the Jacobian matrix guides the search for updated and improved input values and better model fit. The method is most robust when the derivatives calculated by perturbation are largely independent of the exact size of the perturbation. This robust condition is demonstrated when a graph of parameter perturbation increments versus target value yields a trend that approximates a straight line.

The parameter estimation code PEST contains a useful utility (called JACTEST; see Doherty, 2008b) that allows the behavior of derivatives to be tested and the results graphed for selected parameters and targets. For the LMB model, the tests indicate that the linearity of the derivatives is strongly influenced by both the size of convergence criteria and whether the model was run under unconfined or confined conditions. An example is the drawdown simulated at six observation wells produced by perturbations of the vertical hydraulic conductivity of the Maquoketa shale unit below the Southeastern Wisconsin subregion of the model (SE_WI, fig. 44). For an unconfined model with relatively larger (looser) convergence criteria (though one that still produces an acceptable mass water-budget error between 0.1 and 1 percent), the simulated model outputs resulting from successively increasing small perturbations are irregular, without an obvious single trend or slope (fig. 44). Such results are representative of highly nonlinear derivatives—derivatives that can confound nonlinear regression methods. For a confined model with smaller (tight) convergence criteria (tolerances reduced by about 20 times, producing water-budget errors on the order of 0.1 percent), the relation is generally linear (fig. 44). This analysis can be further extended by separating out effects of convergence criteria and unconfined/confined model and quantifying the linearity of the slope by means of a R^2 term arising from applying standard linear regression to the JACTEST graphs, where a R^2 of 1.0 indicates a perfectly linear response. By using a larger number of targets (189) linked to the Maquoketa K_v parameter, median R^2 values were about 0.10 for both unconfined and confined models with larger (looser) PCG2 convergence criteria, indicating nonlinear behavior and inaccurate derivatives in the inversion routines. For the unconfined model with tight convergence criteria, the linearity improved modestly (median R^2 equal to 0.38). It is likely that the persistent nonlinearity (deviation from 1.0) is related to trouble obtaining accurate saturated thicknesses and to the development of desaturated conditions under confined aquifers in later stress periods. For the confined model with small (tight) convergence criteria, the R^2 improves to 0.96, indicating fairly linear behavior and appreciably more reliable derivatives.

---

[21] In **unconfined mode** the MODFLOW-2000/SEAWAT-2000 codes calculate the downward flow between a fully saturated cell in an overlying layer and a partially saturated cell (that is, one containing a water table) in an underlying layer as the product of the vertical conductance between the layers (fixed by the model input) and a head difference equated with the difference between the head in the overlying cell and the overlying cell’s bottom elevation. When a cell is simulated as completely dry in unconfined mode and is, therefore, inactive, no vertical exchange occurs across it. When a layer in MODFLOW-2000/SEAWAT-2000 is restricted to confined model, desaturation of cells is not simulated, and all cells are assumed to be fully saturated throughout the simulation. A simulated water level may be within the cell, above the cell top, or below the cell bottom. The vertical flow between a cell in a confined and an overlying cell is determined by the heads in the two cells and the vertical conductance between the cells. Although a cell in a confined mode layer cannot be desaturated from the standpoint of the flow equation, it is also true that if the water level is below the cell top, then the the confined solution is implying that the cell is either partially dewatered (water level between the top and bottom of the cell) or fully dewatered (water level below the bottom of the cell).

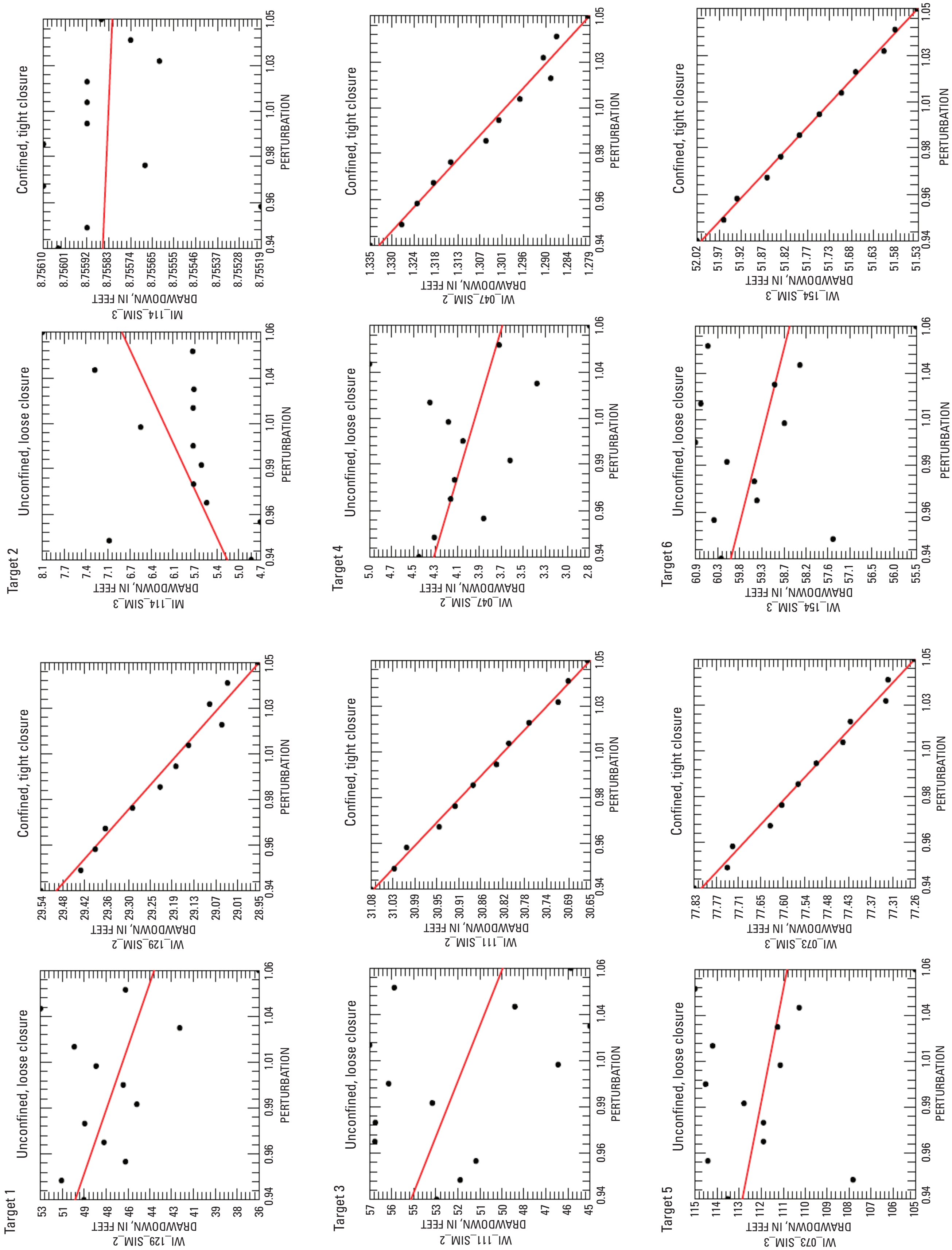

Figure 44. Sample plots of Jacobean derivatives for vertical hydraulic conductivity in the Maquoketa confining unit.

Though responding more linearly to parameter perturbation, the confined version of the LMB also must approximate actual water levels and responses to stresses measured in the groundwater flow system. Therefore, actual deviations from confined conditions were accounted for by modifying a subset of the confined model input, those involving transmissivity and storage. It is fairly easy to approximate the effect of partially (or wholly) desaturated layers on transmissivity as input into the adjusted confined model, and solutions of the unconfined simulation and confined simulation with adjusted parameters did not differ dramatically at initial or final optimal parameter values. The agreement in solutions is especially close for the water-table surface, owing to the effect of locally pinning or "stapling" of heads near head-dependent boundaries representing surface-water features (see section 3). Thus, it is possible to convert the transmissivity in cells that go dry to an extremely low value to simulate inactive conditions, and, in cells only partly saturated, to reduce the full-thickness transmissivity by the difference in saturated thickness in order to simulate water-table conditions. Both conversions are made by means of changes to the K_h cell value: in the case of dry cells it is reduced to 1 E−5 ft/d; in the case of water-table cells the initial value is multiplied by the ratio of the saturated thickness to the total thickness. The calculation is made for the minimum saturated thickness recorded for the initial simulation at the end of any stress period. The revised K_h value is used in parameter estimation for the adjusted confined version of the model, where it is then subject to decrease or increase during calibration.

The treatment of the storage parameter in the adjusted confined model is generally similar to the treatment of transmissivity in the case of dry or water-table cells. For a dry cell the storage parameter should be effectively zero, whereas for a water-table cell it should be proportional to the specific yield (S_y). The confined version of the LMB model does not have the option for unconfined cells of substituting S_y directly for the product of specific storage (S_s) and cell thickness because in confined mode the MODFLOW code permits the application of only one type of storage term. However, the S_s term can be adjusted so that its product with cell thickness approximates the value of S_y and, thereby, provide a more realistic treatment of storage release in cells which contain a water table. Accordingly, construction of the confined version of the LMB model entails setting S_s to 1 E−10 for dry cells and setting S_s to the value of S_y divided by saturated thickness (to yield an effective S_s parameter) for water-table cells. A special difficulty arises in the transition case when drawdown around wells causes desaturation of deep cells and formation of stacked water tables within a given stress period. Because of the relatively coarse time discretization, it is not clear which storage parameter is most representative for the deep layer during the transition—the original S_s value proper for the original confined conditions or the S_y value proper for the eventual water-table conditions. (Note that the input to MODFLOW-2000/SEAWAT-2000 does not allow either the hydraulic conductivity or storage input to change in time.) Unlike the case of transmissivity, where the water-table condition typically produces a fraction of the original horizontal hydraulic conductivity with an expected value in the neighborhood of 0.5, the transition from a fully saturated to partly saturated condition produces a dramatic increase in the storage capability on the scale of several orders of magnitude.

To handle the possibility of this nonlinear behavior, the algorithm to convert storage in the adjusted confined model contains two steps. For the steady-state solution corresponding to predevelopment conditions, no deep dewatered zones overlying deep water tables are present because no deep wells are pumping to induce unconfined conditions. Accordingly, the initial steady-state solution can be applied to the uppermost water-table cell at a row/column location to convert specific yield to specific storage as a function of the degree (or absence) of saturation. The second step applies to cells in layers 2–20 that desaturate after the first steady-state stress period when pumping is active. An initial rough approximation is used to estimate the combined specific storage term—it is set to twice the geometric mean of the initial S_y and S_s assigned to the cell. Initial comparison simulations showed that this compromise value serves to roughly approximate the storage release behavior of the direct unconfined solution. However, the inevitable result of using a geometric mean is the introduction of some error by causing the storage release to be overestimated in the adjusted confined model version before the water-table condition occurs in a deep cell and to be underestimated after they occur.

The scaling of K_h and S_s as a function of unconfined or dry conditions to mimic unconfined conditions in confined mode was done once at the beginning of the calibration process by using the solution obtained with initial parameter values. In principle, the scaling should be updated during intermediate solutions when parameters are updated during calibration, but this refinement was not made on the assumption that the saturated thickness of cells does not change appreciably as parameters are updated and that the initial scaling is adequate to reliably capture the effect of partial saturation on groundwater flow.

The need for these simplifications notwithstanding, the adjusted confined version of the model is superior to the unconfined model for parameter estimation because it inherently keeps all targets and pumping wells active and its linearity promotes numerical stability, shortens runtimes, and preserves the integrity of the derivatives (high linearity of the Jacobian matrix). Nonetheless, it is prudent to compare the calibration and findings of the confined model to those obtained with the unconfined model to assess the effects of the simplification. To that end, two calibration processes were followed: one for the confined version of the model adjusted as described to approximate unconfined conditions, and one for the original unconfined version. The first calibration is presented in this section of the report, and its findings with respect to water levels and fluxes are presented in section 6. Both the calibration and results of the second, unconfined version are presented in section 7, which is devoted to alternative models.

5.2 Calibration Parameters

Some model parameters—for example, the K_h and K_v of the QRNR system, the conductance of RIV cells, and recharge—vary across layers or across stress periods on a cell-by-cell basis. Other inputs—for example, the K_h and K_v of the bedrock aquifers and the K assigned lakebed of Lake Michigan—vary within each layer on a block basis. Still other inputs—for example, storage terms—vary by layer or by groups of layers. It is not practical given the number of parameters, nor even desirable given the limited number of informative calibration targets, to attempt to adjust every input value. Rather, it is necessary to group inputs in ways representative of the system and in a way that obtains a unique set of optimal parameters. In this work, grouping was accomplished by estimating a single multiplier that scales initial values of a particular parameter for a specified collection of cells grouped into a zone. The multipliers applied to zones are adjusted during the calibration and are applied to all values in the zone, thus maintaining the original relative nodal differences present in initial parameter values. By way of example, a single recharge multiplier is applied to the recharge array; thus, the array can be thought of as a single zone that incorporates the highest active cell at every row/column location. A second example involves K_h and K_v of the glacial sediments: six multipliers are estimated for each of the six glacial categories (zones), which are distributed over three model layers. A single multiplier is also applied to the vertical anisotropy (K_h/K_v) in each glacial category[22] and to all the conductance terms accompanying RIV cells in each glacial category, resulting in 12 more parameter-estimation multipliers that are applied within these same six zones. A final example is the most complicated. In the case of the bedrock hydraulic conductivity, K_h and K_v input is grouped according to the grouping described in appendix 4. A zone multiplier varied in parameter estimation can correspond to a single block in a layer that incorporates a single initial value, or it can correspond to multiple blocks in a layer that incorporates multiple initial values. Two rules were developed to assign multipliers to bedrock hydraulic conductivity: (1) no bedrock layer can contain more than nine K_h or nine K_v zones (to reduce the total number of parameters estimated but still maintain calibration flexibility), and (2) zones primarily combine blocks by geographic contiguity and secondarily combine blocks with similar values. As always, a single parameter is estimated during the calibration process that serves to multiply the initial bedrock K values assigned all the cells in the corresponding zone.

The foregoing discussion requires one qualification. Not all zones are subject to an estimated multiplier in the form of a calibration parameter. In some cases, the initial value in a zone is left unchanged either because the flow component is not appreciable and thus is insensitive (K_h in confining units the bed of Lake Michigan) or because values were estimated implicitly through estimation of an associated parameter (K_v in aquifer units estimated indirectly as a ratio of the estimated K_h value). The total number of zones corresponding to unestimated parameters is 38; they are listed and characterized in terms of initial input values in appendix 5, table A5−1. The remaining 165 zones subject to parameter estimation are listed and described in appendix 5, table A5–2. Estimated parameters include recharge (1 parameter), Quaternary sediment K_h (QRNR, 6 parameters), Quaternary sediment vertical anisotropy (QRNR, 6 parameters), lakebed of Lake Michigan K_v (1 parameter), K_h for bedrock layers (81 parameters), K_v for bedrock layers (53 parameters), RIV conductance (7 parameters), and storage terms (5 parameters in the confined model or 10 parameters in the unconfined model). For calibration with the confined version of the LMB model, five S_s parameters that represent both confined and unconfined conditions are estimated, whereas for the unconfined version of the LMB model, five S_s and five S_y parameters are estimated. The configuration of K_h zones and a statistical summary of initial values is shown for nine (mostly aquifer) layers in appendix 6*A*; the pattern of K_v zones with accompanying statistical summaries is shown for nine (mostly confining unit) layers in appendix 6*B*. One set of inputs is estimated on a cell-by-cell rather than zonal basis—the K_v of the Maquoketa hydrogeologic unit in two subregions, Southeastern Wisconsin and Northeastern Illinois (SE_WI and NE_ILL). The use of pilot points in this context is discussed later in this section.

5.3 Calibration Targets

Diverse types of calibration targets can enhance the parameter-estimation process. The most common type of target for groundwater-flow-model calibration is water-level data derived from well measurements or contour maps. Water-level data provide information on the configuration of the water-table surface and of water-level surfaces corresponding to elevations below the water table, which, in turn, helps to

[22] The K_v of the unconsolidated deposits, initialized as 1/20 the value of K_h and therefore, like K_h, varying on a cell-by-cell basis, is not estimated directly but indirectly by means of the vertical anisotropy ratio. The six anisotropy multipliers are estimated with the benefit of the *updated* K_h values from an earlier sweep of the inversion algorithm; the new anisotropy ratios for each zone are then applied to the updated K_h arrays, and this procedure results in updated values of K_v that again vary cell by cell.

estimate horizontal hydraulic conductivity, recharge, and, to a lesser extent, the RIV conductance values. However, K_h and recharge values often correlate because, in principle, increases in one can be offset by increases in the other, thus resulting in a similar simulated head (see Haitjema, 1995). Moreover, either term can be adjusted to handle the degree of water-level mounding resulting from grid discretization (Feinstein and others, 2003; see also "Target Filtering," section 5.3.2). The addition of base-flow targets, which sum the groundwater contribution upgradient from the streamgage where flow is measured, can constrain the estimation of recharge, which in turn can help constrain estimation of hydraulic conductivity and storage (Poeter and Hill, 1997; Hill and Tiedeman, 2007). Vertical-head-gradient targets from nested shallow and deep wells and packer intervals in a same well also facilitate estimation of vertical hydraulic conductivity, and head changes over time (drawdown and recovery) also can constrain storage estimates. Finally, distribution of calibration targets in time and space can also be important for identifying unique optimal values. In the LMB model calibration, targets from both predevelopment and postdevelopment periods were included and were spread over every model subregion, where possible. Like most regional models, the LMB model is characterized by a large cell size. Thus, it is worth noting that an algorithm was employed to interpolate values spatially between cell centers (so that the exact location of a target was honored) and temporally between model stress periods (so that the timing of the measurement was respected).

5.3.1 Target Composition

The sets of targets applied to the calibration of the confined version of the LMB model are listed in table 11*A*, along with the number of targets in each set and other information pertaining to their role in the parameter-estimation process. The targets include representative water levels, base flow, vertical head gradients, and drawdown and recovery differences. Some sets are linked to the pre-1940 period and some to the post-1940 period. Many target types are divided into geographic subsets. Figure 45 presents the spatial coverage as well as the data sources for

(a) USGS network wells, household wells, and contour-derived targets, serving as *predevelopment* and *early postdevelopment* (1860–1940) water-level targets;

(b) USGS network wells, serving as *postdevelopment* (1940–present) water-level targets;

(c) USGS network wells, as well as RASA packer tests from the early 1980s, serving as vertical-head-gradient targets;

(d) multiple observations from USGS network wells and differences computed between contour maps at different times, serving as head-change (drawdown and recovery) targets;

(e) USGS streamgages, serving as base-flow targets; and

(f) household wells, serving as *postdevelopment* water-level targets.

Several target sets merit special attention. In general, it is possible to identify the unit(s) penetrated by USGS network wells and by household wells on the basis of the wells' geologic logs. Where multiple units are penetrated, depth information in the log is juxtaposed with land-surface data and stratigraphic layering used to construct the LMB model layers for the cell corresponding to the well location. In this cell, the water level is assigned to the thickest aquifer unit penetrated by the well, where the thickest unit is used as a surrogate for the most transmissive unit encompassed. When unit information is missing, the total depth of the well, in conjunction with the model layering, is used alone to identify the target layer.

Mapped predevelopment and postdevelopment head contours for the C-O aquifer system are composite heads that reflect conditions in the multiple units extending from the Sinnipee (SNNP) aquifer (layer 14) to the Mount Simon (MTSM) aquifer (layer 19 or layer 20). Where flow is not strictly horizontal, the contours are assumed to reflect average head conditions in the aquifer system. For the purposes of calibration of the LMB model, the targets derived from these contour maps are assigned to a single intermediate layer in the C-O aquifer system corresponding to the Prairie du Chien-Franconian (PCFR) aquifer (layer 16).

Postdevelopment water-level targets that correspond to household wells were not used (not given weight) in the parameter estimation process on account of their shallowness and the inability of LMB model cell size to simulate the actual groundwater-surface water interaction in the basin. However, residuals for 50,000 measurements in the model nearfield were computed and qualitatively evaluated as a check on calibration.

Results from multiple base-flow estimation methods were tested for this study, but the regression base-flow method of Gebert and others (2007) was selected to generate the 62 base-flow targets. Appendix 7 describes the selected regression equations, which estimate base flow as a function of coefficients and exponents computed from (1) the amount of streamflow under low-flow conditions and (2) the upstream basin area. The Gebert method equates the low-flow term in the regression with the flow exceeded 90 percent of the time (the Q_{90} value) at a streamgage location for a given period of record. Appendix 7 also contains a table with the names of the 62 streamgages (referenced to locations in fig. 45*E* and grouped by model subregion). Each gage is accompanied by its upstream basin area, duration of record, the base-flow estimate based on the Gebert equations, base-flow estimates derived from five other base-flow estimation methods, and comparison of the Gebert-method results to the Q_{50}, Q_{75}, and Q_{90} values from the stream's flow-duration curve. Summary statistics for basin area, duration of record, and base-flow comparisons are compiled at the foot of the table.

Table 11. Calibration target sets and target groups for model calibration.

11*A*. Confined conditions.

Target set / Target subset	Number of observations	Individual (observation weight)^2	Weighted sum of squares of calibrated residuals (feet squared)	Percent contribution to weighted sum of squares of residuals: By subset	Percent contribution to weighted sum of squares of residuals: By set
"Predevelopment"—before 1940					**22.8**
USGS network water levels	11	1	6,776	1.45	
Driller-log water levels	51	0.25	4,826	1.03	
Wisconsin Cambrian-Ordovician head contours	233	.04	30,995	6.62	
Michigan Pennsylvanian head contours	115	.04	20,183	4.31	
Michigan Marshall head contours	103	.04	20,810	4.44	
Indiana miscellaneous water levels	19	.16	4,712	1.01	
Illinois Cambrian-Ordovician head contours	231	.04	18,422	3.93	
USGS network wells—"historical" water levels					**40.0**
Southern Lower Peninsula, Michigan	1,761	.01–.04	18,032	3.85	
Northern Lower Peninsula, Michigan	272	.01	11,727	2.51	
Upper Peninsula, Michigan	426	.01–.04	1,565	.33	
Northeastern Wisconsin	1,964	.01–.04	75,631	16.16	
Southeastern Wisconsin	1,149	.01–.04	58,905	12.62	
Northern Indiana	294	.01	1,709	.37	
Farfield	2422	.0025–.01	19,685	4.20	
Northeastern Illinois Cambrian-Ordovician					**4.3**
2000 water-level contours	248	.01	7,434	1.59	
Drawdown, 1864–2000 contours	248	.01	6,398	1.37	
Recovery, 1980–2000 contours	267	.0025–.01	6,133	1.31	
Decadal head changes in USGS network wells					**21.1**
Southern Lower Peninsula, Michigan	1	49	530	.11	
Northeastern Wisconsin	22	1–4	38,359	8.19	
Southeastern Wisconsin	40	1	59,875	12.79	
Vertical head differences					**4.9**
USGS network wells	41	.25–4	10,231	2.19	
USGS RASA packer tests in early 1980s	31	4	12,763	2.73	
Base-flow targets at USGS streamgages in 2000					**6.9**
Southern Lower Peninsula, Michigan	17	3.60E−11	7,582	1.62	
Northern Lower Peninsula, Michigan	11	3.60E−11	4,846	1.04	
Upper Peninsula, Michigan	9	3.60E−11	3,455	.73	
Northeastern Wisconsin	12	3.60E−11	6,138	1.31	
Southeastern Wisconsin	4	3.60E−11	2,864	.61	
Northern Indiana	3	3.60E−11	676	.14	
Northeastern Illinois	6	3.60E−11	6,749	1.44	
Total	**10,011**		**468,011**	**100.00**	**100.0**

Table 11. Calibration target sets and target groups for model calibration.—Continued

11*B*. Unconfined conditions.

Target set	Number of observations	Individual (observation weight)[2]	Weighted sum of squares of calibrated residuals (feet squared)	Percent contribution to weighted sum of squares	
Target subset				By subset	By set
"Predevelopment"—before 1940					**23.2**
USGS network water levels	11	1	6,847	1.48	
Driller-log water levels	51	0.25	5,097	1.10	
Wisconsin Cambrian-Ordovician head contours	233	.04	31,071	6.72	
Michigan Pennsylvanian head contours	115	.04	21,129	4.57	
Michigan Marshall head contour	103	.04	20,616	4.46	
Indiana miscellaneous water levels	19	.16	4,837	1.05	
Illinois Cambrian-Ordovician head contours	231	.04	17,941	3.88	
USGS network wells—"historical" water levels					**40.6**
Southern Lower Peninsula, Michigan	1,761	.01–.04	18,840	4.07	
Northern Lower Peninsula, Michigan	272	.01	13,309	2.88	
Upper Peninsula, Michigan	426	.01–.04	1,506	.33	
Northeastern Wisconsin	1,964	.01–.04	76,691	16.58	
Southeastern Wisconsin	1,149	.01–.04	55,868	12.08	
Northern Indiana	294	.01	1,849	.40	
Farfield	2,422	.0025–.01	19,862	4.29	
Northeastern Illinois Cambrian-Ordovician					**5.7**
2000 water-level contours	248	.01	8,640	1.87	
Drawdown, 1864–2000 contours	248	.01	9,103	1.97	
Recovery, 1980–2000 contours	267	.0025–.01	8,658	1.87	
Decadal head changes in USGS network wells					**17.5**
Southern Lower Peninsula, Michigan	1	49	543	.12	
Northeastern Wisconsin	22	1–4	32,373	7.00	
Southeastern Wisconsin	40	1	48,056	10.39	
Vertical head differences					**6.3**
USGS network wells	41	.25–4	13,460	2.91	
USGS RASA packer tests in early 1980s	31	4	15,831	3.42	
Base-flow targets at USGS streamgages in 2000					**6.6**
Southern Lower Peninsula, Michigan	17	3.60E−11	7,265	1.57	
Northern Lower Peninsula, Michigan	11	3.60E−11	4,241	.92	
Upper Peninsula, Michigan	9	3.60E−11	3,751	.81	
Northeastern Wisconsin	12	3.60E−11	5,568	1.20	
Southeastern Wisconsin	4	3.60E−11	2,488	.54	
Northern Indiana	3	3.60E−11	895	.19	
Northeastern Illinois	6	3.60E−11	6,327	1.37	
Total	**10,011**		**462,662**	**100.00**	**100.0**

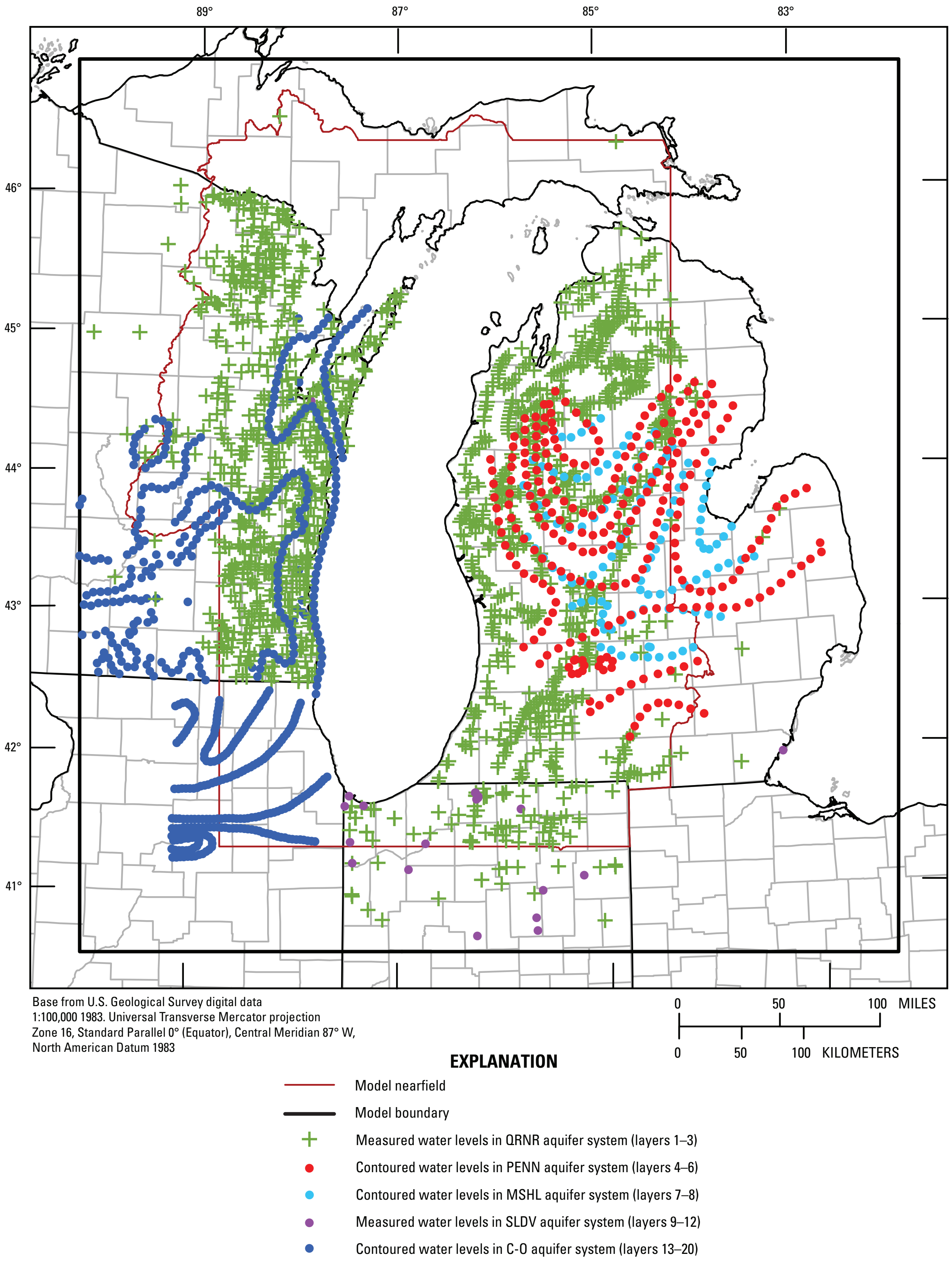

Figure 45*A*. Spatial distribution of calibration targets: USGS network wells, household wells, and contour-derived targets, providing predevelopment water-level targets (Sources: U.S. Geological Survey, National Water Information System, *http://waterdata.usgs.gov/nwis*; Arihood, 2009; Barton and others, 1996; Weidman and Schultz, 1915; Capps, 1910; Visocky and others, 1985; Mandle and Kontis, 1992).

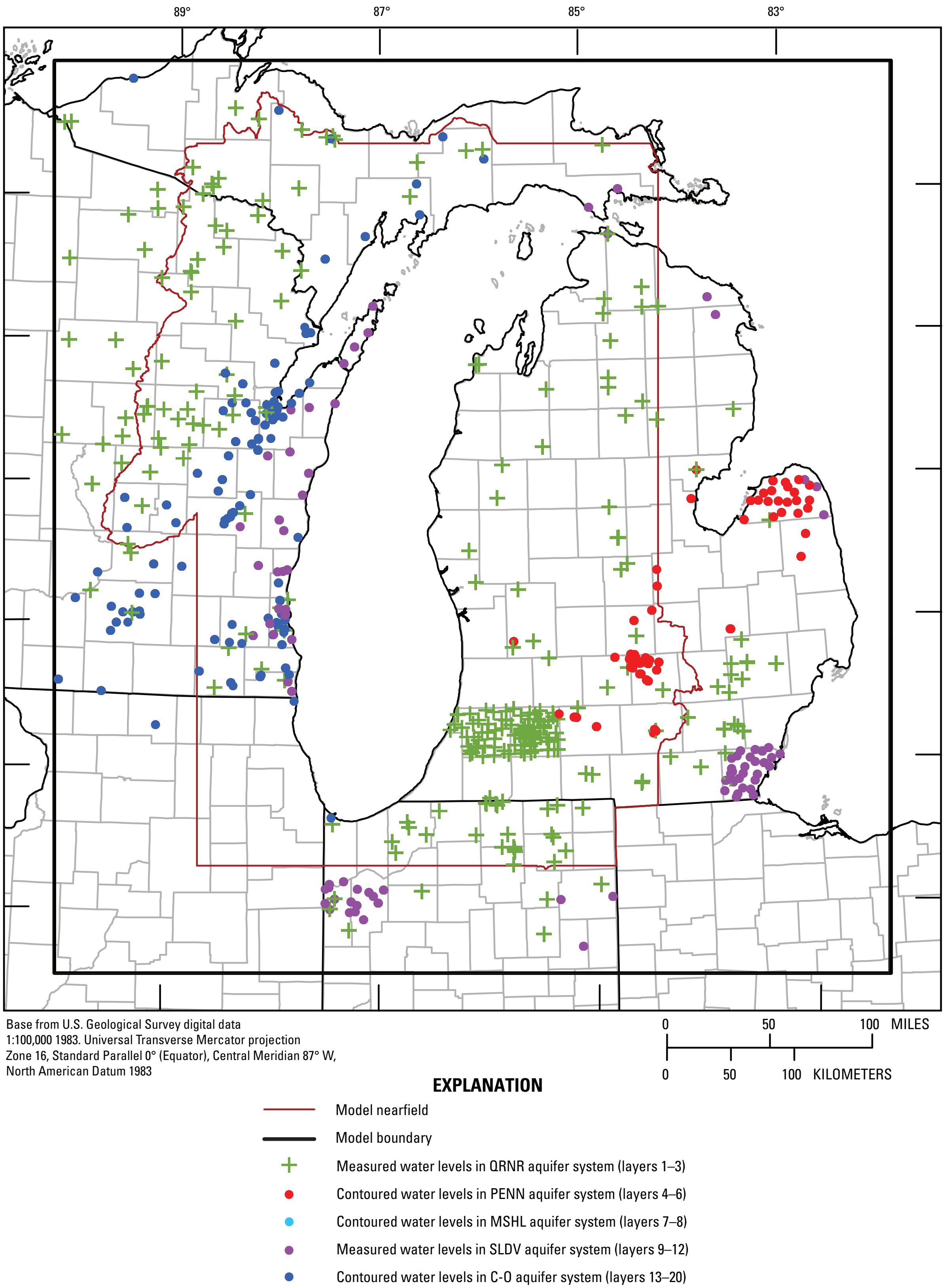

Figure 45*B*. Spatial distribution of calibration targets: USGS network wells, providing postdevelopment water-level targets (Source: U.S. Geological Survey, National Water Information System, *http://waterdata.usgs.gov/nwis*).

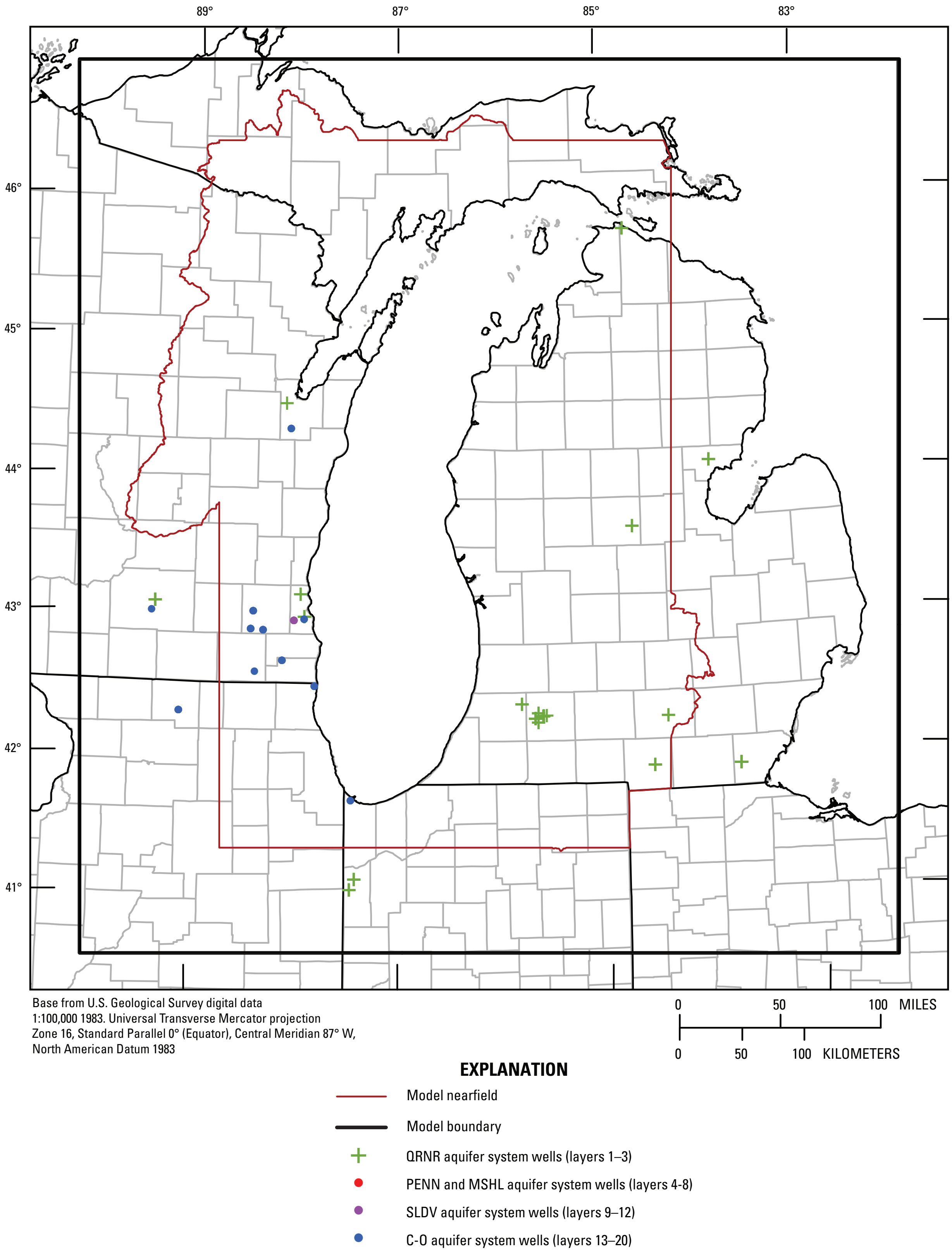

Figure 45*C*. Spatial distribution of calibration targets: USGS network wells as well as RASA packer tests from the early 1980s, providing vertical-head-difference calibration targets (Sources: U.S. Geological Survey, National Water Information System, *http://waterdata.usgs.gov/nwis*; Young, 1992; Nicholas and others, 1987).

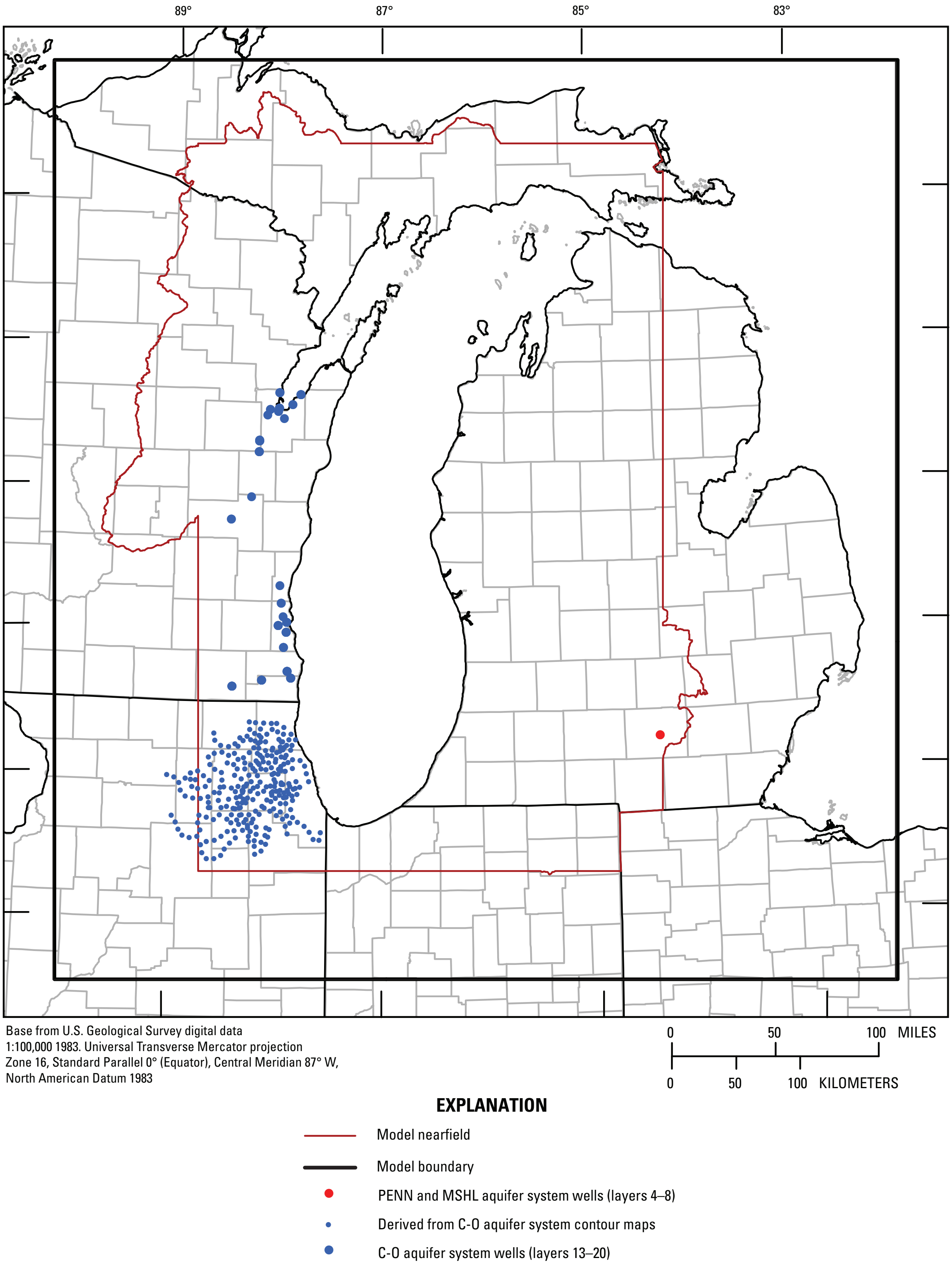

Figure 45*D*. Spatial distribution of calibration targets: Multiple readings from USGS network wells supplemented by targets based on differences between contour maps over time, providing head change (drawdown and drawup) targets (Sources: U.S. Geological Survey, National Water Information System, *http://waterdata.usgs.gov/nwis*; Visocky and others, 1985; Burch, 2002).

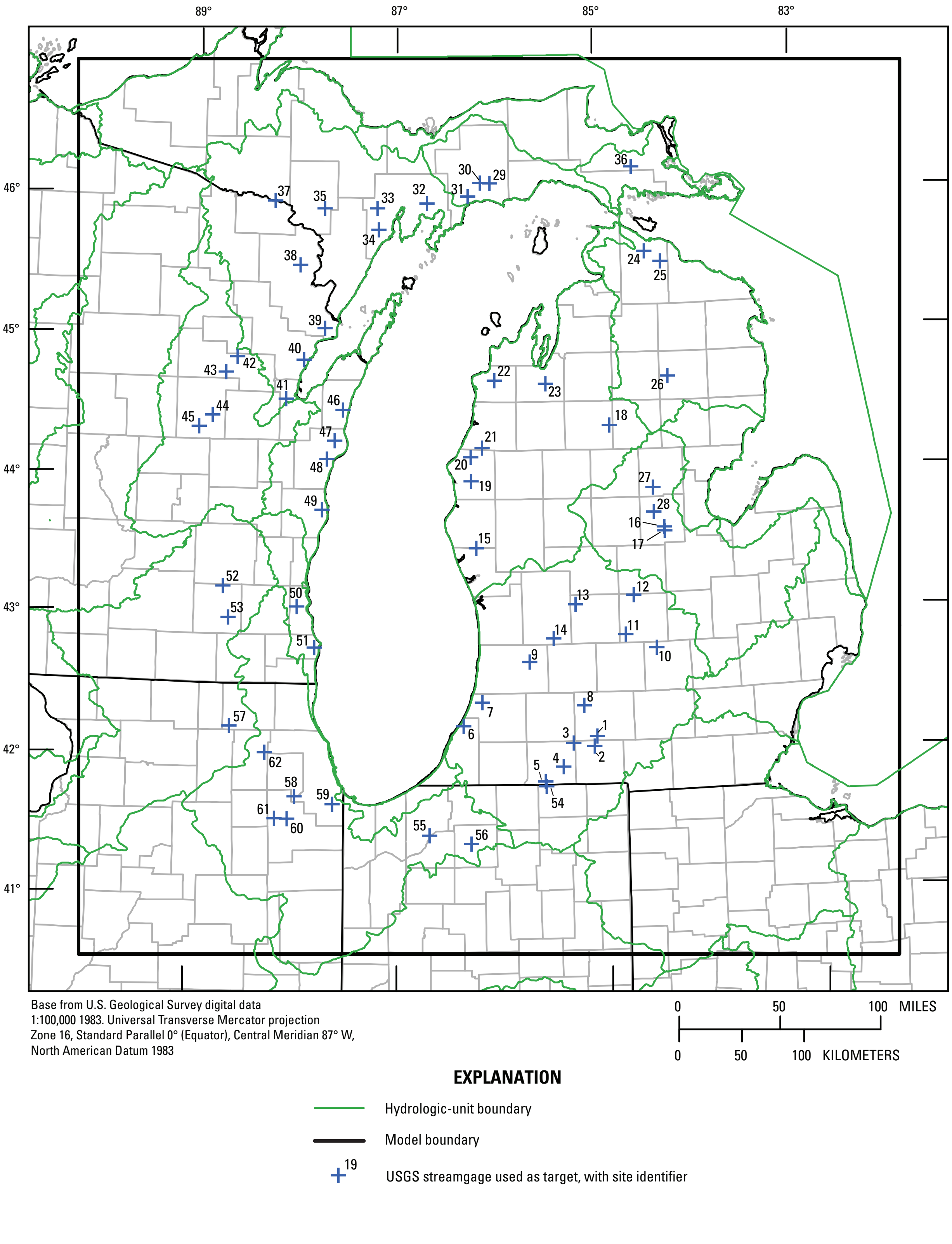

Figure 45*E*. Spatial distribution of calibration targets: USGS streamgages, providing base-flow calibration targets (Source: U.S. Geological Survey, National Water Information System, *http://waterdata.usgs.gov/nwis*).

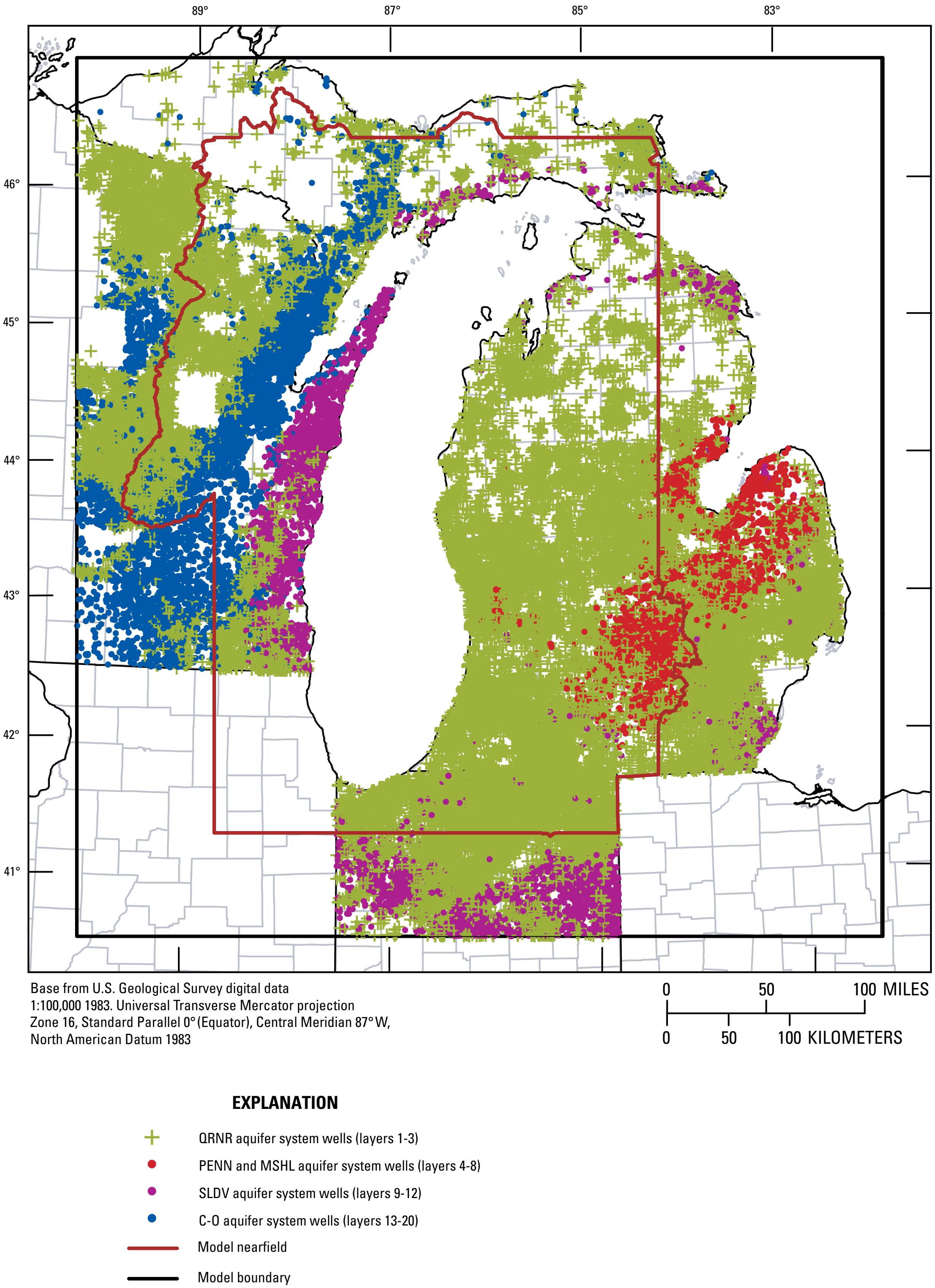

Figure 45*F*. Spatial distribution of calibration targets: household wells, providing postdevelopment water-level targets (Arihood, 2009).

The summary statistics for the 62 streamgage locations suggest that base-flow discharges estimated with the Gebert method are similar to those estimated with other methods. It is also informative to compare base-flow discharges to streamflow exeedances to obtain an idea of what fraction of the annual average streamflow is attributable to base flow. The base-flow discharges are typically less than Q_{50} and greater than Q_{75}, implying that on average the base flow is between streamflow discharges that are exceeded one-quarter and one-half of the time on an annual basis. The relation of base flow to streamflow exceedances varies by subregion and is influenced by the texture of unconsolidated deposits in different parts of the model. For example, in the Northern Lower Peninsula of Michigan (NLP_MI) where material is predominantly sandy, the base-flow discharge is generally close to the Q_{50} discharge rate, whereas in Northeastern Illinois (NE_ILL) where the material is generally fine grained, it is generally substantially less than the Q_{50} rate. In areas underlain by outwash, it is likely that recharge rates are high, yielding high discharges for base flow; in areas underlain by clayey till, recharge is less because more precipitation is diverted through overland runoff, resulting in less base flow.

The 62 base-flow targets provide information for many areas of the model nearfield and are distributed fairly evenly across subregions. (See colored stream and water bodies in figs. 28*A* and *B*). The entire surface-water network captured by nodes upgradient from a streamgage is assumed to contribute to the estimated base flow. However, surface-water network may not always be completely integrated and routed to the streamgage. For example, isolated wetlands can lose groundwater discharge to evapotranspiration rather than transport to an outlet stream. Consequently, the targets used in model calibration may overestimate base flow, and the parameter estimation may reduce the multiplier on recharge to compensate. As discussed in the section 8 (“Model Limitations”), this artifact is only one of several probably small and possibly offsetting interferences that affect the estimation of recharge.

Estimates of direct discharge of groundwater to Lake Michigan were not included in model calibration given their uncertainty. Direct discharge has been estimated from several field studies and models that have reported a wide and uncertain range of results (for example, see Grannemann and Weaver, 1998). Neff and Nicholas (2005) estimate that the whole-lake direct-discharge estimates for the Great Lakes range between 0.5 and 2.0 ft^3/s per mile of shoreline. The results of the calibrated model are qualitatively compared to this target range in section 6 (“Model Results”) and section 7 (“Alternative Models and Model Sensitivity”).

5.3.2 Target Filtering

Two calibration issues arise from the abundance of surface-water features in the Lake Michigan Basin and the relatively coarse discretization used to define the model grid. First, many shallow water-level targets correspond to RIV cells and, therefore, are too constrained by the influence of the head-dependent boundary to be useful for calibration; consequently, they are summarily filtered or removed from the targets used for parameter estimation and do *not* appear in table 11*A* or figure 45. Second, these surface-water features can act as model boundaries, thus limiting the model’s ability to accurately simulate the transient response of the water table to pumping from shallow wells. In parts of the model domain (notably Michigan and Indiana), almost all the pumping is from the Quaternary (QRNR) aquifer or shallow unconfined bedrock aquifers (see table 9*B*). Because the model cannot simulate the groundwater/surface-water interaction with a meaningful resolution, it returns a poor match to observed drawdown produced by shallow pumping in these areas. Moreover, inclusion of these shallow drawdown targets in the calibration process obfuscates information available from targets that can be properly simulated given the model resolution (for example, drawdown targets in the confined bedrock aquifers), thereby undermining parameter estimation. For this reason, all the shallow drawdown targets also were removed from the target list and do *not* appear in table 11*A* or figure 45. Finally, water-level targets derived from contour maps are omitted in areas where the contours cross saline water. This filtering affects some targets derived from predevelopment contours in the Marshall Aquifer (MSHL) unit and, to a lesser extent, predevelopment and postdevelopment contours in the Cambrian-Ordovician (C-O) aquifer system in northeastern Illinois. Targets are restricted to freshwater areas because extremely few measurements of water levels in the Michigan Basin have been collected in brackish water (defined here as those with concentrations between 10,000 mg/L and 100,000 mg/L) or brines (defined here as those with concentrations greater than 100,000 mg/L).

5.3.3 Target Weights and Bounds

The parameter-estimation program PEST uses algorithms to modify parameter values so as to minimize the objective function; that is, the sum of squares of the weighted target residuals.[23] The modeler-assigned target weights are a primary mechanism for translating the modeler’s relative ranking of target fit used to assess calibration quality; consequently, the weights are important for guiding the search for optimal parameters. For this study, target weights were selected to balance the contribution to the objective function among the different target types so that information contained in targets can influence the inversion regardless of the small number of targets contained in that target type.

The weights for each target carry units that, when multiplied by the residuals, yield dimensionless weighted residuals. In the calibration process the targets and residuals corresponding to water levels, change in water levels, vertical difference between water levels, or water levels derived from contour maps carry units of *feet*; therefore, their weight units are ft^{-1}.

[23] The target residual is equal to the measured value minus the simulated value at the target location for the appropriate model time step.

The targets corresponding to base-flow estimates in the calibration process carry units of *cubic feet per day* (ft^3-day^{-1}); therefore, their weight units are day-ft^{-3}. Water-level measurements obtained largely from the USGS monitoring-well networks are plentiful, and many targets are available. However, the value of individual measurements to improving model fit is highly variable because the model results are insensitive to some observations. In this study, the most value belongs to the relatively small number of measurements that allow for matching predevelopment conditions, for determining aquifer responses to pumping, and for properly simulating vertical gradients. These select head targets, in addition to base-flow targets (that break the correlation between hydraulic conductivity and recharge), were deemed important for constraining the parameter estimation. By adjusting an observations' weight, it is possible to avoid having the inversion routine "chase noise" (obtain slightly better fits at unimportant targets at the expense of fitting important targets). The final roster of weights for the confined version of the LMB model (column 3 in table 11*A*) ensures that all the target types ultimately contribute at least 4 percent to the objective function that drives the parameter-estimation process (column 6 in table 11*A*).

Another important modeler-specified constraint on the PEST parameter estimation is the presence of upper and lower parameter bounds that limit the range of potential values. The range used in this study was informed in part by the coarse grid spacing (5,000 ft on a side in the model nearfield) necessitated by the extent of the regional model. As discussed in section 3 (and also section 8, which is devoted to model limitations), the large cells require a compromise between a version of the model that incorporates the entire surface-water network, including first-order streams, and largely fixes the water table prior to simulation and, alternatively, a version that inserts only major surface-water features and is liable to distort the value of model input in order to control excessive water-table mounding. Because some groundwater-discharge features are absent in the compromise configuration, the inversion routines tend to raise the shallow horizontal hydraulic conductivity of the unconsolidated and shallow bedrock units higher than evidence indicates in order to match the degree of observed water-table mounding in between surface-water bodies. By bounding the maximum value of K_h for these parameters at levels only somewhat higher than initial values, one can generate reasonable values for these inputs while achieving most of the reduction in the objective function potentially obtainable given the model discretization. The parameters affected by this strategy include the multipliers for the K_h of the six glacial categories and also some multipliers assigned K_h zones of the Silurian-Devonian (SLDV) bedrock unit, which subcrops west of Lake Michigan. For these parameters, the upper bounds lead to final values that are less than 10 times the initial values (lower bounds are less than 0.1 times the initial value). For all other parameters in the adjusted confined model calibration, the upper and lower bounds are set to 10 times and 0.1 times, respectively. Appendix 5, table A5–2, tabulates the bounds for each of the 160 parameters estimated for the confined model calibration.

5.4 Regularized Inversion Techniques

Unique calibration of the large and complex LMB model is tractable only if the parameter estimation process operates on an input structure that simplifies the complexity of the natural world. As explained previously, the simplification involves grouping input variables into a restricted number of multiplying parameters applied to zones of cells. The zones group either areas with cell-by-cell variation or areas with block variation. Zonation of inputs is a common simple form of "regularization" applied during model construction and calibration (Hunt and others, 2007). However, there are other forms of regularization that can facilitate the inversion process. These other forms can be particularly important when, as in this study, the combined number of parameters (even after zonation) cannot be uniquely estimated. Moreover, for a complex model it can be important to use inversion methods that minimize the number of times the Jacobian matrix—consisting of derivatives for each calibration target relative to each estimated parameter—is recalculated in the effort to identify the objective function minimum.

The LMB model calibration is notable for its use of the sophisticated regularized inversion tools available in the parameter-estimation computer code PEST (Doherty, 2008a; Doherty and Hunt, in press). Specifically, the calibration approach used here differs from traditional nonlinear regression parameter estimation in its use of (1) pilot points (Doherty, 2003; Doherty and others, in press), in addition to a traditional parameter zone approach in one area of the model; (2) Tikhonov regularization (Tikhonov, 1963a, 1963b; Doherty, 2003; Fienen and others, 2009); and (3) hybrid singular value decomposition (Tonkin and Doherty, 2005; Hunt and others, 2007; Doherty and Hunt, in press), also referred to as SVD-Assist (SVDA) by Doherty (2008a). Application of these advanced tools not only enhanced the calibration of the complex LMB model but also helped demonstrate the utility of innovative methods, a goal of the broader pilot-study design.

5.4.1 Pilot Points

During calibration, it became apparent that one important area of the regional model—the SE_WI and NE_ILL pumping centers—was parameterized by using zones that were too large to accurately simulate local water levels and vertical gradients. The leakage of water from the shallow flow system to underlying confined aquifers of the deep pumping centers is controlled in large measure by the resistance posed by the Maquoketa confining unit. Thus, rather than employ large blocks of homogeneous values to characterize the hydraulic conductivity of the bedrock, as done elsewhere in the model domain, the vertical hydraulic conductivity of the Maquoketa confining unit in this part of the model is simulated by means of pilot points as a way to constrain cell-by-cell variation of the K_v value within this area of the model domain. Kriging (a geostatistical algorithm) is used to interpolate values estimated at the 78 pilot-point locations (fig. 46) to the other cells in the unit. The pilot points are used to characterize conditions in two zones, one representing a subcrop area where the Maquoketa is subject to enhanced weathering, and a second to the east where the unit is overlain by SLDV. The method is "regularized" by using a preferred homogeneity condition, by which one attempts to minimize variation between values at pilot points within each zone by penalizing deviations from "smoothness." Regularization and interpolation between pilot points are limited to cells within their respective zones, and this restriction conforms to the geologic conceptualization of the two zones. This approach facilitates geologic continuity where it is believed to exist but still allows heterogeneity to be expressed within zones as informed by the observations of water-level, vertical gradient, and head-change targets. In sum, the pilot point approach allows the use of "soft" knowledge (based on geologic zonation) that it is not "hardwired" to one fixed parameter value over the entire zone as in a traditional calibration approach. The ability of observed data to inform the parameterization is enhanced by an appreciable number of representative targets that pertain to the parameter used for a pilot-point representation. Thus, in this study, pilot points and related regularization were restricted to evaluating the Maquoketa K_v in two subregions where vertical head and gradient targets are plentiful and where the calibration proves highly sensitive to its values. (See discussion of model fit below.)

5.4.2 Tikhonov Regularization

A groundwater-flow model with many parameters is commonly affected by parameter insensitivity and correlation, which in turn lead to solution non-uniqueness and an ill-posed inverse problem. Two forms of Tikhonov regularization were used to counter these problems in the LMB model: preferred value and preferred homogeneity (Tikhonov 1963a, b). Preferred value regularization was applied to non-pilot-point parameters such as the hydraulic conductivity in zones, anisotropy, storage, and river-conductance parameters. The preferred values were set at the initial parameter values that resulted from previous modeling in the basin (for example, Krohelski, 1986; Mandle and Kontis, 1992; Young, 1992; Arihood and Basch, 1994; Conlon, 1998; Eberts and George, 2000; Krohelski and others, 2000; Reeves and others, 2004; Luukkonen and others, 2004; Feinstein, Eaton, and others, 2005; Meyer and others, 2009). As discussed above, preferred homogeneity regularization was specified for the pilot points within each weathering zone; thus, homogeneity was preferred within a weathering zone, but the preferred condition was not expressed across zones. Finally, the compromise between model fit and the preferred conditions was initially weighted in favor of model fit and later weighted to favor the preferred condition (PEST variable PHIMLIM— Doherty 2003; 2008a; and Fienen and others, 2009).

5.4.3 Singular Value Decomposition

In addition to the Tikhonov regularization, subspace methods were also employed through hybrid singular value decomposition (SVD) (see Tonkin and Doherty, 2005). SVD uses the Jacobian matrix to divide the full parameter space (as defined by all the original or "base" parameters) into linear combinations of base parameters (hereafter referred to as "superparameters") from those parameters that cannot be estimated by using the available targets due to parameter insensitivity or correlation; only the former are included in the parameter-estimation process. As discussed in Doherty and Hunt (in press), SVD can be relentless in pursuit of a best fit even at the expense of realism, which can result in unreasonable and extreme parameter values considered optimal because of small improvements in fit. Tikhonov regularization and specification of parameter bounds were used to balance model fit with parameter reasonableness.

In this pilot application, the Jacobian matrix (containing the 238 original, or "base," parameters for the confined model: 160 zone multipliers plus 78 pilot points) was reconfigured to define 40 superparameters used for model calibration. The estimation of 40 superparameters was found to be a stable process over the range of values evaluated during the parameter estimation (as indicated by a matrix condition number less than 1 E6 for all parameter-estimation iterations; see Doherty and Hunt, in press, for more information). The parameter-estimation problem was run on an 80-processor modeling array by using Parallel PEST (Doherty 2008a), facilitating runtime reductions of two orders of magnitude in the parameter-estimation operation.

5.4.4 Integrity of Derivatives

Beyond its use of sophisticated regularized inversion tools for parameter estimation, the LMB pilot application is also notable for its employment of new tools for assessing the quality of the model for nonlinear-regression parameter-estimation techniques. As described previously, nonlinear regression is based on the expectation that the derivative of the change in parameter value to the change in observation is a smooth function. However, the number of significant figures carried through the computations, the tightness of solver solution-convergence criteria, solution thresholds such as those involving dry nodes, and nonlinearities such as those generated by fluctuations in saturated thickness can degrade the smoothness of this function by introducing granularity in the derivatives. Granularity can be expressed as jumps, thresholds, and other irregularities in the derivative, often manifesting itself as a seemingly random variation of the observed quantity to regular changes in the parameter value. Regardless of the form, granularity decreases the signal-to-noise ratio of the target-to-parameter sensitivity information contained in the Jacobian matrix; if sufficiently degraded, the Jacobian matrix can become so noisy that the quality of the parameter upgrade calculated from that Jacobian matrix could be compromised.

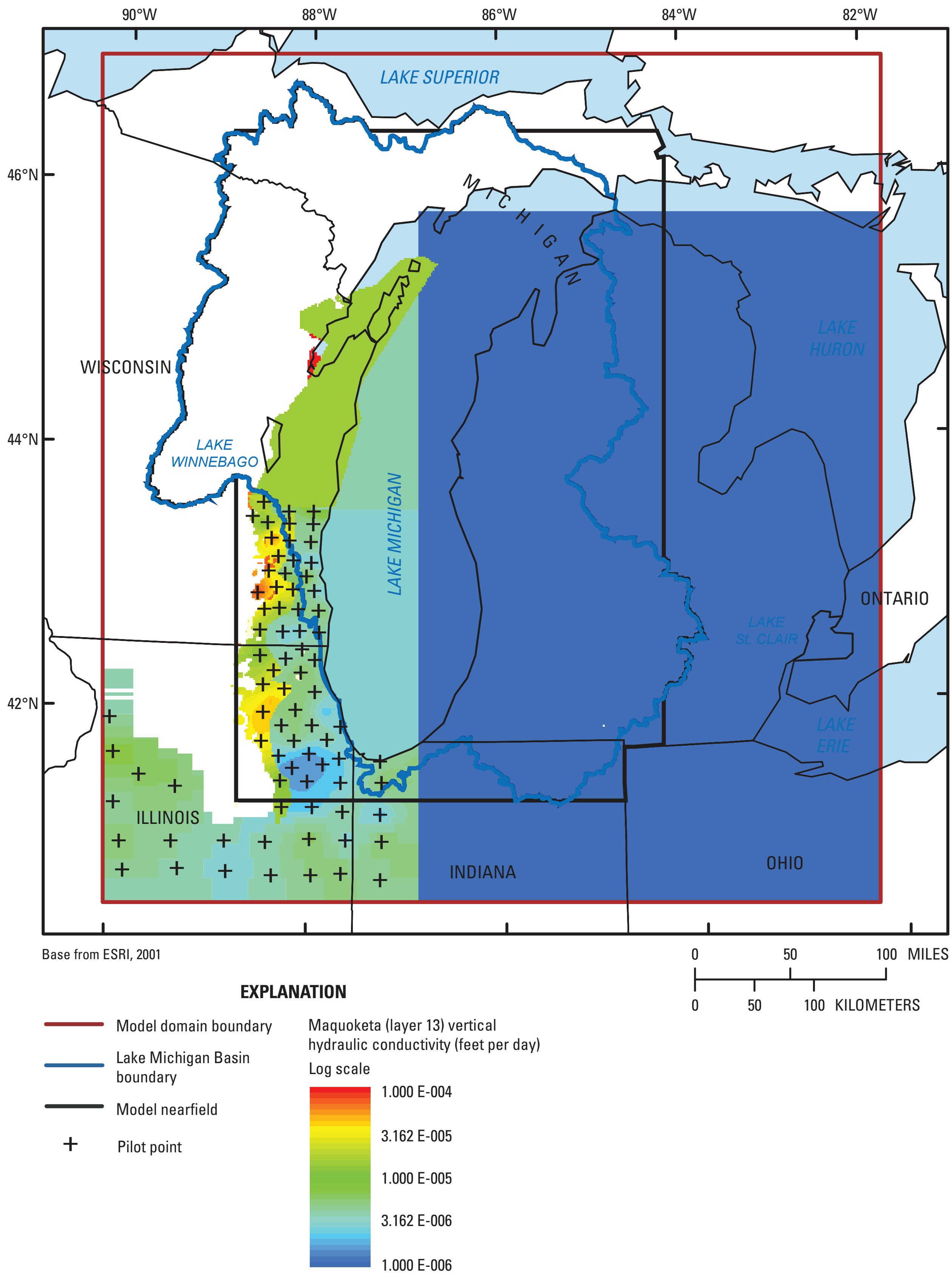

Figure 46. Pilot point locations and calibration results for vertical hydraulic conductivity of the Maquoketa confining unit.

As discussed previously in this report and also by Feinstein and others (2008), the unconfined SEAWAT model exhibited appreciable granularity, so most parameter estimation was done on the confined case where the granularity was reduced.[24]

5.5 Calibration Results

In the following subsections, the results of the calibration process are evaluated in terms of (1) improvements in the model fit between the measured and simulated targets and (2) plausibility of parameter values estimated from the calibration process.

5.5.1 Model Fit

The initial model input for the confined version of the LMB model yielded a value for the sum of squares of weighted residuals—the objective function measuring overall model error—equal to 9.43 E5. After five iterations of nonlinear regression, the model error was approximately halved, to a value of 4.68 E5. Additional iterations result in very small reduction of the model error at the expense of having more parameter estimates approach unreasonable and extreme values. The final calibrated confined version of the LMB model was chosen before the extreme values dominated, and it is called SLMB-C (SEAWAT-LMB-confined). Table 11*A* records the contribution of each target type and the total objective function for SLMB-C. Table 12 lists summary calibration statistics across head target subsets for SLMB-C.[25] The first statistic, mean error (*ME*) is a measure of bias; that is, the tendency of the simulated targets values to be less than measured values (positive *ME*) or greater than measured values (negative *ME*). It is computed as the average of the weighted residuals in a target subset. The second statistic, mean absolute error (*MAE*), is computed as the average of the *absolute values* of the weighted residuals in a target subset and is always positive. For the targets related to water levels or differences in water levels, the *ME* across target subsets for SLMB-C ranges from about −21 to +16 ft; the *MAE* ranges from about 1 to 50 ft.

Two different calibration statistics are computed for the base-flow targets to account for the different scale of units associated with these observations (typically 1 E7 ft^3/d). The *ME* is computed as the average ratio of the measured to simulated target flows, and the *MAE* is the average of the absolute value of the flow ratios. The *ME* (1.07) indicates that the simulated flux is, on average, 7 percent smaller than the estimated base-flow targets, and the *MAE* (1.25) indicates an average error of about 25 percent.

The model fit for each target subset in the confined SLMB-C model is displayed visually in appendix 8 by means of scatterplots that show model error and the degree of bias about the 1:1 line. Most plots show close agreement over the entire range of targets in the subset; but a few (for example, the plot for predevelopment water levels in the Marshall unit (MSHL)) show some bias and large residuals over part of the range, indicating that the model could be improved in those areas with a different conceptualization. Plots for the target subsets involving drawdown, recovery, and vertical gradient targets indicate the SLMB-C model reasonably reproduces the formation of cones of depression around deep pumping centers, as well as the recovery of water levels in deep aquifers in the northeastern Illinois area after communities there shifted to a Lake Michigan water source. Vertical gradients measured in packer tests and between nested USGS network wells also are well reproduced. The base-flow residuals are plotted on a log scale and show that, in general, the model preserves the relative rank of observed fluxes estimated at streamgages. Finally, the qualitative comparison between the water levels observed in household wells and the water levels simulated at those locations shows reasonable agreement over the entire range of values, indicative of a consistently close average match across model subregions.

In order to gain additional insight into the quality of the calibration of the SLMB-C model, a subset of the calibration targets was selected for additional analysis. The subset incorporated all water-level measurements, both predvelopment and postdevelopment, that contributed to the calibration process—a total of 8,350 targets. The *ME* for the subset was −1.97 ft and the *MAE*, 25.21 ft. An additional statistic, equal to the square root of the average of the squared residuals of the targets and called the root mean squared error (Anderson and Woessner, 1992), is more sensitive to outlier values than is the *MAE*. For the ensemble of measured head targets (unweighted), the root mean squared error was 36.78 ft. This statistic is often compared to the range of measurements as a general way of indicating agreement between measured and simulated values. The smaller the ratio, the better the overall model fit. For the SLMB-C model, measured water-level altitudes vary between 195 and 1,650.7 ft, yielding a ratio of 0.025. This value is well below the 0.100 threshold for the ratio commonly posited to indicate a good fit (Spitz and Moreno, 1996).

[24] In cases where granularity cannot be addressed within the model itself, global search methods within PEST such as shuffle-complex evolution (Duan and others 1992; 1993) or covariance matrix adaptation evolution scheme methods (Hansen and Ostermeier, 2001; Hansen and others, 2003) can be used in place of nonlinear regression methods. However, these nonregression methods were not needed in the LMB model application.

[25] The comparison in table 12 between the results for SLMB-C and those for the unconfined calibratred model, SLMB-U, are discussed in section 7.

Table 12. Confined and unconfined model calibration statistics for weighted targets and for driller-log targets.

[Arrows indicate which version of the model performed better in terms of calibration statistics. Double arrow indicates large discrepancy]

Target subset	Confined model (SLMB_C)			Unconfined model (SLMB_U)		
	Mean error	Mean absolute error		Mean error	Mean absolute error	
Predevelopment USGS network water levels (pre-1940)	−5.36	14.94	<==	−5.89	15.13	
Predevelopment driller-log water levels (pre-1940)	.01	14.09	<==	−.78	14.60	
Predevelopment Wisconsin Cambrian-Ordovician head contours	−19.97	41.26	<==	−20.03	41.49	
Predevelopment Michigan Pennsylvanian head contours	−8.56	49.91	<==	−9.41	50.64	
Predevelopment Michigan Marshall head contours	9.07	44.52		7.92	43.92	<==
Predevelopment Indiana miscellaneous water levels (pre-1940)	−11.24	22.99	<==	−13.11	23.80	
Predevelopment Illinois Cambrian-Ordovician head contours	4.63	31.07		5.79	29.96	<==
2000 Illinois Cambrian-Ordovician head contours	−3.27	29.98	<== <==	−17.69	34.84	
1864–2000 Illinois Cambrain-Ordovician drawdown contours	14.82	41.66	<== <==	30.00	47.40	
Base flow	1.07	1.25		1.05	1.24	<==
Vertical head difference—USGS network	9.74	11.03	<== <==	6.91	14.96	
Vertical head difference—USGS RASA packer tests	−1.64	7.80	<==	3.34	8.95	
Southern Lower Peninsula, Mich., network water levels (post-1940)	−13.74	20.83	<==	−14.74	21.40	
Northern Lower Peninsula, Mich., network water levels (post-1940)	−21.46	37.71	<== <==	−28.23	41.20	
Upper Peninsula, Mich., network water levels (post-1940)	3.91	11.20		2.54	11.09	<==
Northeast Wisconsin network water levels (post-1940)	−1.79	31.49	<==	−.18	31.56	
Southeast Wisconsin network water levels (post-1940)	−12.81	35.60		−12.09	34.66	<==
Northern Indiana network water levels (post-1940)	−8.84	15.02	<==	−9.70	15.33	
Farfield network water levels (post-1940)	11.37	22.48	<==	11.73	22.60	
Decadal head changes in USGS network wells	−14.60	25.67		−12.39	22.40	<== <==
1980–2000 recovery in Illinois Cambrian-Ordovician head contours	15.57	37.32	<== <==	−28.07	44.25	
Water levels from nearfield driller logs for all time periods*	11.30	19.81		10.13	19.09	<==

* The post-1940 driller logs were assigned zero weight in the parameter inversion.

5.5.2 Estimated Parameter Values

Parameter estimation of the SLMB-C model (1) resulted in some optimal parameter values very close to their initial values (signified by a multiplier close to 1.0), (2) changed most inputs by a moderate amount, and (3) drove a few parameters to the bounds set as user-specified constraint. Appendix 5, table A5–2, tabulates the parameter multiplier for each estimated parameter. Multipliers less than 0.5 and greater than 2.0 are annotated, as are multipliers that are equal to an upper or lower bound. The following calibration results for the confined SLMB-C model are notable:

- The recharge multiplier was constrained when using the most complete dataset—that constructed from measurements from recent conditions corresponding to year 2000; thus, the optimal multiplier of 1.048 is derived from conditions in the final model stress periods (1991 to 2005). This same multiplier is then applied to every cell in the model and to every time step. Thus, the relative distribution of recharge through time and space is unchanged, but all values are increased by about 5 percent relative to the initial recharge arrays generated by the soil-water-balance (SWB) model and shown in figures 30 and 31.
- Storage parameter multipliers (ranging from 0.697 to 1.69) and RIV conductance multipliers (ranging from 0.96 to 1.52) deviate modestly from 1, indicative of relatively small changes to initial storage and conductance inputs compared to changes in hydraulic conductivity discussed below.
- The pilot point cell-by-cell variation in the K_v assigned the Maquoketa (MAQU) confining unit in the SE_WI and NE_ILL subregions (fig. 46) was characterized by overall values consistent with the geologic conceptualization. In the weathered zone at the western fringe, the geometric mean of the updated cell K_v values is 2.61 E−5 ft/d. To the east, where the MAQU does not subcrop and is not weathered to the same degree, the geometric mean of values is lower (6.30 E−6 ft/d). Although the average change from initial values (2.0 E−5 ft/d and 5.85 E−6 ft/d, respectively) is small, the cell-by-cell variation in this parameter is important in reducing the magnitude of the objective function and improving calibration. In particular, the focused use of pilot points allowed a much improved fit to the high-quality targets associated with the RASA packer-test water-level data and, thereby, allowed the model to simulate more closely the gradients controlling vertical leakage within the deep part of the flow system in the SE_WI, NE_ILL and N_IND subregions.
- The following multiplier parameters hit the upper bounds imposed as constraints on the parameter estimation: K_h for clayey till (5.0), K_h for loamy till (2.70), K_h for sandy till (1.73), and K_h for the Silurian-Devonian unit (SLDV) in zone 2 of layer 10 (2.0). In each case, it is likely that horizontal hydraulic conductivities above the bounds (and also above reasonable values for the deposits in question) would lower simulated water-table elevations and reduce the reported model error. This model error could also be reduced by decreasing the model grid spacing to enable better representation of the surface-water network, as discussed previously.
- The following multiplier parameters hit their lower bounds: K_h for the Prairie du Chien-Franconia unit (PCFR) in zones 2 and 6 of layer 16 (0.1) and K_h for the Mount Simon unit (MTSM) in zones 5 and 6 of layer 19 (0.1).
- Out of the 160 parameter multipliers estimated in the SLMB-C calibration, 24 are greater than 2.0 (maximum=6.9 for a K_h MTSM zone in layer 19) and 15 are less than 0.5 (minimum=0.10 for bedrock parameters that hit their lower bounds).

The spatial distribution of calibrated horizontal hydraulic conductivities given the optimal parameter multipliers are shown for layer 1 in figure 47 and for selected layers (upper, middle, and lower QRNR, PEN1, MSHL, upper SLDV, STPT, IRGA, and upper MTSM) in appendix 6*A*. Given the optimal multipliers, the spatial distribution of the calibrated vertical hydraulic conductivities are shown for selected layers (upper, middle, and lower QRNR, PEN2, MICH, DVMS, middle SLDV, MAQU, EACL) in appendix 6*B*. The initial values of hydraulic conductivity are compared to the optimized values in three ways:

1. Comparison of figure 39 to figure 47 shows that the calibration process yielded generally higher hydraulic conductivity values for the upper QRNR deposits in layer 1.

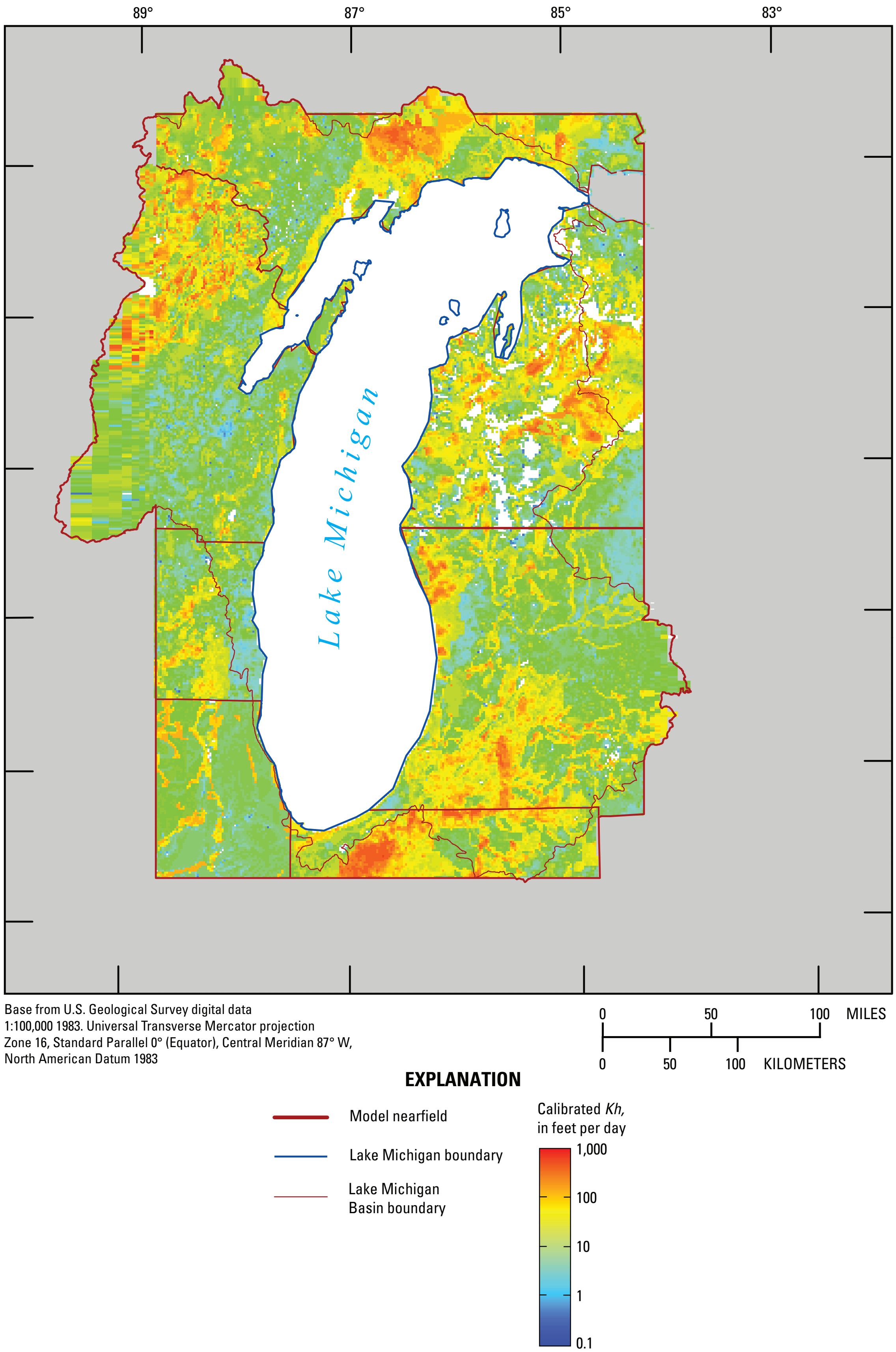

Figure 47. Calibrated horizontal hydraulic conductivity distribution in nearfield area of model layer 1.

2. In appendix 9, the average and geometric mean of thickness-weighted horizontal hydraulic conductivity for aquifer systems is compared for the initial and calibrated SLMB-C input. The calculation is restricted to the inland parts of the nearfield; that is, the seven model subregions.[26] Inspection of the results shows that the average and geometric mean values for the QRNR aquifer system uniformly increase across subregions as a result of calibration. The initial geometric mean values range between 2.5 and 21.0 ft/d by subregion, whereas the calibrated geometric mean values range between 8.0 and 34.1 ft/d. The biggest relative change occurs in NE_ILL; the large increase there can be attributed to the 5.0 calibration multiplier applied to its dominant glacial category, clayey till. The remaining bedrock aquifer systems show less dramatic and systematic changes from initial to calibrated average and geometric mean values. The calibrated K_h values are on average higher for the PENN and MSHL aquifer systems (between 4 and 14 ft/d by subregion) than for the SLDV and C-O aquifer systems (between 0.5 and 3.8 ft/d by subregion).

3. The spatial distributions of initial transmissivity by aquifer system (figs. 41*A*–*E*) can be compared to the distributions of calibrated transmissivity (figs. 48*A*–*E*, starting on p. 142). The higher calibrated *K* input values noted after calibration for the Quaternary (QRNR) sediments are reflected in higher calibrated transmissivities. Other aquifer systems show more muted changes between distributions of initial and calibrated values and generally maintain the pattern of low- and high-transmissivity areas initially imposed as a result of the geologic conceptualization. The calibrated transmissivities are generally highest for the QRNR aquifer system (fig. 48*A*); the bedrock systems, where present, all display bulk transmissivity values roughly similar in magnitude (figs. 48*B*–*E*).

4. The distribution of initial K_v in confining units (fig. 42) can be compared to the distribution of calibrated K_v (fig. 49). Both increases and decreases are evident in the sample cross section, with the biggest relative changes due to calibration occurring in the Salina Group within the SLDV (layer 11), the PCFR unit (layer 16), and the EACL unit (layer 18).

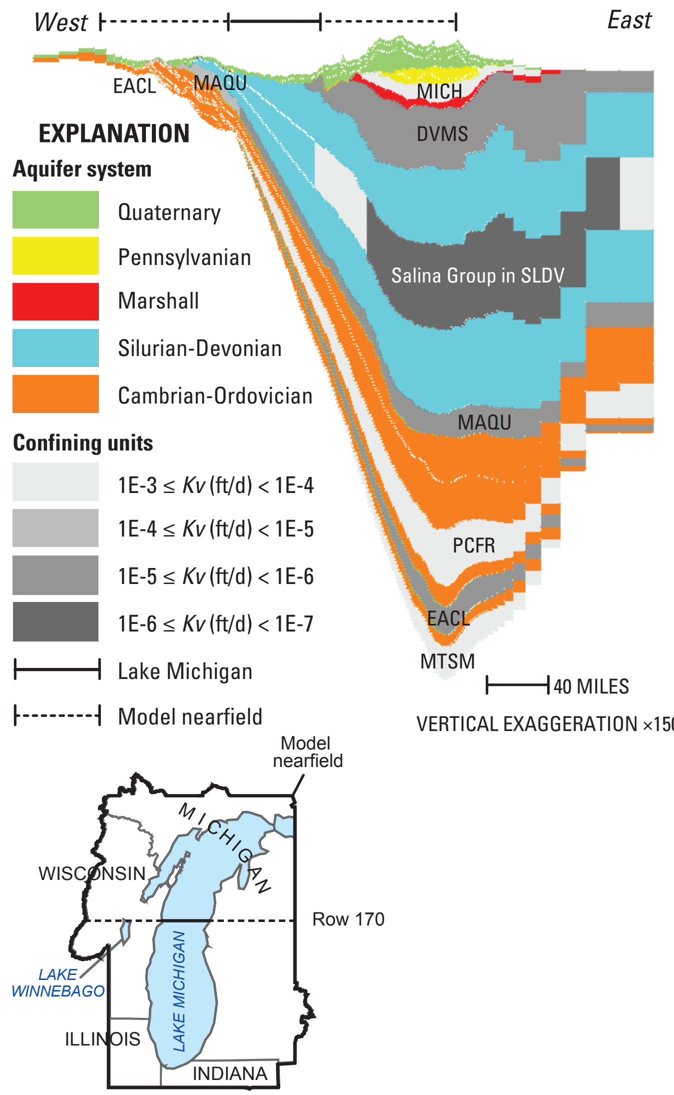

Figure 49. Calibrated vertical hydraulic conducitivity values for major confining units, row 170.

[26] For example, the average thickness-weighted K_h for the QRNR system is calculated by summing the weighted K_h assigned to each subregion cell for layers 1, 2, and 3, where weights are proportional to the thickness of the cell, and then dividing the total by the number of cells. The geometric-mean calculation sums the logs of the thickness-weighted values, divides the total by the number of cells, and then applies the antilog. The average and geometric mean calculations effectively weight the *K* values by the *saturated* thicknesses used in the confined version of the LMB model.

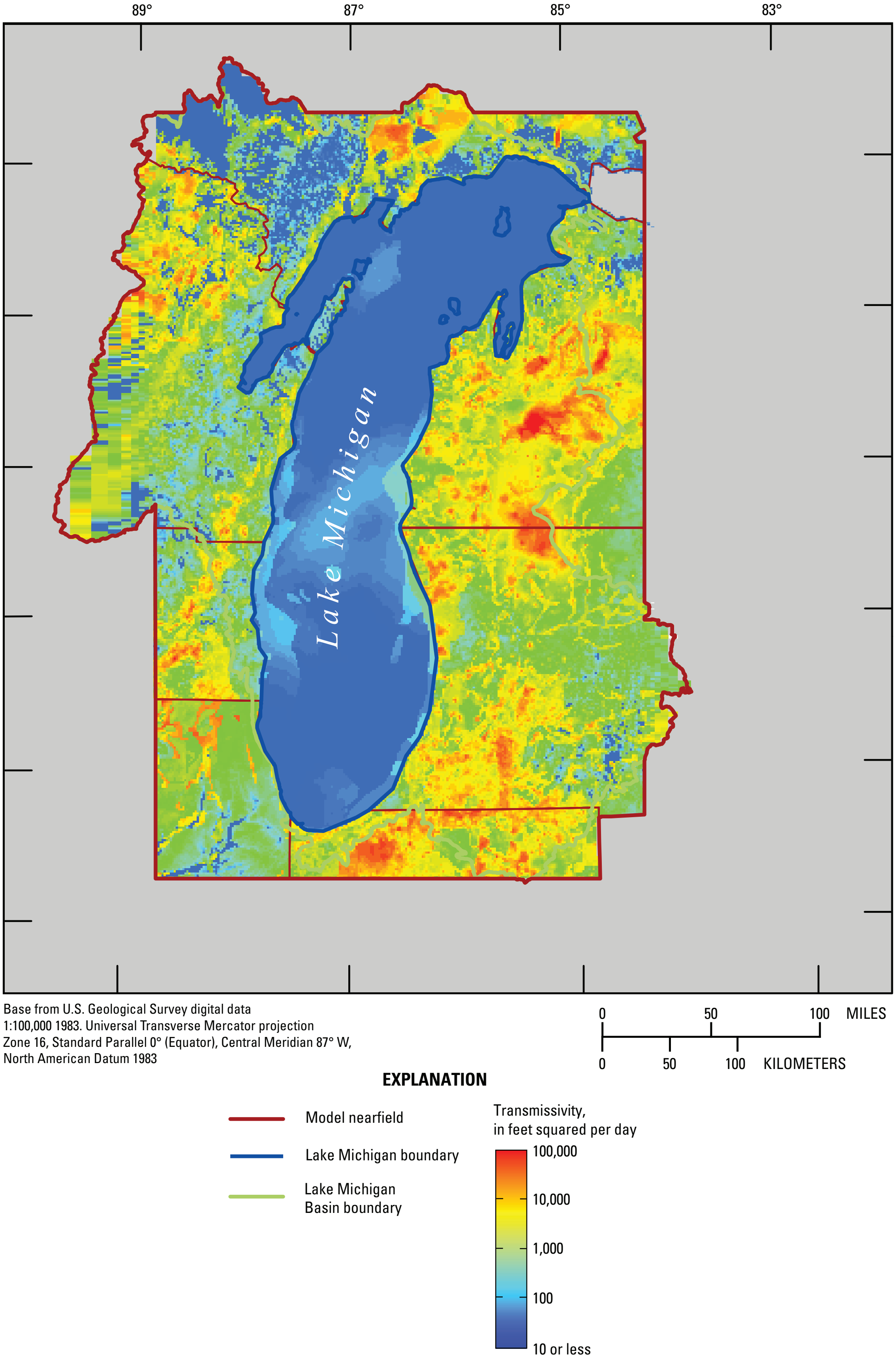

Figure 48*A*. Calibrated transmissivity distribution in aquifer system QRNR.

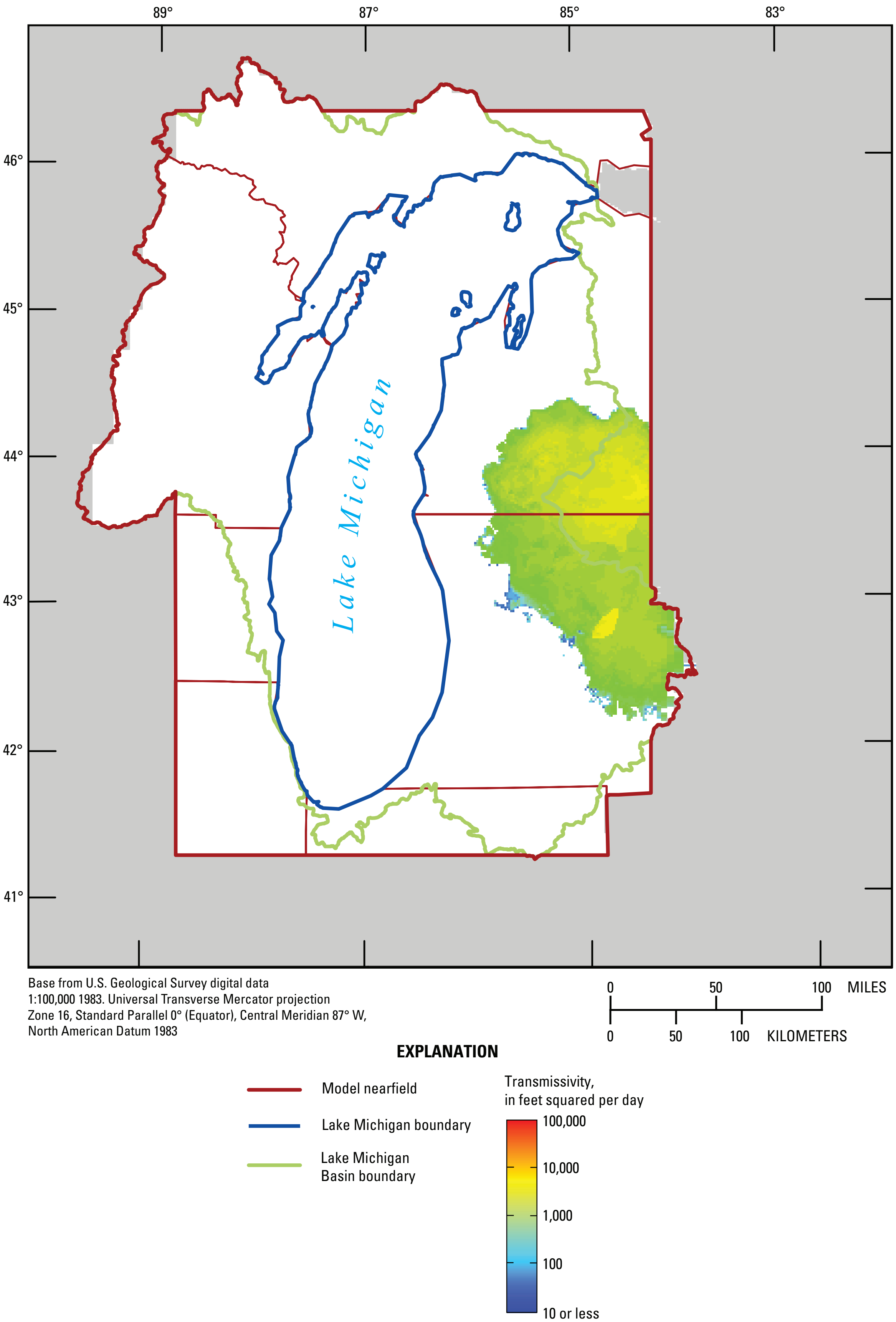

Figure 48*B*. Calibrated transmissivity distribution in aquifer system PENN.

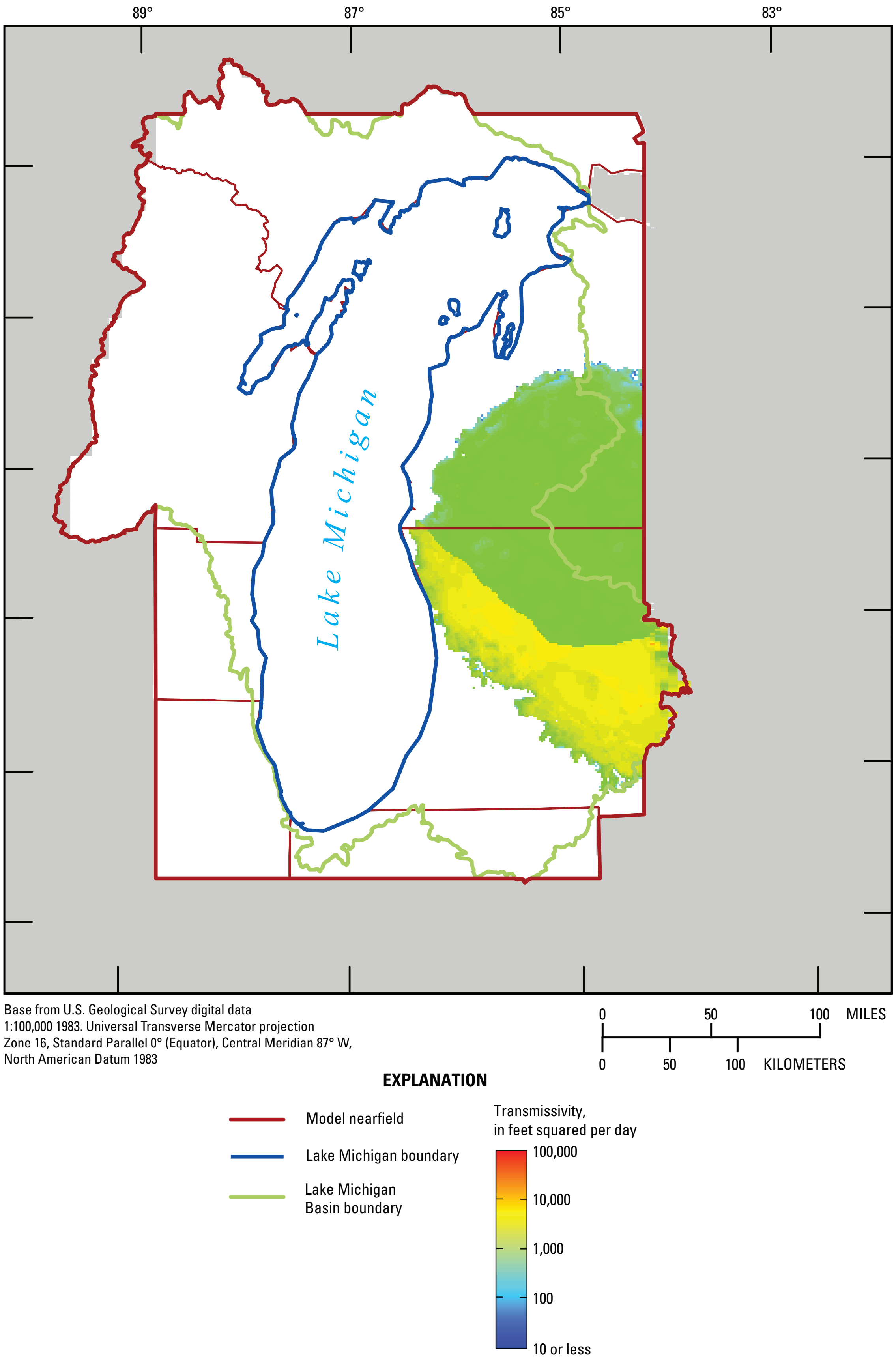

Figure 48*C*. Calibrated transmissivity distribution in aquifer system MSHL.

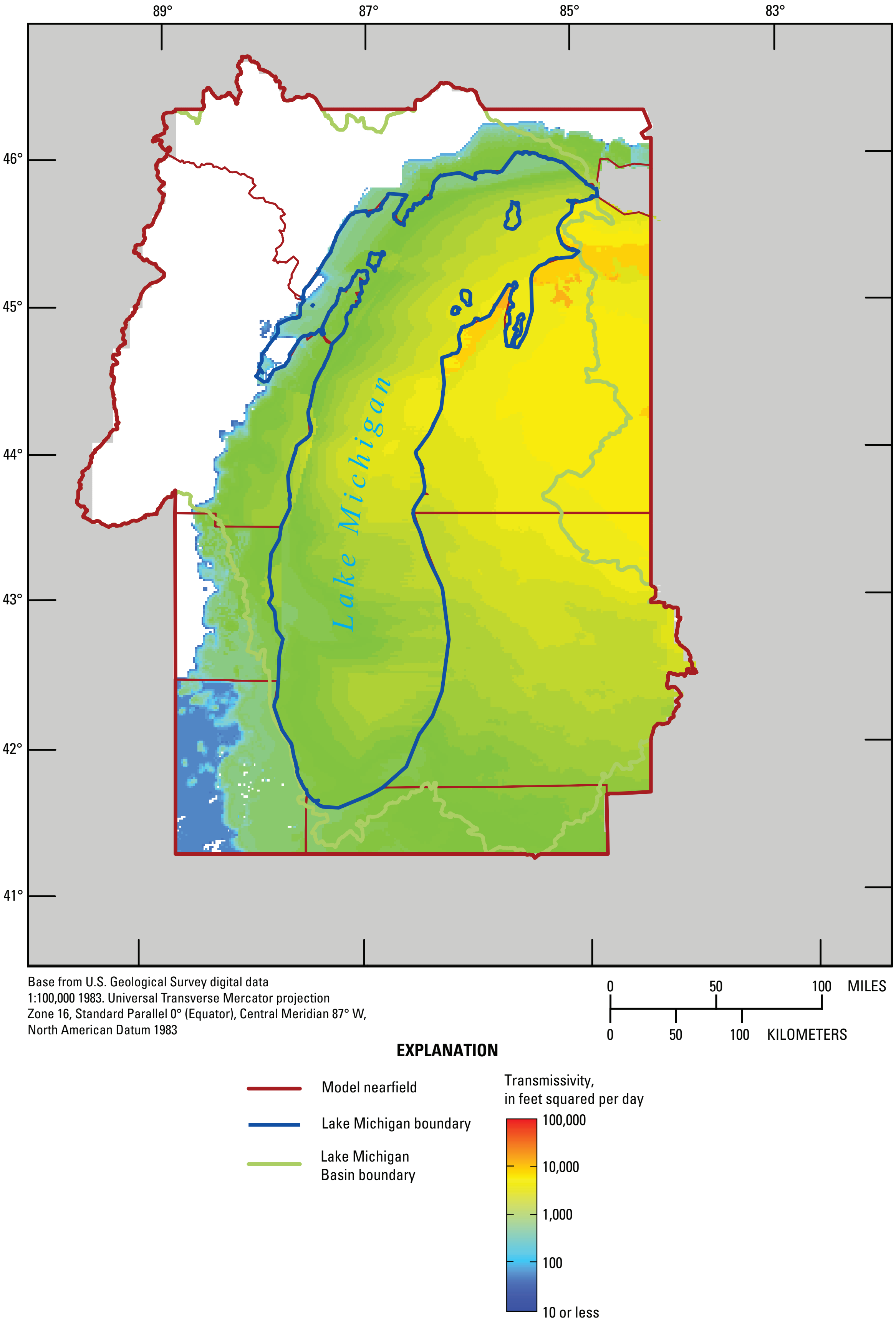

Figure 48*D*. Calibrated transmissivity distribution in aquifer system SLDV.

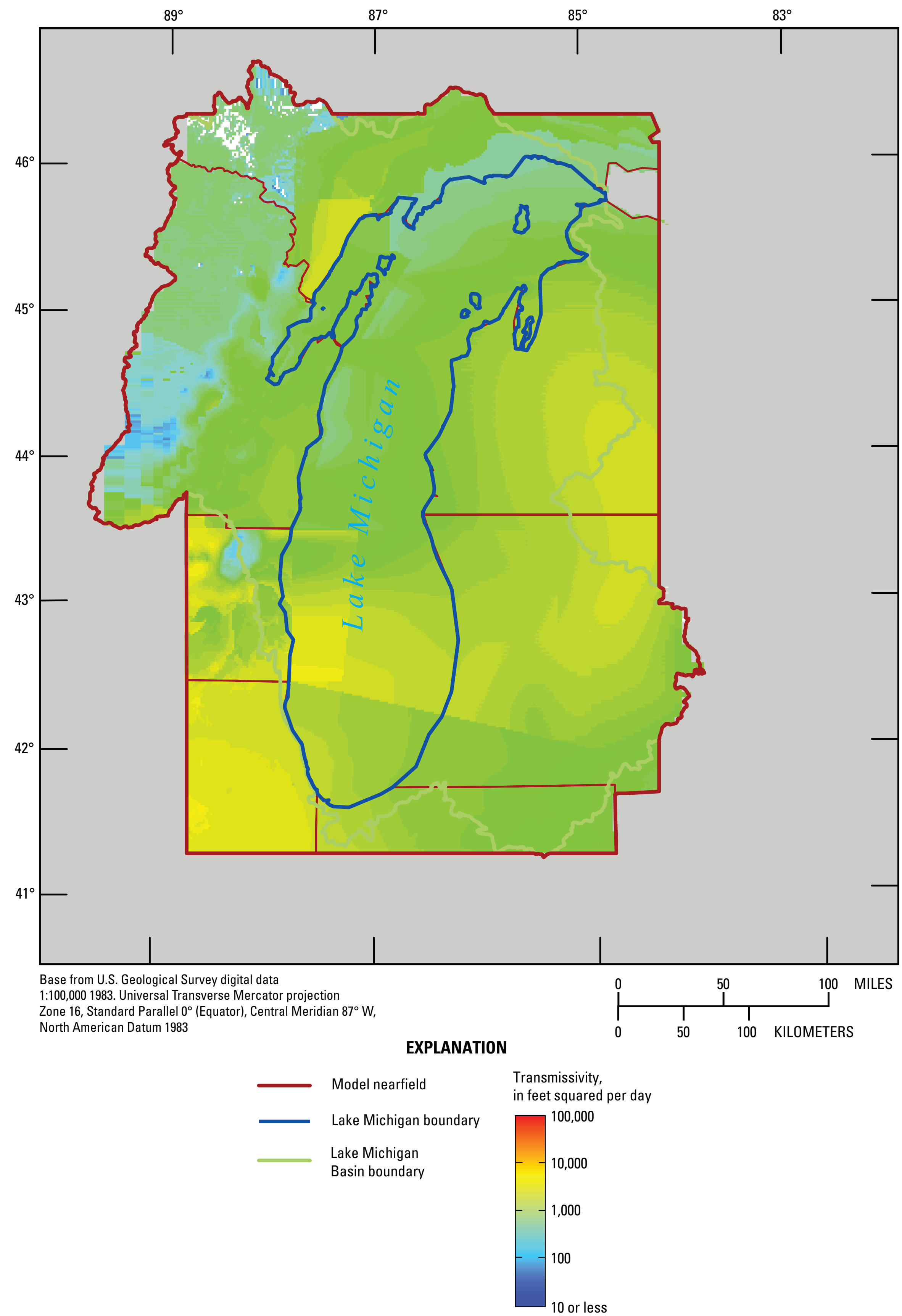

Figure 48*E*. Calibrated transmissivity distribution in aquifer system C-O.

5.6 Parameter Sensitivity

Parameter estimation generates output that ranks the sensitivity of the weighted ensemble of simulated target values to perturbations in individual parameter values. It is convenient to group the individual parameter values by “composite sensitivity,” a measure of the sum of all observation sensitivity reported for each parameter. This measure provides a visualization of information content in the dataset for the parameters included in the calibration.

The model input is divided into 14 parameter groups, which include between 1 and 78 individual parameters (the largest group being the set of pilot points for the Maquoketa K_v in the SE_WI and NE_ILL subregions). The groups are ranked by the composite sensitivity across the individual parameters and the sum of composite sensitivity (table 13*A*). The two rankings are in some respects quite different. Whereas the sensitivity of the single parameter in the recharge group is relatively quite high, the larger number of individual parameters in other groups renders them collectively more important to the calibration process. About 60 percent of the summed composite sensitivity is attributable to three parameter groups associated with the C-O aquifer system. The remaining sensitivity is distributed roughly equally among K_h and K_v parameter groups of other aquifer systems, plus RIV conductance, storage, and recharge parameter groups.

Consolidation of the base parameters into eight parameter groups further illustrates the pronounced sensitivity of the SLMB-C calibration to the *K* parameters for the C-O aquifer system compared to the sensitivity toward other types of inputs (fig. 50). Part of this difference is due to the high number of water-level, vertical-head-difference, and time-dependent head-change targets in the C-O system, and part is due to the dramatic effect deep pumping west of Lake Michigan has had on the groundwater-flow system (see section 6, “Model Results”). Shallow-aquifer parameters as a whole tend to be less important than deep-aquifer parameters because the water-table solution in the regional model is constrained by head-dependent boundaries in the form of RIV cells. These constraints particularly affect the ability of the calibration process to inform the estimation of the specific yield of unconfined aquifers (as illustrated by low composite sensitivity). The relative weakness of recharge in guiding the calibration process can be attributed, at least somewhat, to the relatively small weights assigned to the base-flow targets and, by extension, the comparatively modest contribution of these targets to the final objective function. The decision to limit the importance of recharge via weighting was imposed on the calibration process because the base-flow targets used to calibrate recharge in the SLM-C groundwater-flow model were also used to calibrate the SWB recharge model that created the recharge array (see last section of appendix 7).

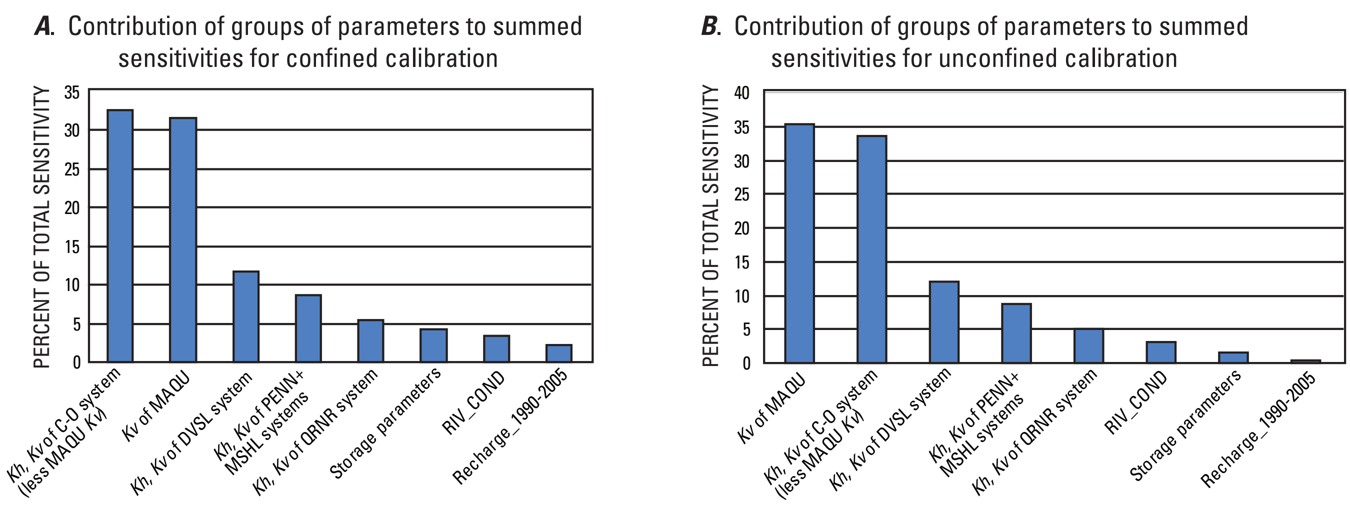

Figure 50. Composite sensitivities of calibration targets to eight parameter groups for *A*, confined (SLMB-C) calibration and *B*, unconfined (SLMB-U) calibration.

Table 13*A*. Composite sensitivities by parameter groups for confined calibration (SLMB-C).

[The 238 estimated parameters (including 78 pilot points) are divided into 14 groups. See appendix 5, table A5–2 for groupings]

Sorted by number of parameters in group		Sorted by average composite sensitivity in group		Sorted by sum of composite sensitivities in group		Percent of sum
Kv_MAQU-pilot_points	78	Ss_C-O	0.115	Kv_MAQU-pilot_points	1.43	29.47
Kh_C-O	46	Recharge_1991-2005	.108	Kh_C-O	.95	19.56
Kv_C-O	30	Kh_QRNR	.025	Kv_C-O	.63	13.11
Kh_SLDV	21	Ss_QRNR-PENN-MSHL-SLDV	.024	Kh_SLDV	.37	7.75
Kh_PENN-MSHL	14	RIV_COND	.023	Kh_PENN-MSHL	.27	5.52
Kv_SLDV	11	Kv_PENN-MSHL	.022	Kv_SLDV	.19	3.99
Kv/Kh_QRNR	7	Kv_C-O	.021	RIV_COND	.16	3.39
RIV_COND	7	Kh_C-O	.021	Kv_PENN-MSHL	.15	3.19
Kv_PENN-MSHL	7	Kv_MAQU-zone	.020	Kh_QRNR	.15	3.06
Kh_QRNR	6	Kh_PENN-MSHL	.019	Ss_C-O	.11	2.37
Kv_MAQU-zone	5	Kv_MAQU-pilot_points	.018	Kv/Kh_QRNR	.11	2.33
Ss_QRNR-PENN-MSHL-SLDV	4	Kv_SLDV	.018	Recharge_1991-2005	.11	2.23
Ss_C-O	1	Kh_SLDV	.018	Kv_MAQU-zone	.10	2.06
Recharge_1991-2005	1	Kv/Kh_QRNR	.016	Ss_QRNR-PENN-MSHL-SLDV	.09	1.95
Total number	**238**			**Total composite sensitivity**	**4.84**	**100.00**

Table 13*B*. Composite sensitivities by parameter groups for unconfined calibration (SLMB-U).

[The 243 estimated parameters (including 78 pilot points) are divided into 16 groups. See appendix 5, table A5–2 for groupings.]

Sorted by number of parameters in group		Sorted by average composite sensitivity in group		Sorted by sum of composite sensitivities in group		Percent of sum
Kv_MAQU-pilot points	78	Kv_PENN-MSHL	0.108	Kv_MAQU-pilot_points	7.45	33.35
Kh_C-O	46	Recharge_1991-2005	.107	Kh_C-O	4.37	19.56
Kv_C-O	30	Kv_C-O	.105	Kv_C-O	3.15	14.07
Kh_SLDV	21	RIV_COND	.096	Kh_SLDV	1.89	8.44
Kh_PENN-MSHL	14	Kv_MAQU-pilot_ points	.096	Kh_PENN-MSHL	1.22	5.44
Kv_SLDV	11	Kh_C-O	.095	Kv_SLDV	.81	3.62
Kv/Kh_QRNR	7	Kh_QRNR	.095	Kv_PENN-MSHL	.76	3.39
RIV_COND	7	Kv_MAQU-zone	.092	RIV_COND	.67	3.02
Kv_PENN-MSHL	7	Kh_SLDV	.090	Kh_QRNR	.57	2.54
Kh_QRNR	6	Kh_PENN-MSHL	.087	Kv/Kh_QRNR	.56	2.49
Kv_MAQU-zone	5	Kv/Kh_QRNR	.080	Kv_MAQU-zone	.46	2.06
Ss_QRNR-PENN-MSHL-SLDV	4	Kv_SLDV	.074	Sy_QRNR-PENN-MSHL-SLDV	.13	.56
Ss_C-O	4	Ss_C-O	.055	Ss_QRNR-PENN-MSHL-SLDV	.12	.54
Sy_QRNR-PENN-MSHL-SLDV	1	Sy_C-O	.044	Recharge_1991-2005	.11	.48
Sy_C-O	1	Sy_QRNR-PENN-MSHL-SLDV	.031	Ss_C-O	.05	.25
Recharge_1991-2005	1	Ss_QRNR-PENN-MSHL-SLDV	.030	Sy_C-O	.04	.19
Total number	**243**			**Total composite sensitivity**	**22.35**	**100.00**

6. Model Results

Quantitative results from the calibrated SLMB-C model provide a portrait of the groundwater resource in the Lake Michigan Basin and its evolution through space and time. Some results provide an overview of the resource's status at the regional scale:

- Water levels and drawdown by aquifer system
- Relative strengths of sources and sinks in the groundwater budget
- Change through time of groundwater flow rates and patterns

Other indicators address questions pertinent to protecting the long-term sustainability of the water supply:

- Sources of water to shallow and deep wells
- Shifting groundwater divides between the Lake Michigan Basin and surrounding basins
- Groundwater interactions with Lake Michigan

All these model findings, based on the calibrated confined model SLMB-C, reflect the changes introduced by two time-dependent stresses: variable recharge and pumping.

6.1 Water Levels and Drawdown

The LMB model simulates water levels in QRNR and bedrock units for both the fresh and saline parts of the model domain. However, only the results for the freshwater part indicate the lateral direction of flow in each unit as a function of the water-level gradients. The interpretation of water levels and of the direction of flow in the saline part of the model is complicated by the influence of density on head elevations and head gradients (Christian Langevin, U.S. Geological Survey, oral commun., April 4, 2008). For this reason, predevelopment (pre-1864) water levels (fig. 51) are presented only where salinity is less than 10,000 mg/L, a common threshold for distinguishing freshwater from saline water. The predevelopment water table is shown regardless of the layer it occupies (fig. 51*A*), although typically the water table is at the top of the hydrogeologic system in the QRNR aquifer system, in model layer 1. Other plots show predevelopment water levels for layers within each bedrock aquifer system: the PENN system is represented by layer 5 (fig. 51*B*), the MSHL system by layer 8 (fig. 51*C*), the SLDV system by layer 10 (fig. 51*D*), and the C-O by the IRGA unit in layer 17 (fig. 51*E*).

The configuration of the predevelopment water table tends to be a subdued reflection of the land surface (as can be seen by comparing fig. 51*A* to fig. 6). The presence of major discharge areas is evident along river valleys, where the water table occurs at low elevations. Predevelopment water levels in bedrock units also reflect land-surface topography. However, it is possible to detect vertical head differences within the groundwater flow system that influence flow. For example, comparison of the simulated water table (fig. 51*A*) to simulated head conditions in the C-O (fig. 51*E*) indicates that deep water levels, which are lower than shallow water level in the western parts of NE_WI, SE_WI, and NE_ILL, become higher than shallow levels in the vicinity of Lake Michigan. This pattern defines a regional flow system characterized by recharge areas to the west (where water leaks to deep layers) neighboring discharge areas to the east (where water eventually circulates back upward and flows toward Lake Michigan). The first wells installed in the Cambrian-Ordovician rocks around Chicago and Milwaukee encountered artesian (flowing) conditions, with water levels in the deep confined aquifer registering more than 100 ft above land surface in some locations (Weidman and Schultz, 1915). The model reproduces this condition for the predevelopment stress period and suggests that artesian conditions continued in the early postdevelopment stress periods at the beginning of the 20th century.

Pumping has perturbed parts of the predevelopment regional flow system. Simulated drawdown at the water table is hardly detectable for any stress period, largely because the proximity of surface water restricts the effects of wells to a radius smaller than the 5,000-ft spacing of the regional grid. In bedrock layers and particularly in confined parts of the flow system, however, drawdown is substantial in both freshwater and saline areas.[27] Inspection of the simulated head change between predevelopment and 2005 along four east-west cross sections (fig. 52) demonstrates the regional extent of the drawdown cones. Sections along rows 260 (fig. 52*C*) and 350 (fig. 52*D*) show clearly that well withdrawals from centers west of Lake Michigan influence simulated conditions under Lake Michigan and to the east.

The pumping centers east of Lake Michigan caused much less drawdown than the centers to the west of the lake. Both the extent and depth of drawdowns attributable to pumping in the MSHL aquifer system (figs. 53*A*–*C*; scale from 1 to 100 ft of drawdown) are smaller than those attributable to pumping in the C-O aquifer system (figs. 54*A*–*C*; scale from 10 to 1,000 ft of drawdown).

[27] The representation of drawdown, as opposed to water levels, is not affected by variable density. It is therefore useful to map the drawdown results continuously from pumping centers through areas of brackish groundwater as far as the brines within the Michigan Basin.

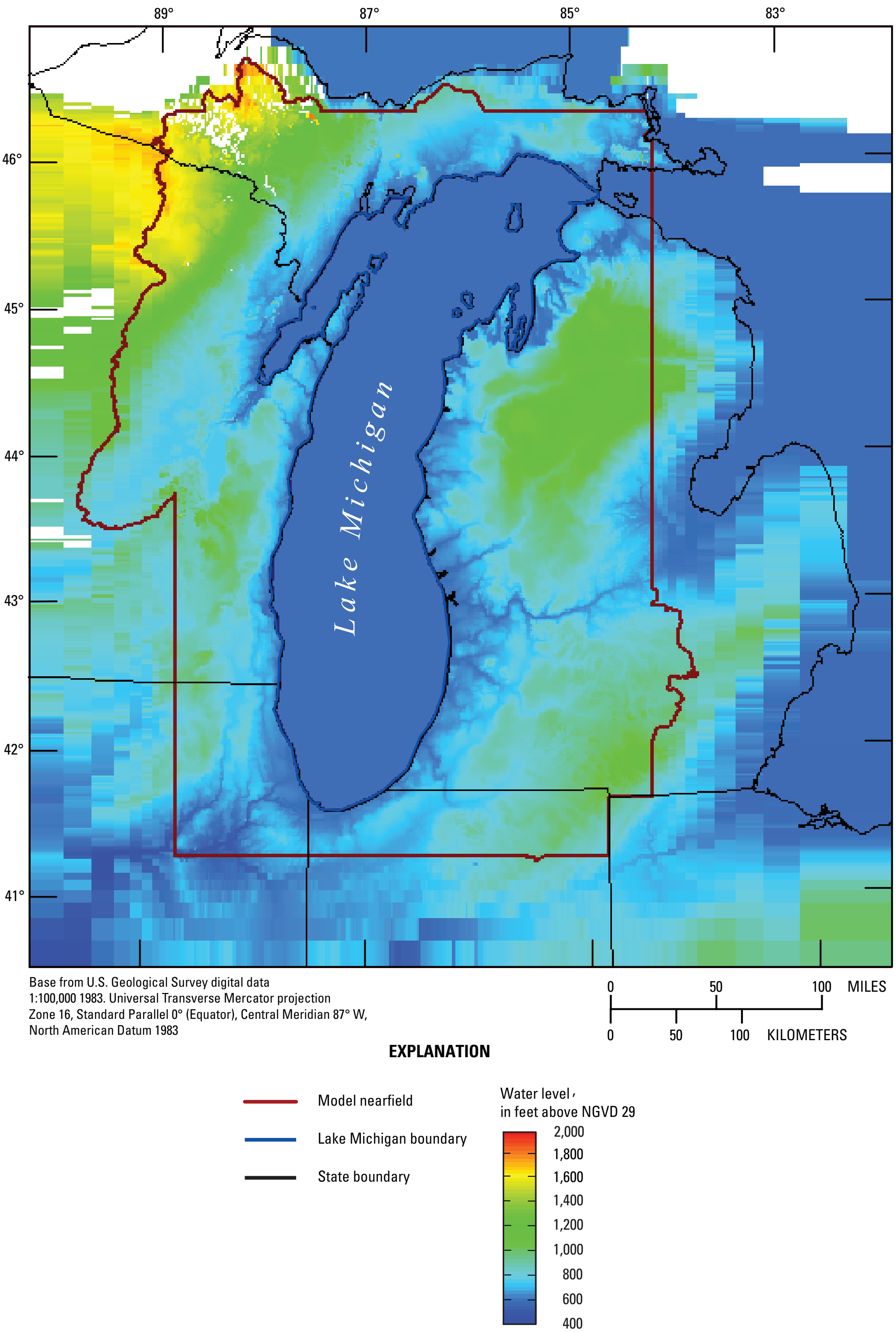

Figure 51*A*. Simulated predevelopment water levels for QRNR aquifer system.

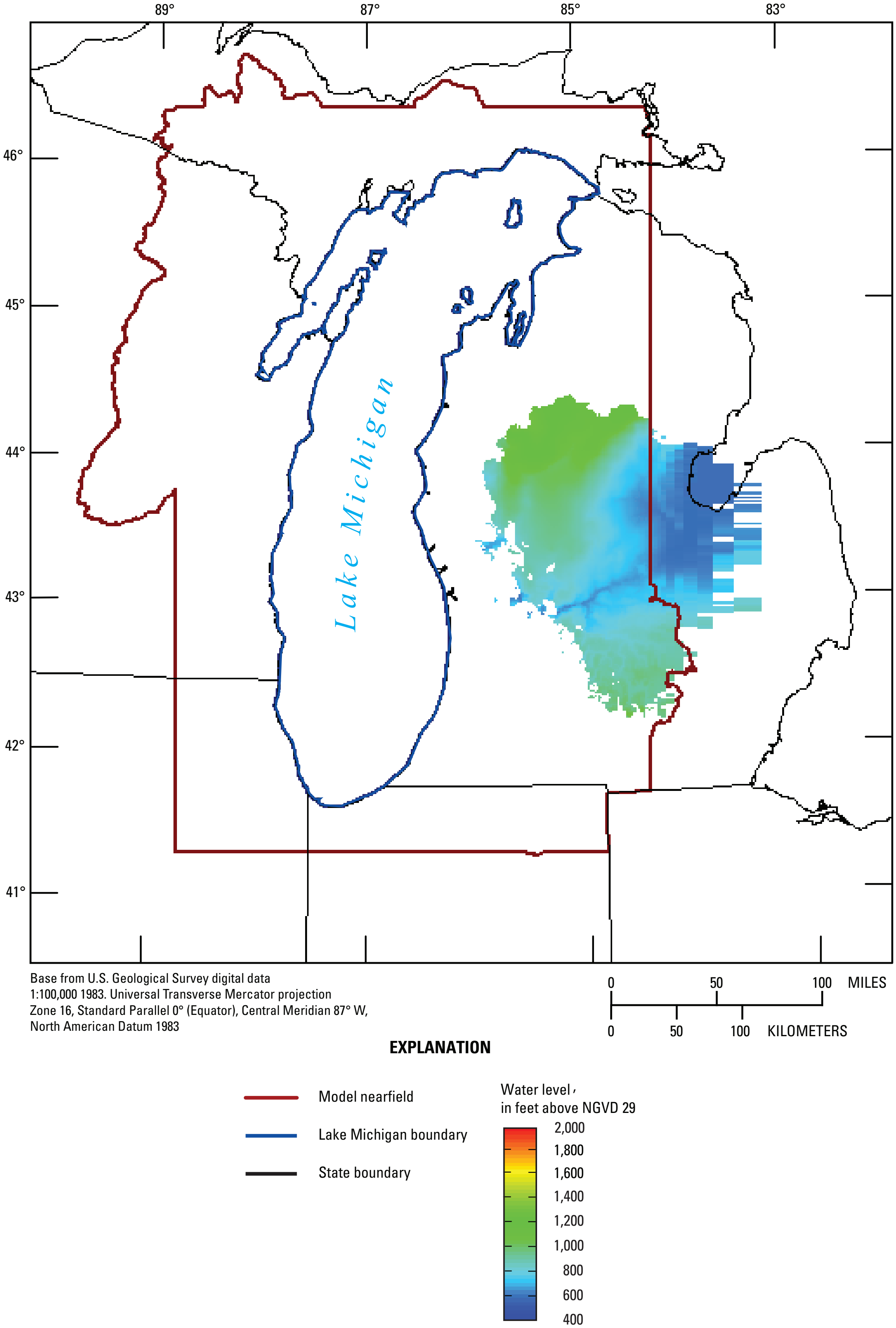

Figure 51*B*. Simulated predevelopment water levels for PENN aquifer system.

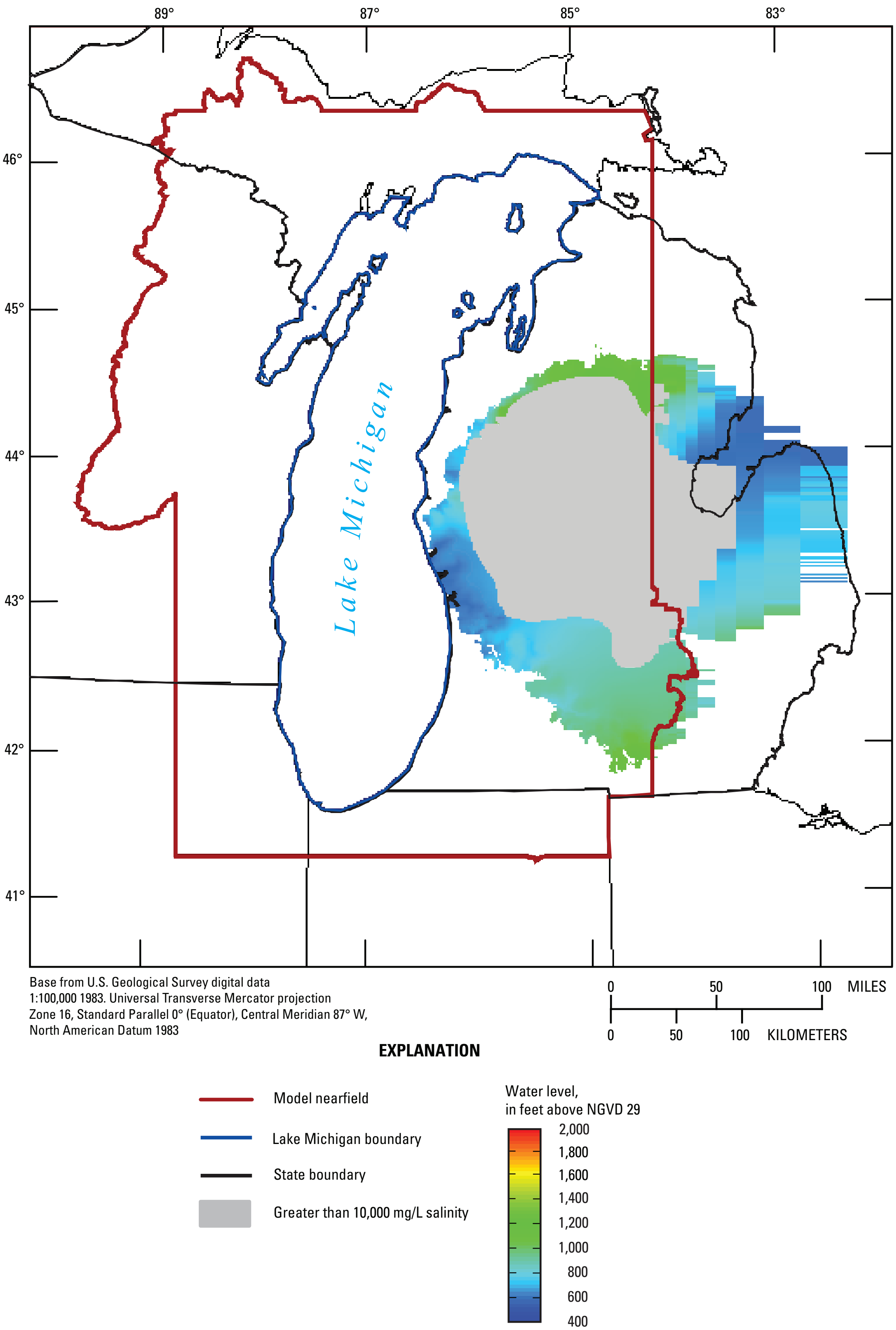

Figure 51*C*. Simulated predevelopment water levels for MSHL aquifer system.

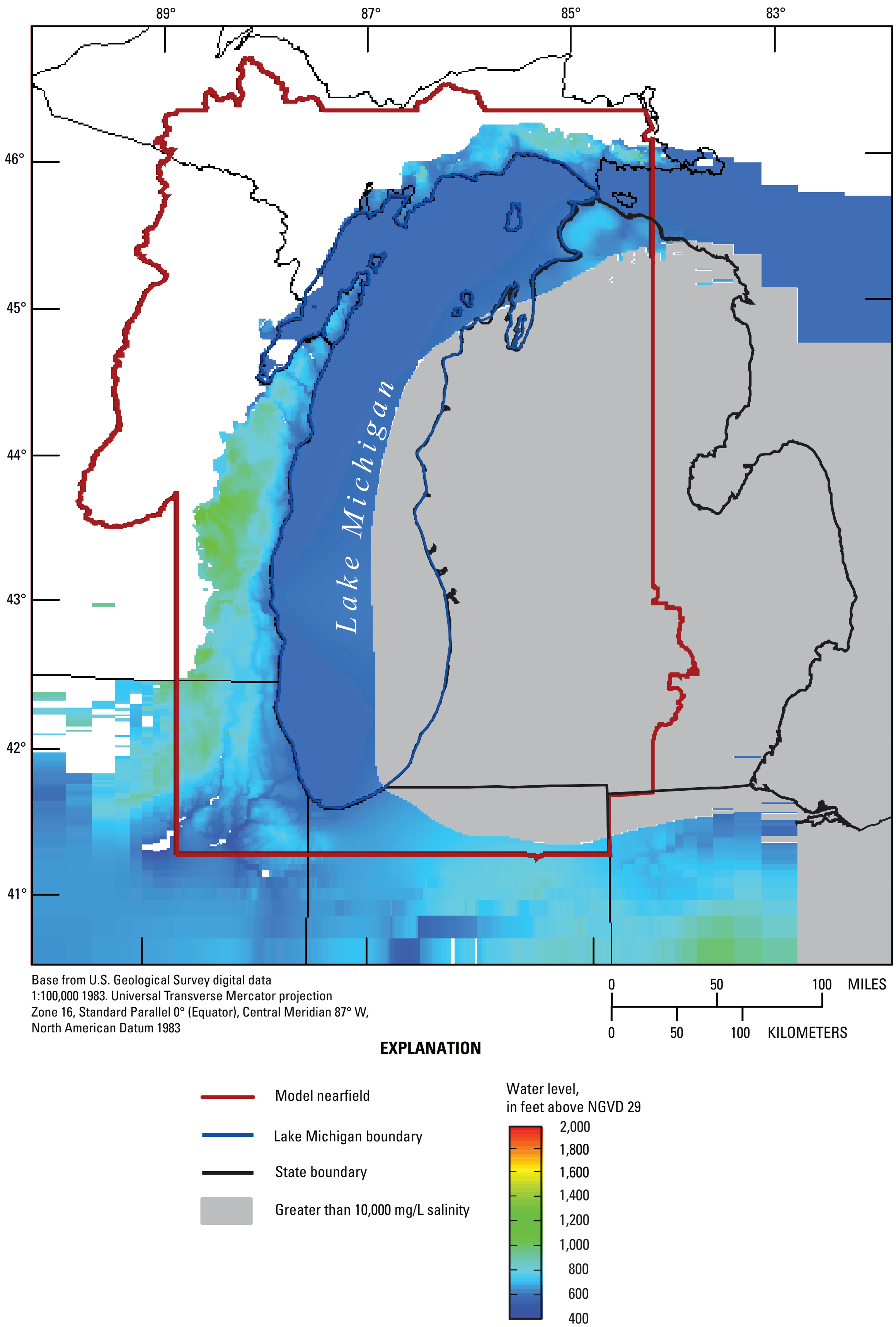

Figure 51*D*. Simulated predevelopment water levels for SLDV aquifer system.

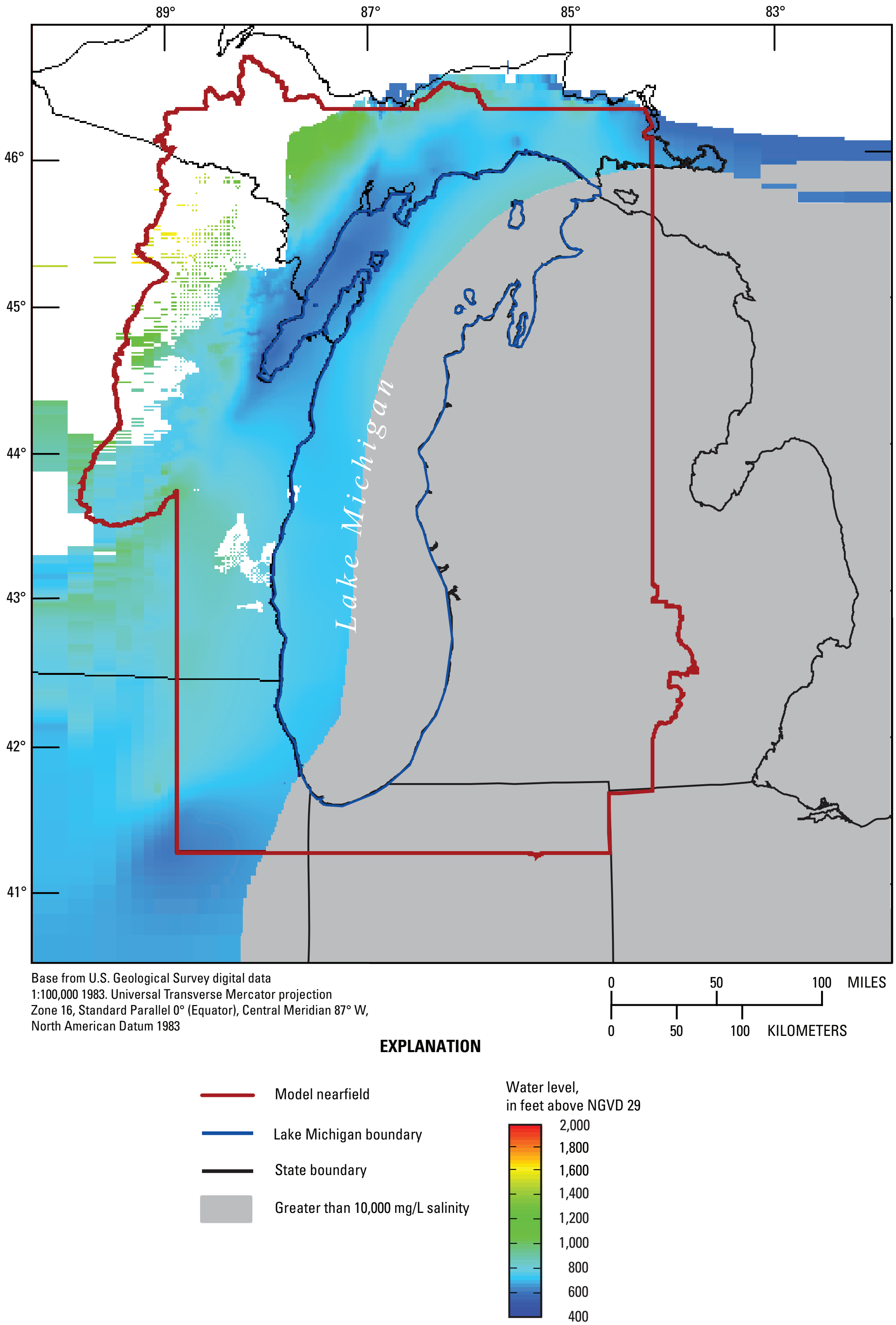

Figure 51*E*. Simulated predevelopment water levels for C-O aquifer system.

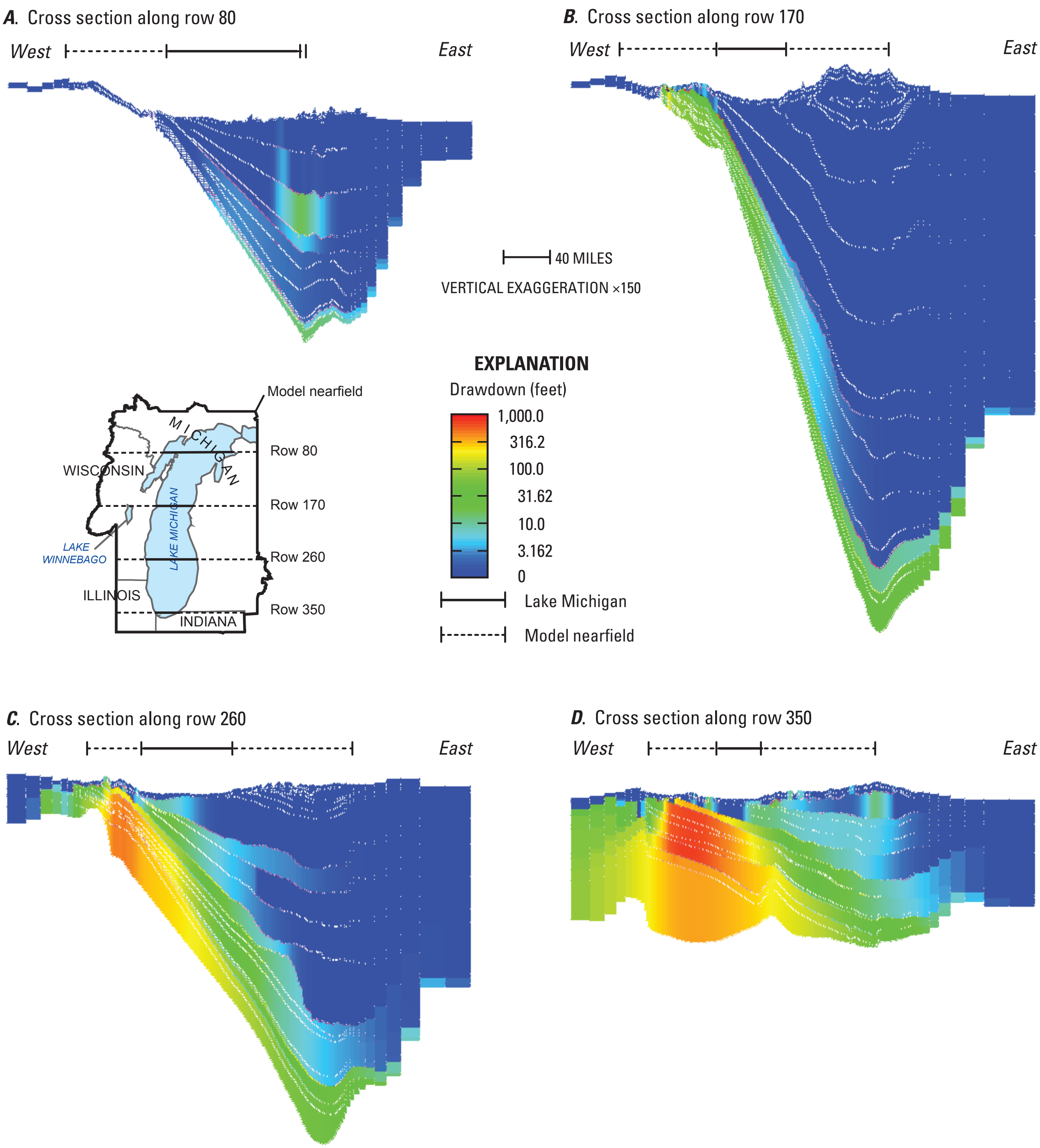

Figure 52. Simulated drawdown in 2005 along selected west/east cross sections.

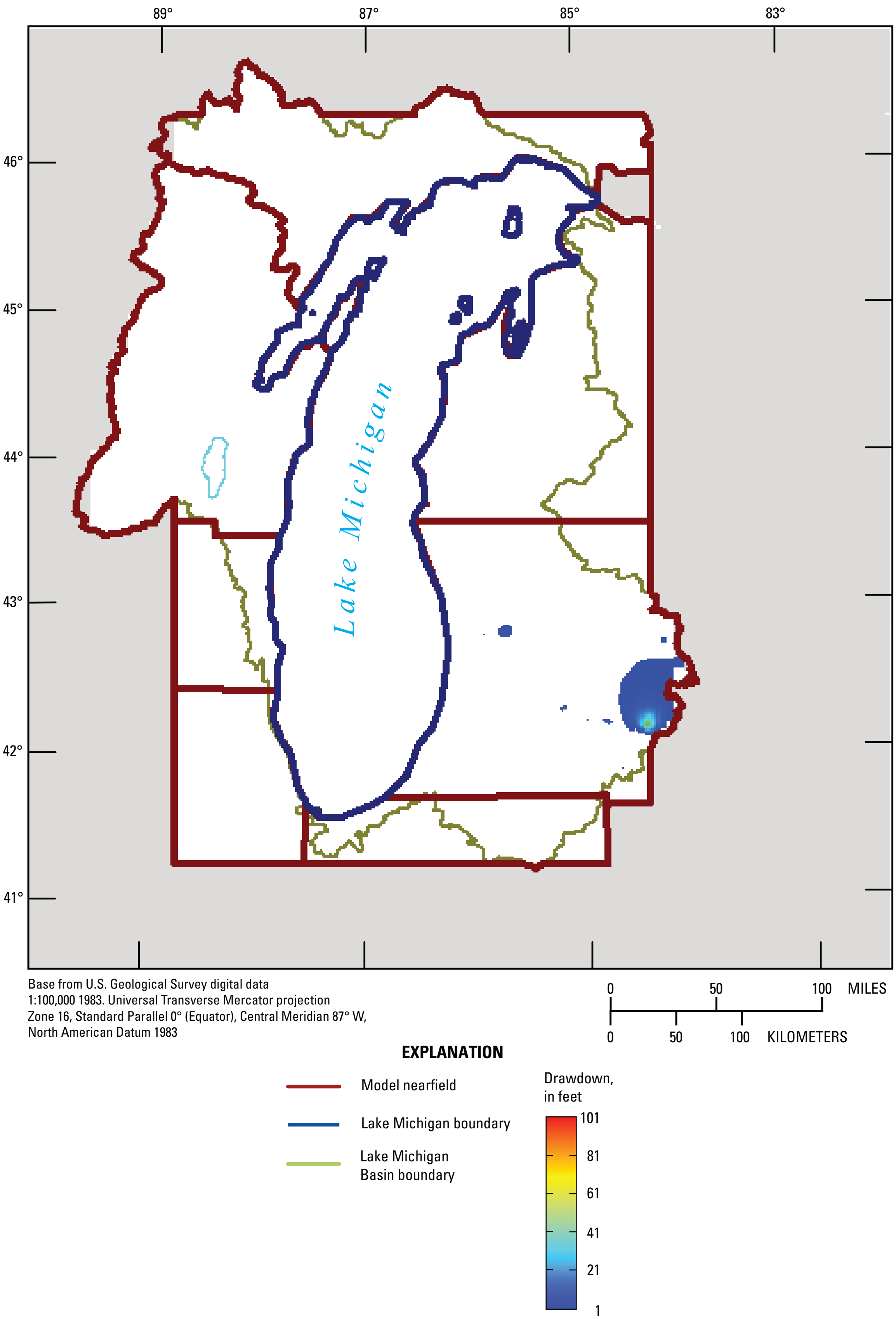

Figure 53*A*. Simulated drawdown in Marshall aquifer, 1950.

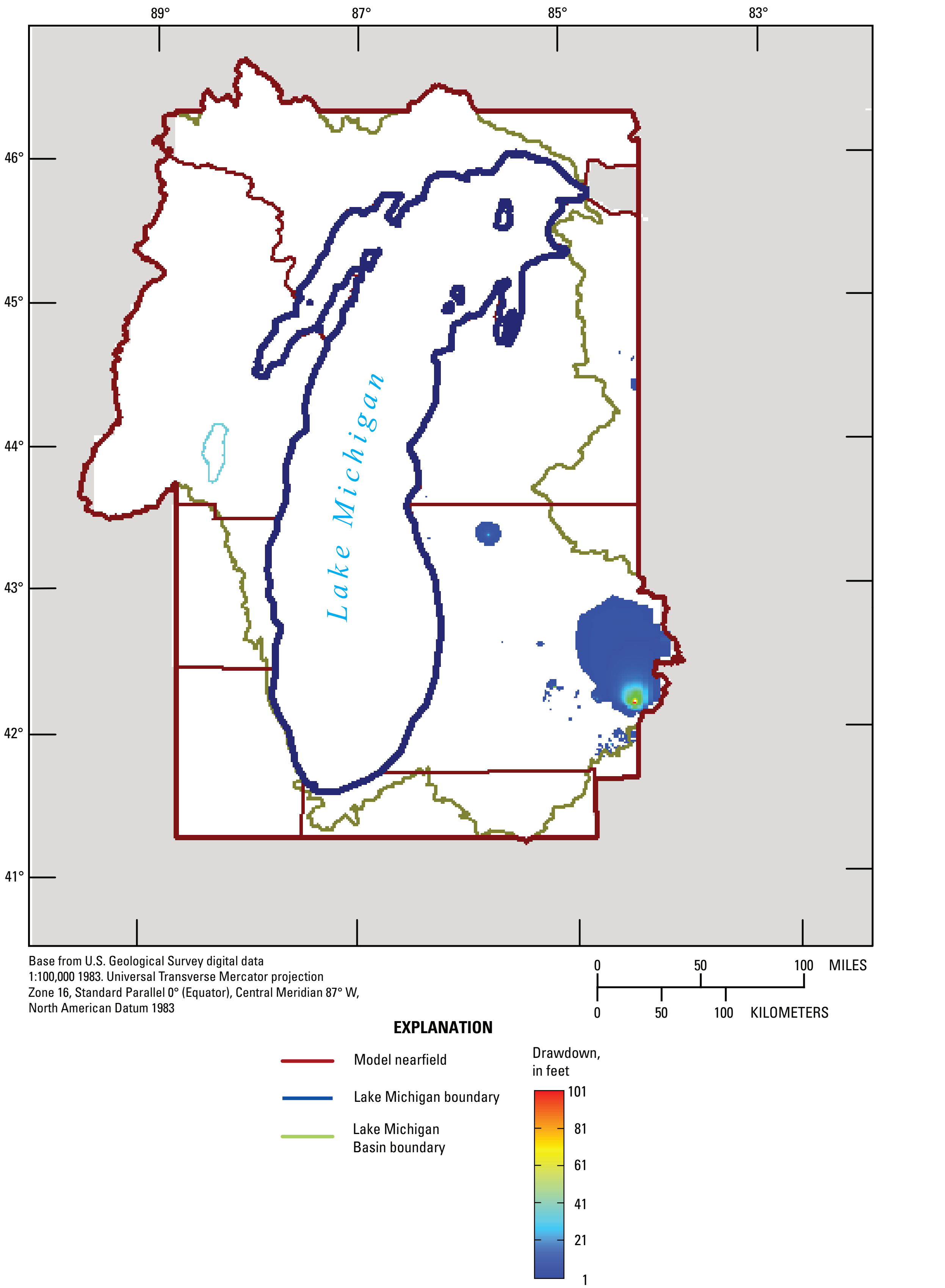

Figure 53*B*. Simulated drawdown in Marshall aquifer, 1980.

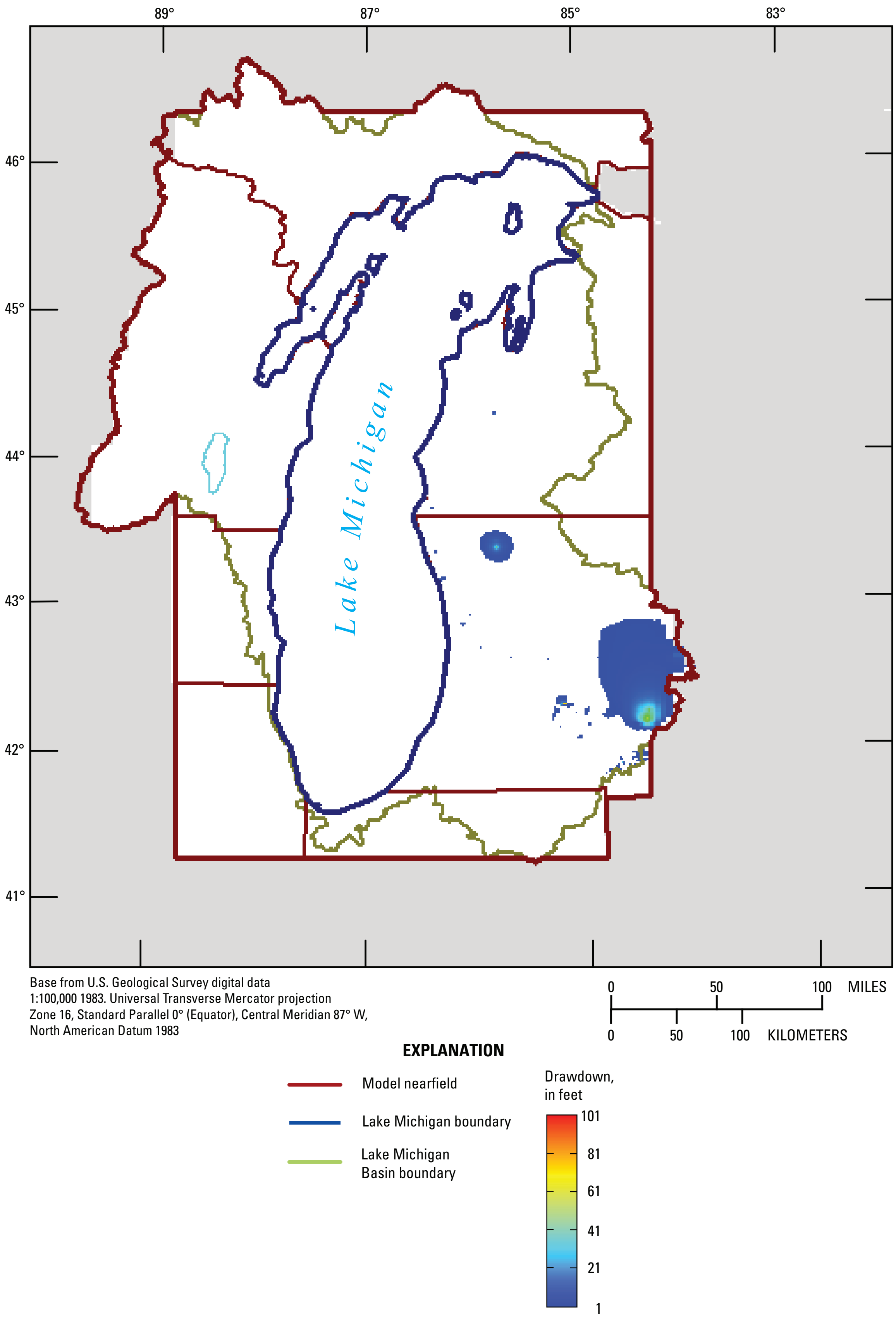

Figure 53*C*. Simulated drawdown in Marshall aquifer, 2005.

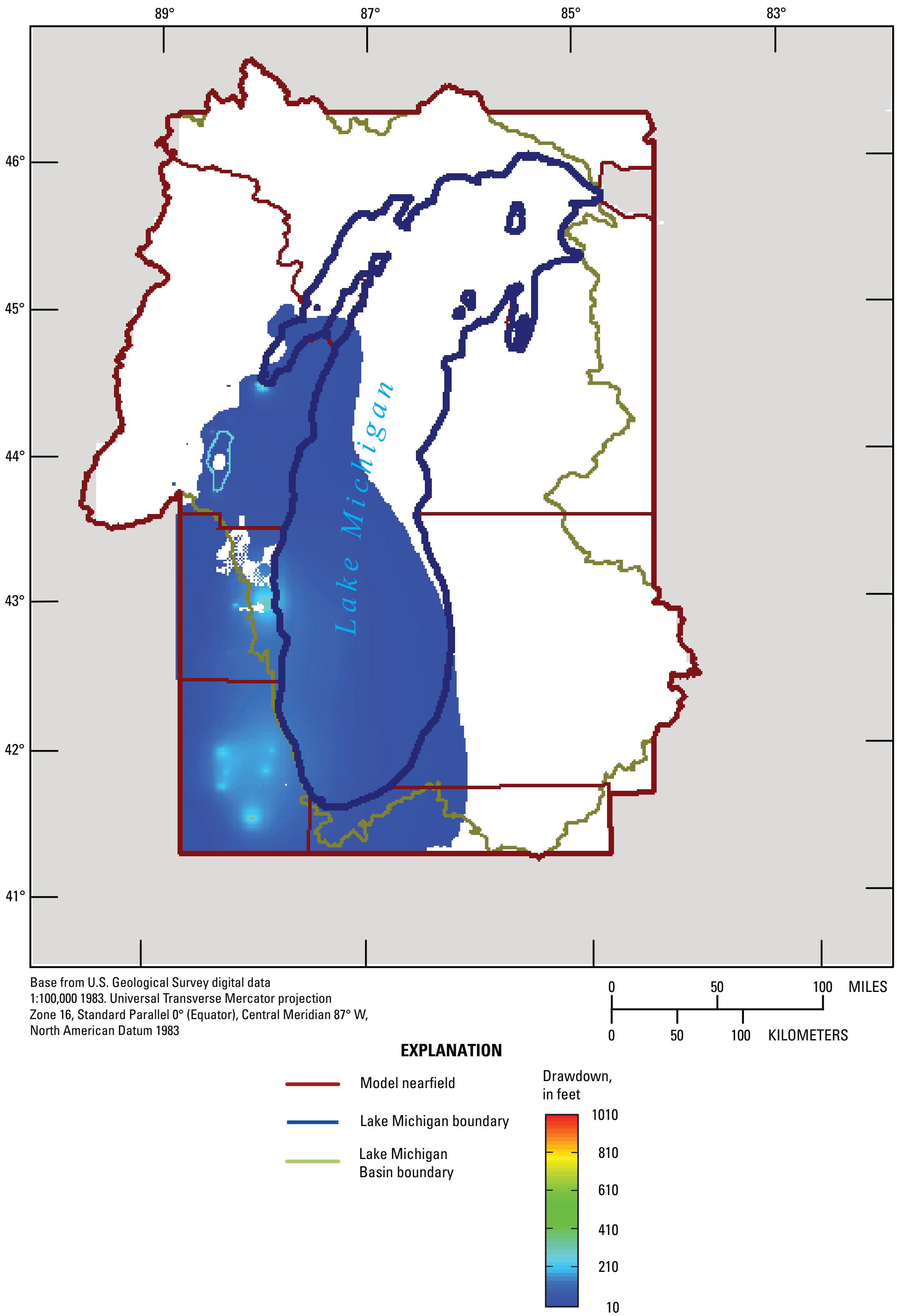

Figure 54*A*. Simulated drawdown in Ironton-Galesville aquifer, 1950.

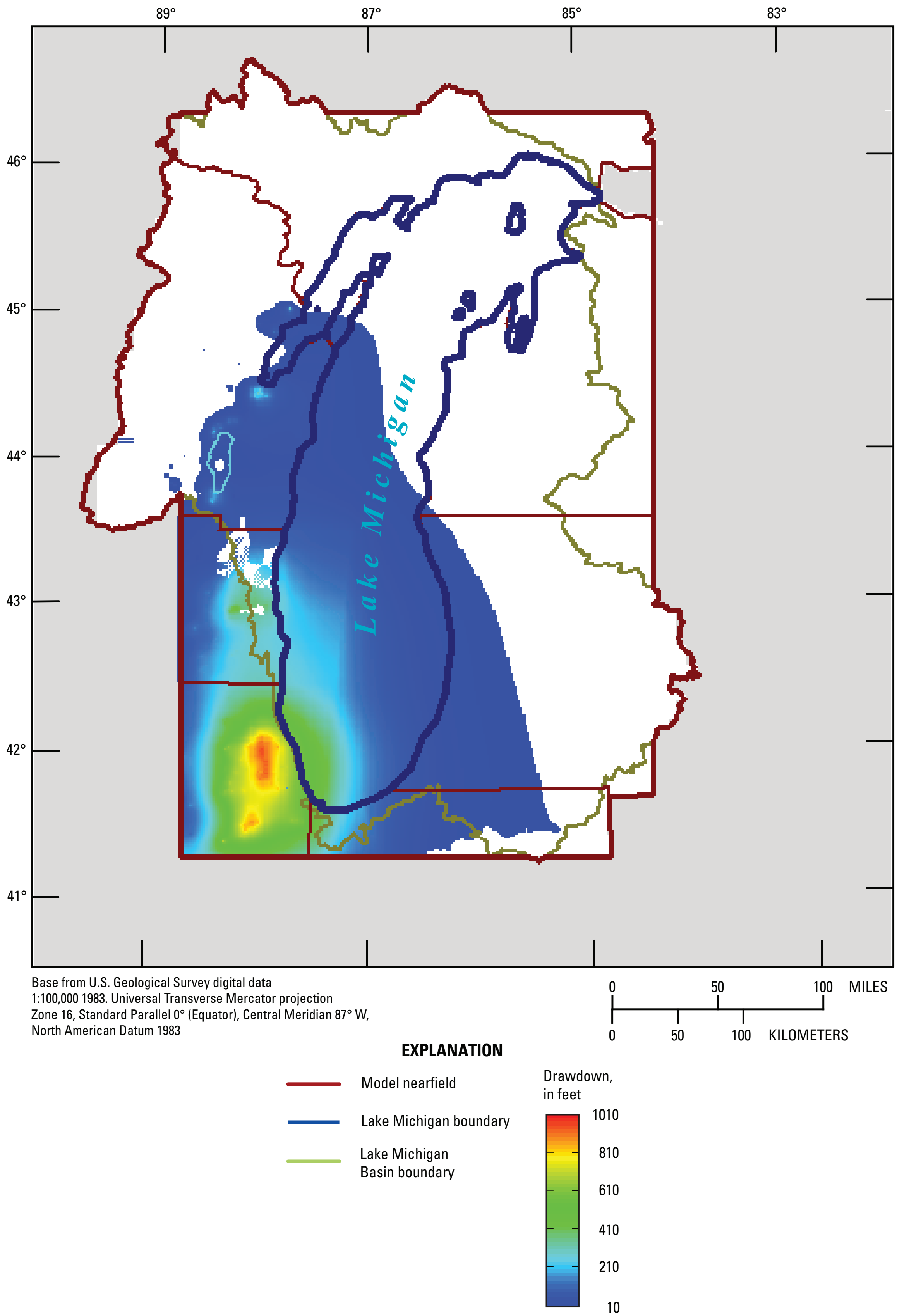

Figure 54*B*. Simulated drawdown in Ironton-Galesville aquifer, 1980.

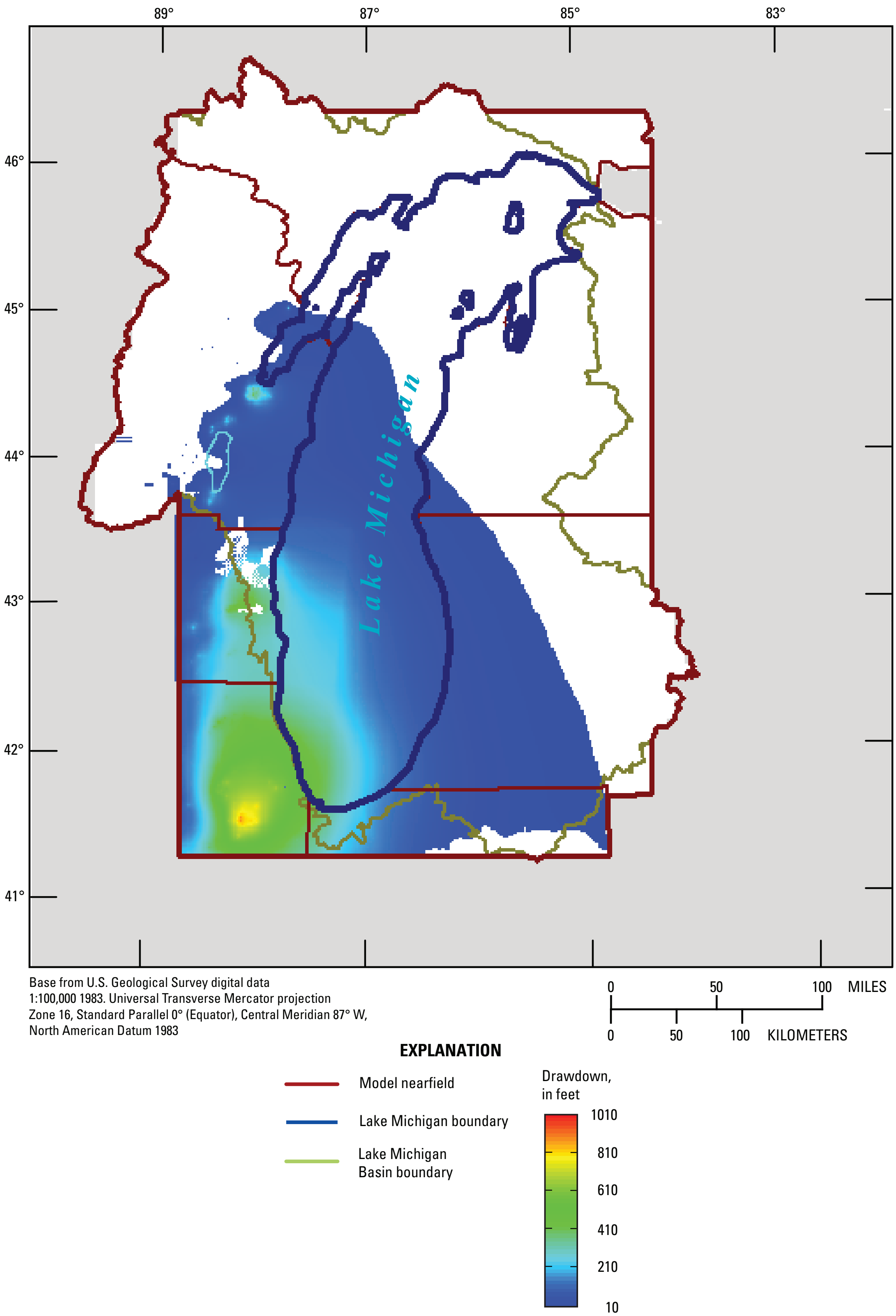

Figure 54*C*. Simulated drawdown in Ironton-Galesville aquifer, 2005.

The trends through time also can be seen by examining hydrographs of water levels at major pumping centers that draw from the MSHL and C-O aquifer systems (fig. 55). The hydrographs indicate that, for each pumping center, periods of both drawdown and recovery are evident and reflect shifting demand and changing sources of water supply. Drawdown in the MSHL system is associated with a major pumping center in the Lower Peninsula of Michigan; after 1960 water levels in this area stabilized or slightly recovered (fig. 55*B*). In the C-O system, three major pumping centers west of the lake are evident; their patterns of drawdown each evolved differently over the postdevelopment period. Pumping in NE_WI increased modestly after 1950—and drawdowns decreased after the city of Green Bay's switch to Lake Michigan surface water in 1957 (fig. 55*B*). Pumping in SE_WI increased rapidly between 1950 and 1980. Drawdowns continued to expand after 1980, but decrease in industrial pumping in the late 1990s and early 2000s slowed declines and sometimes resulted in water-level recovery. The pumping center in NE_ILL is the biggest in the model domain. Even though the wells are outside the Lake Michigan Basin, the influence of pumping continues to extend far into the basin. The maximum drawdown (on the order of 1,000 ft, as simulated for the IRGA aquifer) occurred in the early 1980s before Chicago and surrounding areas switched to Lake Michigan for water supply. By that time the drawdown areas for the C-O aquifer system in SE_WI and NE_ILL had coalesced. At the center of the area affected by drawdown in Illinois, several hundred feet of recovery relative to 1980 remained in 2005, although the rate of recovery peaked earlier than 2005 and, in some areas of NE_ILL, the trend at the end of the model simulation was again toward drawdown.

6.2 Lake Michigan Basin Water Budget

The calibrated model provides quantitative estimates of the sources and sinks in the water budget over the period 1864 through 2005. For the part of the model domain defined by the topographic boundaries of the Lake Michigan Basin, it is convenient to divide the water budget derived from the SLMB-C model into five source terms—

- recharge to the water table
- infiltration from inland surface water
- infiltration from Lake Michigan to groundwater
- release from storage due to declining water levels
- net lateral groundwater flow into the basin

and five sink terms—

- groundwater discharge to streams
- groundwater discharge to inland lakes and wetlands
- groundwater discharge directly to Lake Michigan
- gain to storage due to rising water levels
- well withdrawals

Although groundwater flows laterally both into and out of the Lake Michigan Basin, the simplified budget includes only the net flow into the basin. Similarly, it is possible for groundwater to flow inland from Lake Michigan itself, especially in the presence of pumping, so that the sink term for direct discharge to the lake is net of any inflow. Infiltration from surface water to groundwater is summed as one source term, but the discharge of groundwater to surface water is distributed among three sink terms. Finally, conditions before 1864 are simulated as steady-state conditions, so change in storage is excluded as a source or sink term and no pumping wells are active for the initial predevelopment stress period.

Most of the water-budget changes registered by the LMB model over time (fig. 56) reflect fluctuations in recharge, the major source term; and discharge to streams, the major sink term. The Lake Michigan Basin groundwater system still retains the imprint of predevelopment ("natural") conditions, despite large pumping centers and large shifts in groundwater flow patterns (see below). Withdrawals and storage changes within the basin are relatively small elements in the budget. Release from storage in the Lake Michigan Basin in 2005 (caused by reductions in recharge and by pumping) amounted to 71 Mgal/d, whereas recharge to the basin was about 16,000 Mgal/d or about 230 times that amount (fig. 57*C*). Withdrawals in the basin for 2005 amounted to 580 Mgal/d, whereas the groundwater discharge to surface-water features totaled 18,720 Mgal/d, 32 times that amount (fig. 57*D*). The model indicates that shallow and deep pumping in the Lake Michigan Basin accounted for 3.0 percent of the total discharge (19,313 Mgal/d) from the basin in 2005.

Another way to contrast the magnitude of selected fluxes in the water budget is to tabulate recharge over the Lake Michigan Basin through time and juxtapose these values with the amount of direct discharge to Lake Michigan and the amount of pumping from the basin for the same periods (table 14). Although pumping has increased over this period, it remains a small fraction of inflow from recharge. Discharge to Lake Michigan is more closely related to recharge fluctuations than to trends in pumping.

Although increased pumping over a time period acts to reduce base flow to streams, increased recharge for the same time period can counter the effect of pumping and yield a net increase in base flow. For example, comparison of sources and sinks for predevelopment (fig. 57*A, B*) to the year 2005 (fig. 57*C, D*) fails to show the regional effect of historical pumping as reduced base flow because the general increase of recharge over the same period yields a general increase of simulated base flow to streams and lakes. This increase dominates the regional water budget and masks the decreased flux to local surface-water bodies due to diversion of groundwater discharge to particular pumping centers. In light of the competing effects of time-dependent recharge and pumping, a special analysis is needed to isolate the effect of wells on the natural groundwater flow to Lake Michigan, streams, and inland lakes (see next section).

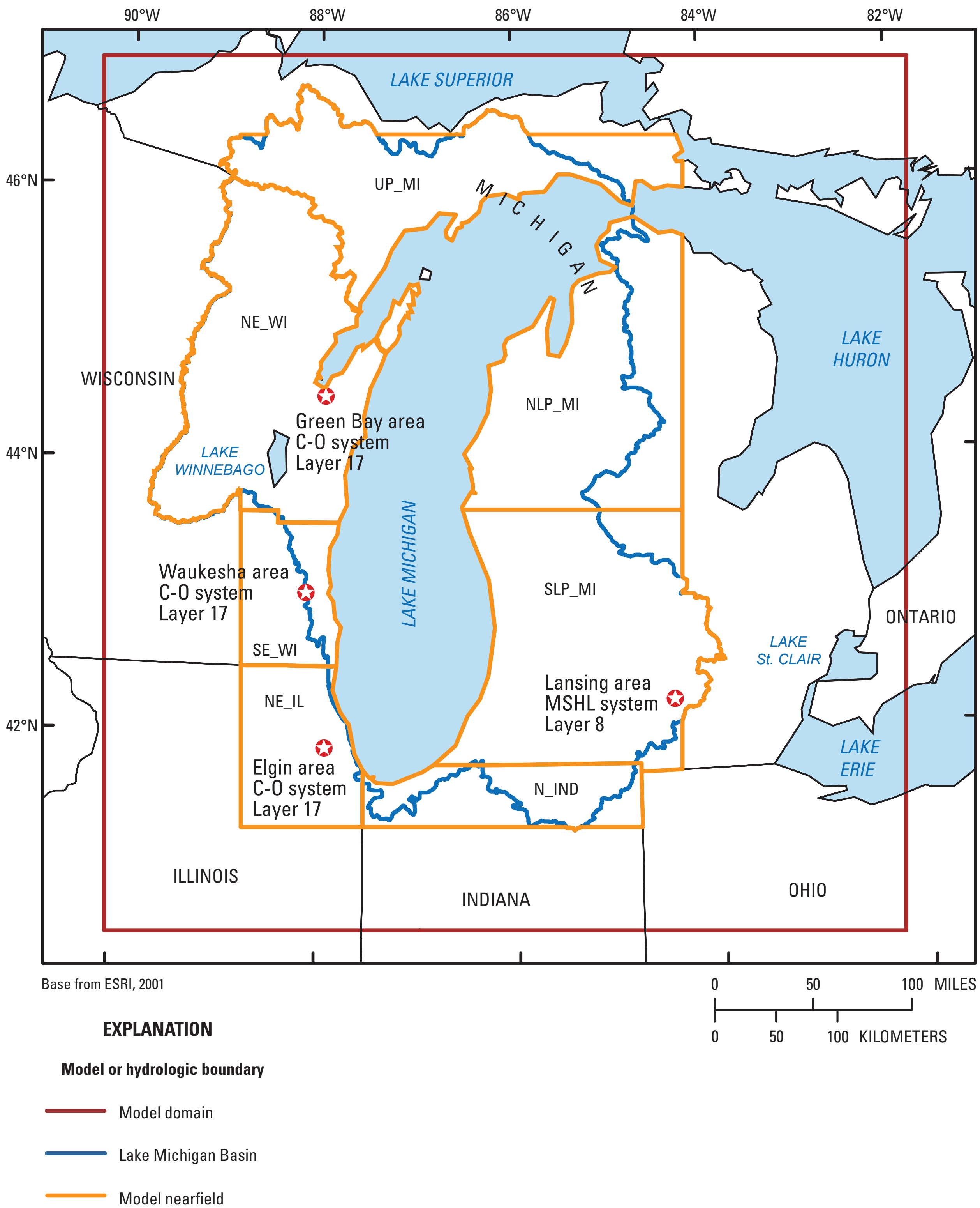

Figure 55*A*. Selected pumping centers.

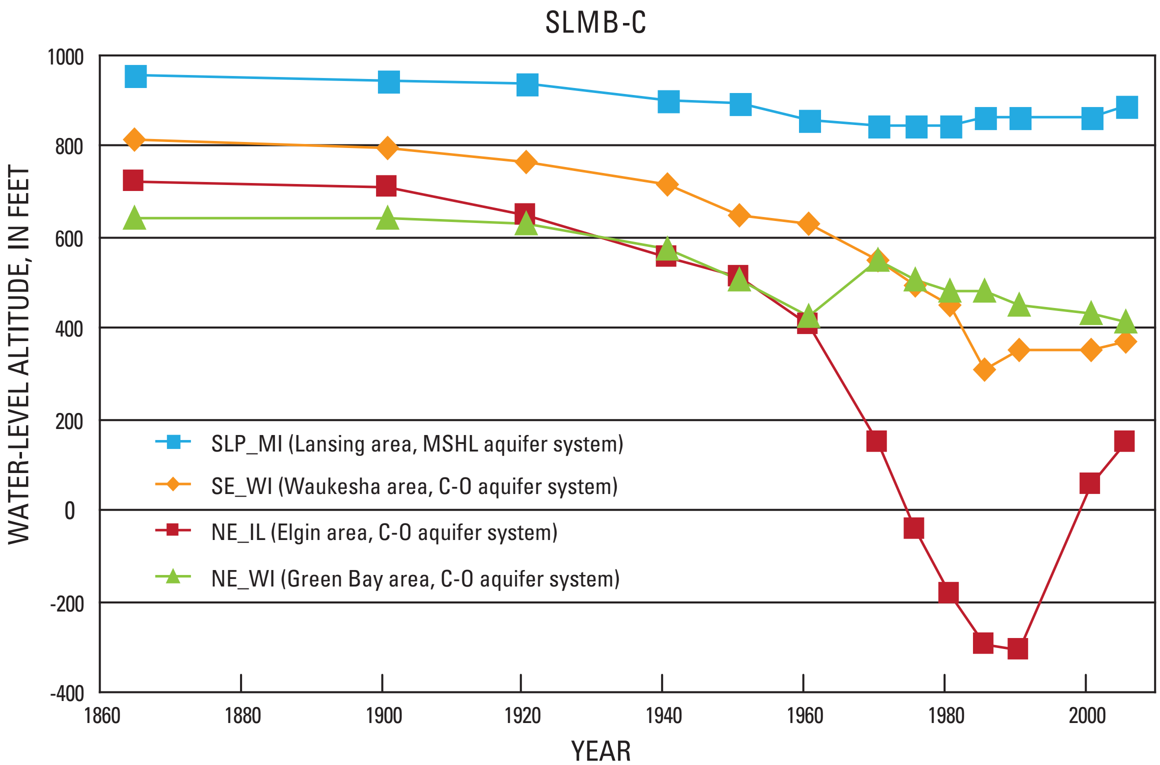

Figure 55*B*. Simulated water-level hydrographs at selected pumping centers.

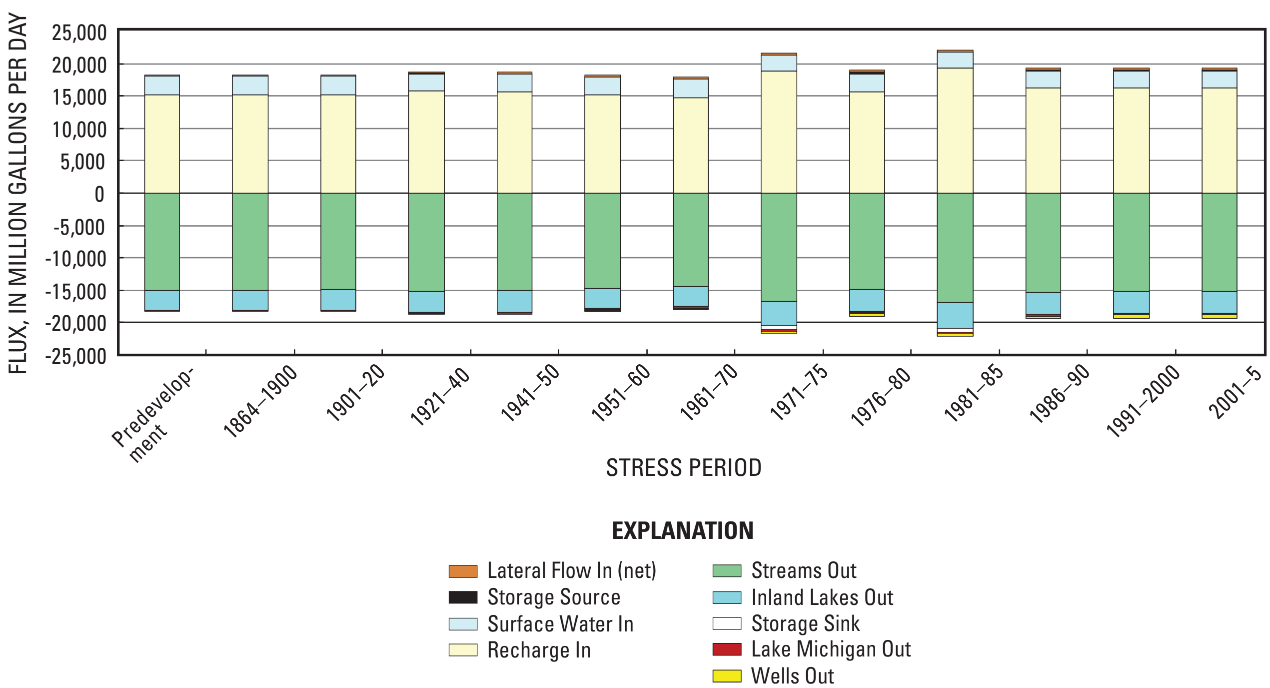

Figure 56. Simulated groundwater budget, by stress period, for Lake Michigan Basin.

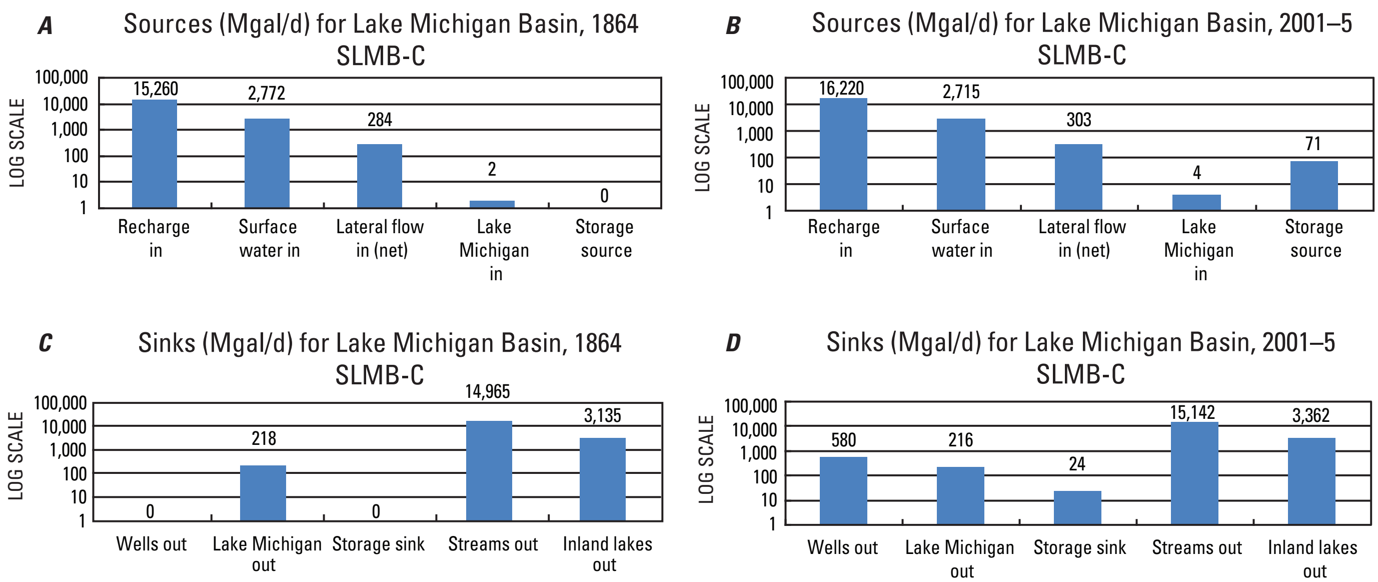

Figure 57. Simulated groundwater sources and sinks in Lake Michgan Basin for predevelopment (1864) and 2001–5 periods.

Table 14. Relative magnitude of recharge, simulated direct discharge to Lake Michigan, and withdrawals by pumping, predevelopment through 2005.

[Values correspond to the confined model, SLMB-C; Mgal/d, million gallons per day]

Stress period	Date	Recharge to Lake Michigan Basin (Mgal/d)	Direct groundwater discharge to Lake Michigan[1] (Mgal/d)	Net pumping in Lake Michigan Basin (net of injection)[2] (Mgal/d)
1	Predevelopment	15,261.15	217.90	0
2	Oct. 1864–Oct. 1900	15,261.15	217.86	8.41
3	Oct. 1900–Oct. 1920	15,261.15	217.28	19.96
4	Oct. 1920–Oct. 1940	15,769.50	223.63	55.38
5	Oct. 1940–Oct. 1950	15,687.74	222.05	118.82
6	Oct. 1950–Oct. 1960	15,131.87	220.82	187.30
7	Oct. 1960–Oct. 1970	14,781.80	219.93	272.29
8	Oct. 1970–Oct. 1975	18,807.74	223.56	317.54
9	Oct. 1975–Oct. 1980	15,639.94	221.64	368.19
10	Oct. 1980–Oct. 1985	19,349.68	224.54	423.60
11	Oct. 1985–Oct. 1990	16,199.12	221.89	435.77
12	Oct. 1990–Oct. 2000	16,221.24	215.93	576.00
13	Oct. 2000–Oct. 2005	16,221.24	215.66	569.52

[1]Lake Michigan is represented by GHB nodes in the model. The flow to the GHB nodes represents the direct discharge to the lake (that is, groundwater flow that discharges directly to the lake rather than indirectly through surface-water bodies that are tributary to the lake) .

[2]Net pumping is pumping minus injection inside the Lake Michigan topographic basin. The model simulates injection at only one cluster of locations (near Kalamazoo), where it amounts to about 10 Mgal/d for 2005.

6.3 Groundwater Flow Rates and Patterns

Simulation of changing water levels and evaluation of regional sources and sinks are two ways to analyze the status of groundwater in and around Lake Michigan. The calibrated model affords a third set of indicators through the depiction and analysis of the magnitude and direction of subsurface flow. Insight into the changing nature of the regional resource is gained by examining flow rates as a function of space and time, by mapping the changing pattern of vertical exchange between shallow and deep parts of the flow system, and by tracking the regional effect of pumping centers on flow rates and directions.

Circulation within this groundwater system is typically most vigorous in shallow unconsolidated deposits. In the model nearfield, the flow rate in the upper 100 ft of the QRNR deposits varies almost everywhere between 0.001 and 1.0 ft/d (fig. 58).[28] The rate of flow is highest where sediments are coarse and where recharge is high; for example, in parts of the northern Lower Peninsula in Michigan. The flow rate is much lower, for example, near the shoreline of Lake Michigan in Wisconsin and northeastern Illinois, areas dominated by clayey tills and fine stratified deposits. In deep bedrock units, flow rates range from 1.0 E−5 to 1.0 E−3 ft/d because the hydraulic gradients are less, and only part of the recharge to the water table reaches the deeper aquifers (fig. 59*A–D*). Lower flow rates, on the order of 1.0 E−6 ft/d, are simulated for the low-permeability confining units that span parts of the Wisconsin Arch and Michigan Basin.

Much information on the flow pattern can be obtained by mapping the proportion of the total subsurface flow through each aquifer system. First for consideration is the distribution of lateral flow under predevelopment conditions (blue bars in fig. 60). The pattern is very different on the east side of Lake Michigan (fig. 60*A*) as opposed to the west (fig. 60*B*). To the east, the QRNR aquifer system is the dominant conveyor of groundwater; in the N_IND subregion, for example, 92 percent of the predevelopment flow (according to the model) passes through unconsolidated deposits. Secondary in importance from the standpoint of lateral flow are the SLDV system in the NLP_MI subregion and the MSHL system in the SLP_MI subregion. To the west, the QRNR aquifer system shares flow with the SLDV and C-O systems. The simulated lateral flow in the unconsolidated deposits averages just over 50 percent of the total predevelopment flow, ranging from 39 percent in the UP_MI to 60 percent in SE_WI. The remainder is shared fairly evenly between the mostly dolomite rocks in the SLDV system and the mostly sandstone rocks in the C-O system. The introduction of pumping changes the mix. Shallow pumping increases the share in the QRNR layers for the Lower Peninsula of Michigan from an average of 61 to 72 percent of total flow. West of the lake, the redistribution is more complicated. In the UP_MI, NE_WI, and SE_WI subregions, shallow 2005 pumping increases the relative proportion of QRNR flow relative to predevelopment conditions, but in NE_ILL deep pumping routes an increased proportion of flow through bedrock units. Although the SLDV aquifer system is an important source of well withdrawals, competing withdrawals from above (QRNR system) and below (C-O system) reduce its relative share with respect to predevelopment in all four subregions west of the lake. There is a striking increase in the proportion of lateral flow through the C-O aquifer system for 2005 in SE_WI and, especially, in NE_ILL; there, despite the availability of Lake Michigan water for supply, the C-O system under the influence of pumping transmits half the total lateral flow.

Much model information that bears on how flow patterns change through time can be gleaned by comparing the vertical flow between the shallow and deep parts of the flow system before and after the installation of high-capacity wells. As defined previously in this report, the deep part of the flow system is all aquifer systems that fall below the first major confining unit at depth at any location. A map of the uppermost deep aquifer system in the model nearfield (fig. 61) indicates that the PENN and MSHL systems constitute the top of the deep part of the flow system in the center of the Michigan Basin (confined by the JURA, PEN2, and/or MICH confining units) whereas the SLDV is the uppermost system along the flanks of the Michigan Basin in the Lower Peninsula of Michigan, in northern Indiana, and under parts of Lake Michigan (beneath the DVMS confining unit). The deep flow system is restricted to the C-O aquifer under parts of Lake Michigan and over most of the model nearfield west of the lake (beneath the MAQU and SNNP confining units), whereas the entire groundwater flow system is unconfined in the northwestern corner of the nearfield because confining units are absent.

---

[28] In this report the term "flow rate" refers to the so-called Darcy flow, defined as the volumetric flux per unit area in the direction of flow ($ft^3/d/ft^2$ or ft/d). A related term is the "advective velocity," which equals the flow rate divided by the effective porosity of the sediments. The flow rate indicates where the amount of groundwater flow is relatively high or low, whereas the advective velocity term is used to compute traveltimes along flow paths. The "lateral flow" for a layer, unit, or aquifer system at a row/column locaton is computed as the Darcy flow moving horizontally across the right and front sides of cell faces, plus the difference between what enters and what exits vertically through the top and bottom of the cell(s).

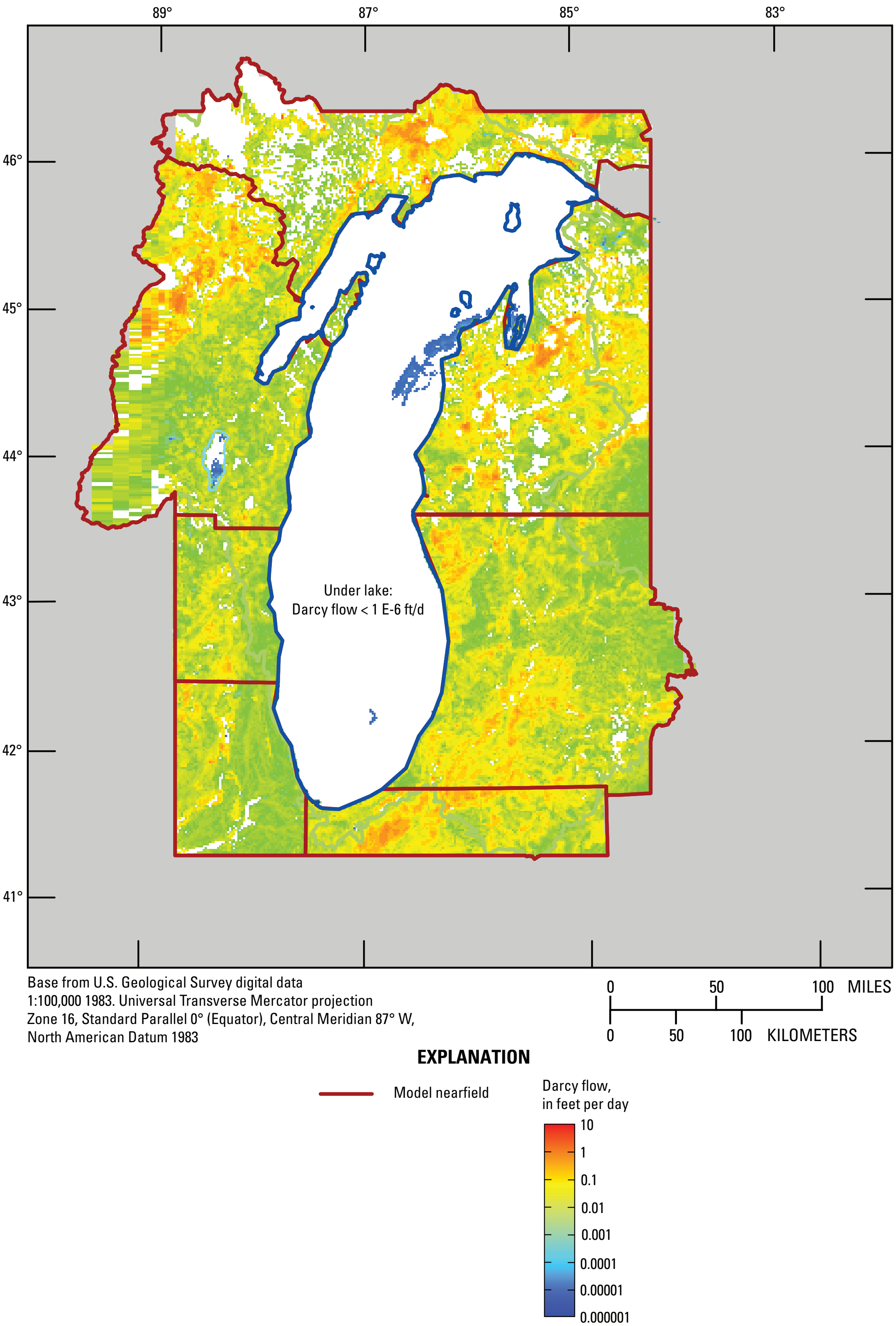

Figure 58. Simulated flow rate (Darcy flow) in model layer 1 for predevelopment conditions.

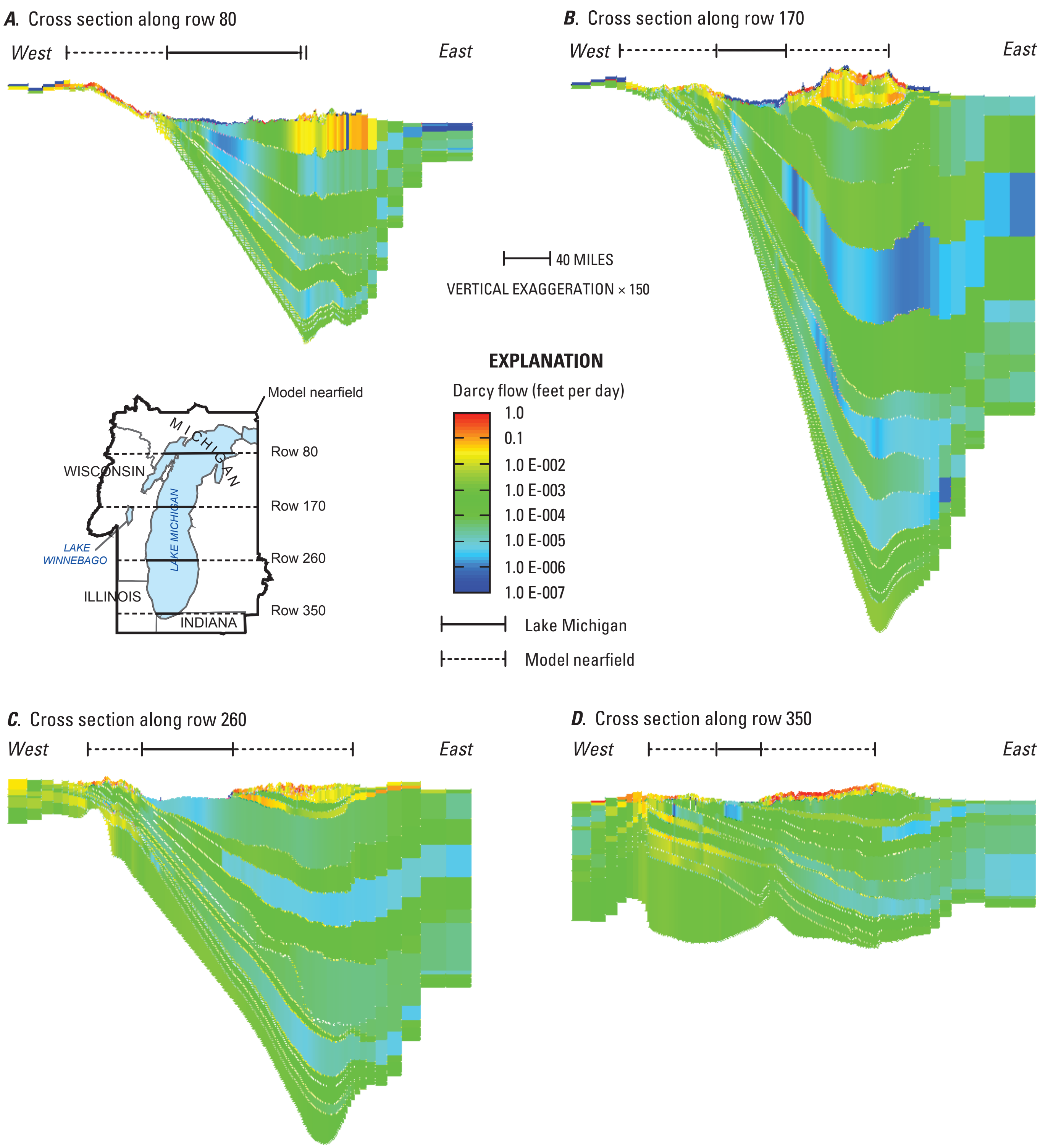

Figure 59. Simulated flow rate (Darcy flow) along selected west/east cross sections for 2005 conditions.

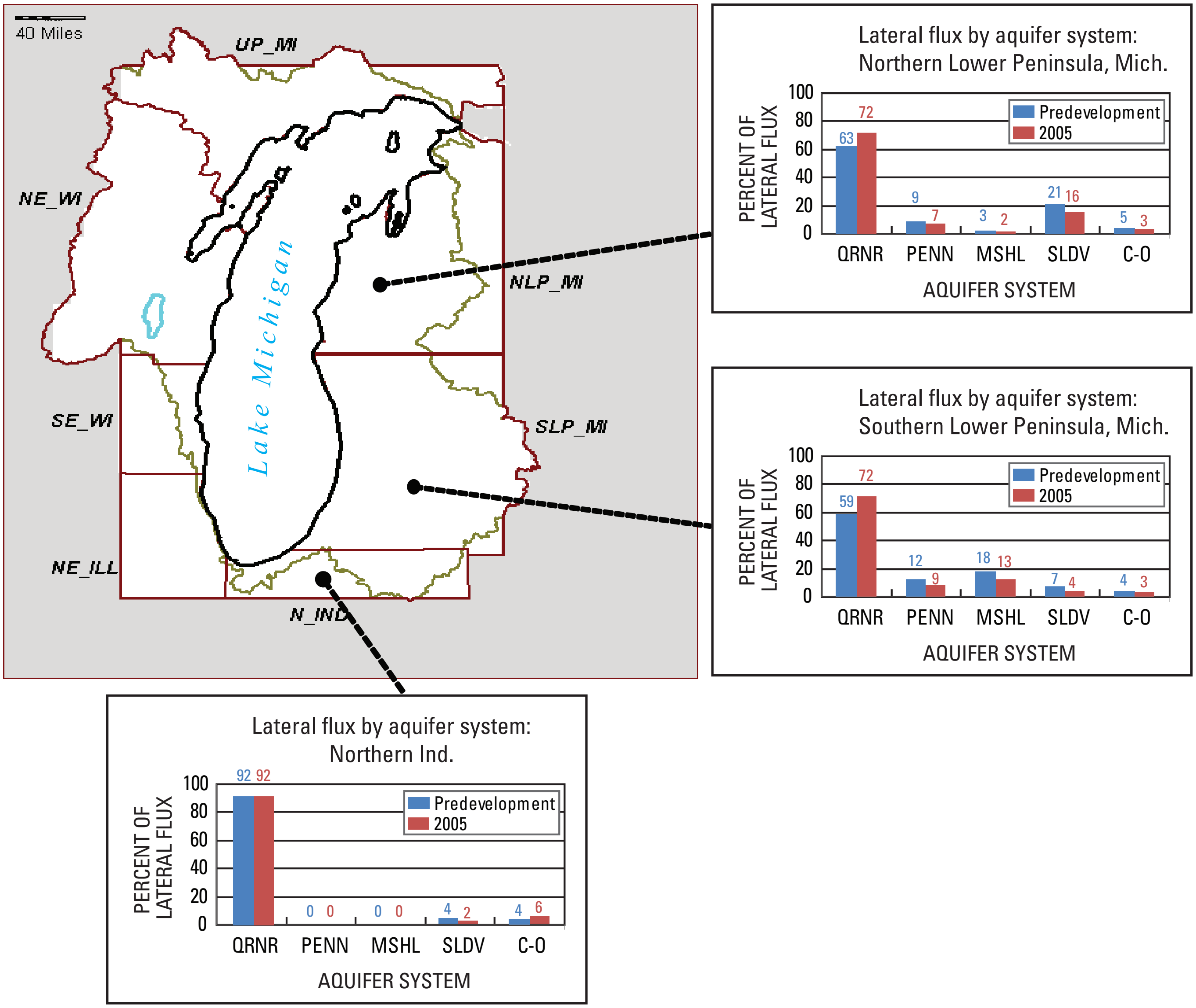

Figure 60*A*. Simulated lateral flux by aquifer system in subregions east of Lake Michigan for predevelopment and 2005 conditions.

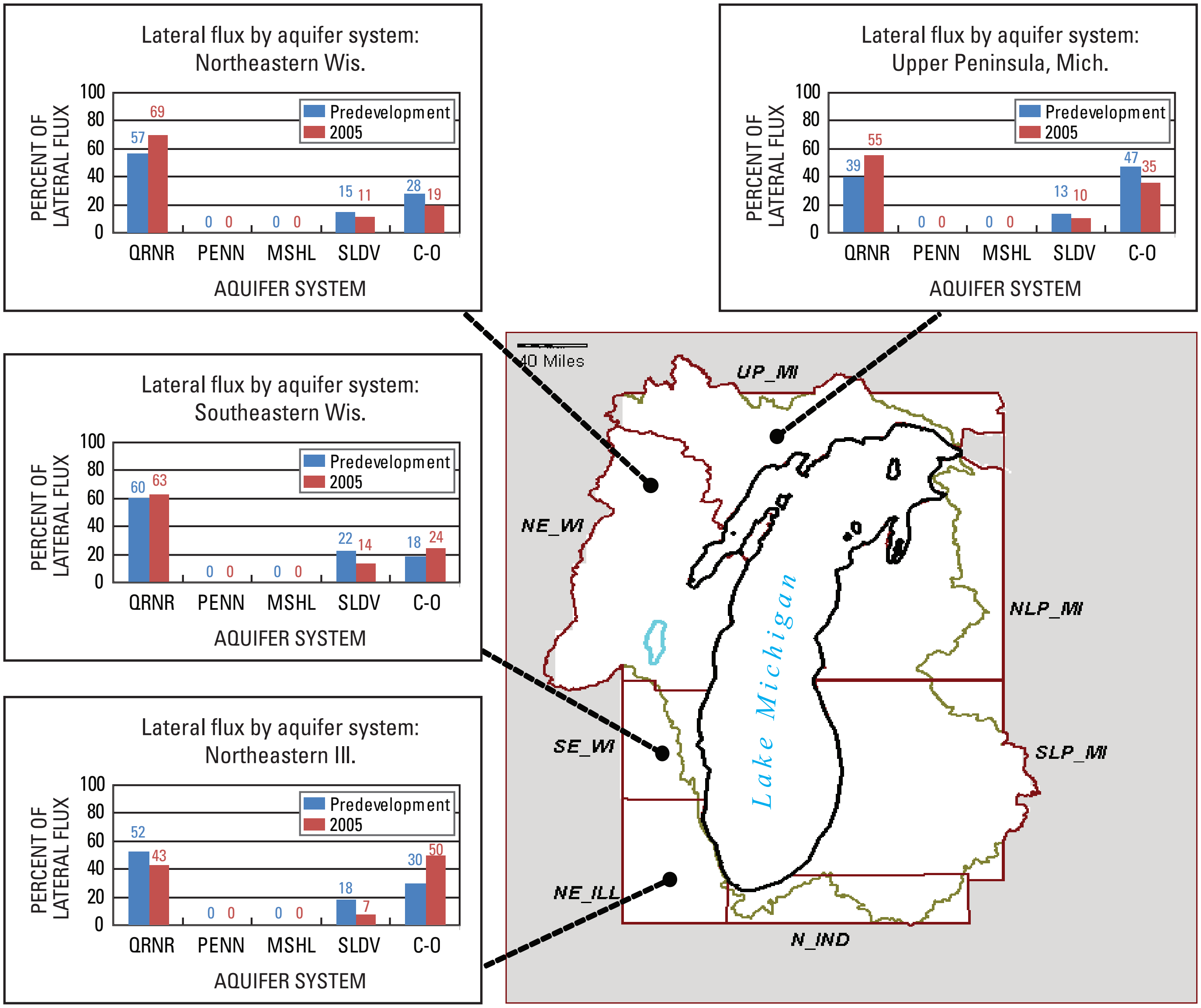

Figure 60*B*. Simulated lateral flux by aquifer system in subregions west of Lake Michigan for predevelopment and 2005 conditions.

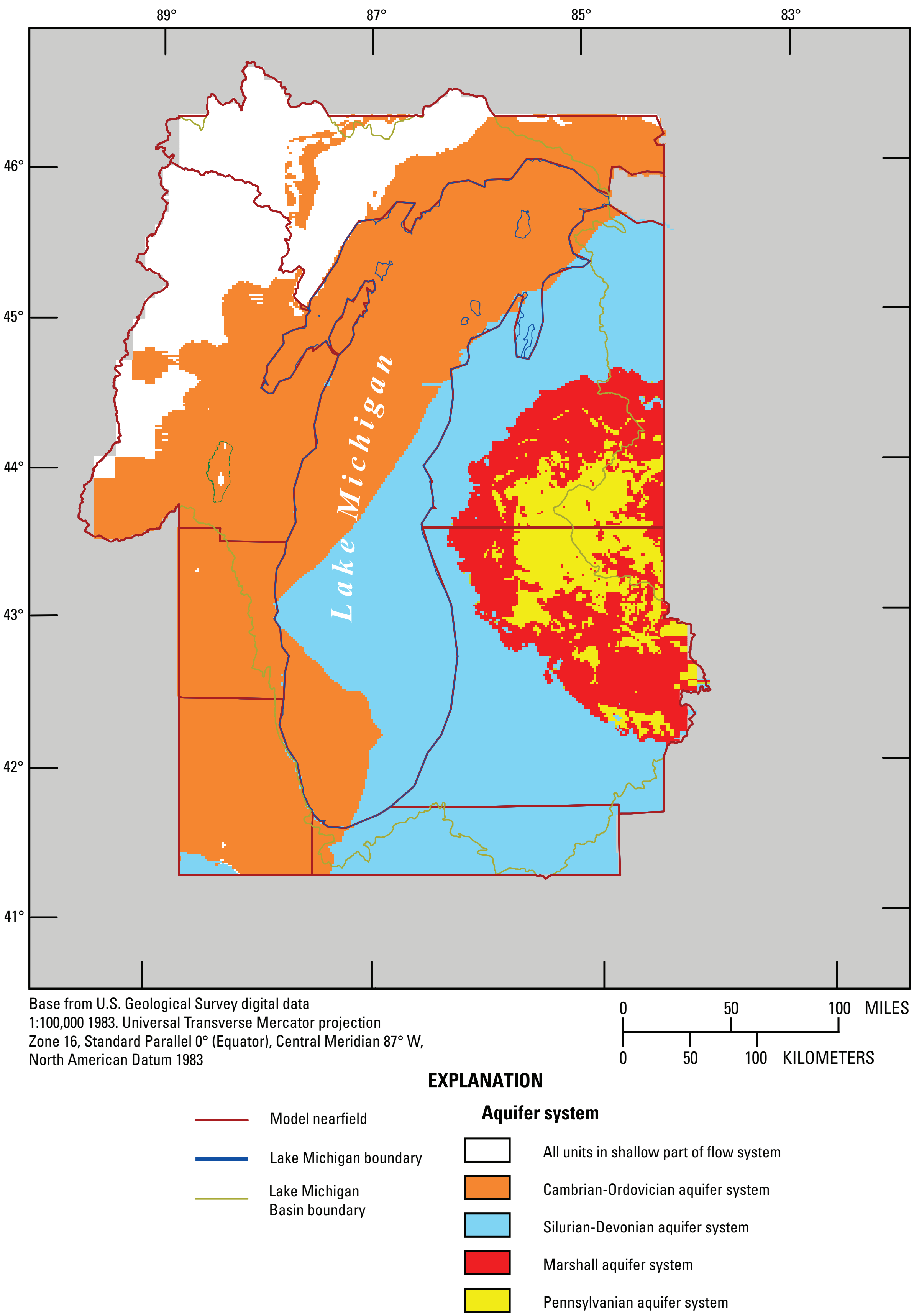

Figure 61. Uppermost aquifer system in deep part of flow system.

The downward leakage of groundwater to the deep part of the flow system under predevelopment conditions accounts for more than 10 percent of recharge in certain nearfield areas in NE_WI and NLP_MI , whereas little downward leakage occurs in broad swaths extending east from the eastern shoreline of Lake Michigan (fig. 62*A*). Flow is *upward* from the deep part to the shallow part of the flow system over large areas bordering the western shoreline of Lake Michigan (white areas in fig. 62*A*). The mixed pattern of upward and downward flow evident in the center of the Michigan Basin and also westward into Wisconsin (including parts of the model farfield not shown in fig. 62*A*) indicates that, in those areas, local circulation extends toward the bottom of the deep part of the flow system, linking recharge zones to discharge zones for the entire thickness of the groundwater system over relatively short distances.

Pumping leaves the pattern of vertical leakage to the deep part of the flow system largely unchanged east of Lake Michigan but decisively alters conditions west of the lake. Mapped conditions in 2005 (fig. 62*B*) show a large area of previously upward flow inland of the Lake Michigan western shoreline where pumping from deep wells now induces downward flow from the shallow part of the flow system to the C-O aquifer system. Over much of SE_WI and NE_ILL, the downward flow is small (on the order of 1 percent of recharge to the water table); but in the western fringe of the model nearfield (and for adjacent areas of the farfield not shown) it increases, according to the model, to well over 10 percent of available recharge. These source areas for deep pumping coincide with areas just west of the subcrop of the Maquoketa Shale where the C-O aquifer system is not confined. The model results indicate that groundwater that once flowed along regional paths to Lake Michigan now is discharged at pumping centers in the vicinity of Milwaukee and Chicago.

6.4 Sources of Water to Pumping Wells

The transfer of water from one part of the flow system to another as a consequence of pumping has implications for groundwater management; for example, source-water protection. In this subsection and the two that follow, confined model results are used to illustrate different ways the groundwater system has responded to pumping. In each case, the analysis applies *particle tracking* to model results by means of MODPATH (Pollock, 1994). This technique moves particles through the simulated flow field in order to delineate the path between sources of water (such as recharge at the water table) and sinks (such as surface water or pumping wells). The procedure also computes the time of travel along a flow path, based on the particle's advective velocity. The advective velocity is equal to the Darcy flow rate simulated by the model at a given location (the sum of the components of flow calculated as the product of hydraulic conductivity and hydraulic gradient in each coordinate direction) divided by the assumed effective porosity (dimensionless) of the sediments. For this application the effective porosity is equated with the specific yields assigned to unconsolidated deposits, carbonate-and-shale-dominated deposits, and sandstone-dominated deposits. The initial specific yields for these three types of units were 0.15, 0.005, and 0.05 respectively (see section 4). On the basis of the calibration of the unconfined version of the model for specific-yield parameter zones (see appendix 5, table A5–2, and section 7), the following values were used:

- QRNR (layers 1–3) = 0.152
- JURA, PEN1, PEN2 (layers 4–6) = 0.070
- MICH, MSHL (layers 7–8) = 0.081
- DVMS, SLDV (layers 9–12) = 0.0049
- MAQU, SNNP (layers 13–14) = 0.0044
- STPT, IRGA, PCFR, EACL, MTSM (layers 15–20) = 0.044

For steady-state conditions before 1864, the flow field is stable, and MODPATH can be applied to the simulation results. After 1864, flow-field conditions changed in response to changes in recharge and pumping. One way to reveal the dynamics of the flow system is to effectively freeze hydraulic gradients and determine particle paths that would exist if conditions corresponding to a particular timeframe were maintained indefinitely. To this end, the input to MODPATH was adjusted to show the rates and directions groundwater flow would tend under conditions that correspond to the end of the model simulation period (1991–2005).[29]

Particle tracking indicates that most recharge under 1991–2005 conditions would circulate through flow paths to surface water or pumping wells in the QRNR aquifer system (fig. 63*A*). However, some of the particles released at the water table infiltrate to bedrock aquifers and discharge to surface water and pumping wells in bedrock aquifers. Contributing areas for wells in both the QRNR and bedrock aquifer systems are delineated by plotting only the particles that terminate at pumped wells (fig. 63*B*). The resulting pattern, for 1991–2005 conditions, indicates that the contributing areas for QRNR wells dominate the areas east of Lake Michigan, with relatively small areas of leakage to PENN and MSHL wells also. West of the lake, contributing areas for SLDV and C-O wells are fairly extensive, with the contributing areas to the C-O wells generally located inland west of the Maquoketa Shale subcrop. According to the model, areas colored white in figure 63*B* are not associated with major contributing areas for wells and indicate source areas that discharge to surface-water features.

[29] To simulate particle tracking under the 1991–2005 conditions, MODPATH was given the head and flux results for the last two stress periods only. In addition, the effective porosities assigned the model were reduced by 1,000 times to speed up the flow sufficiently that the travel between sources and sinks (for example, from the water table to a deep well) is completed over the 15-year period. Subsequently, the output times of flow were multiplied by 1,000 to restore the proper times of flow (for example, if MODPATH reported a traveltime of 12 years, it was corrected to 12,000 years).

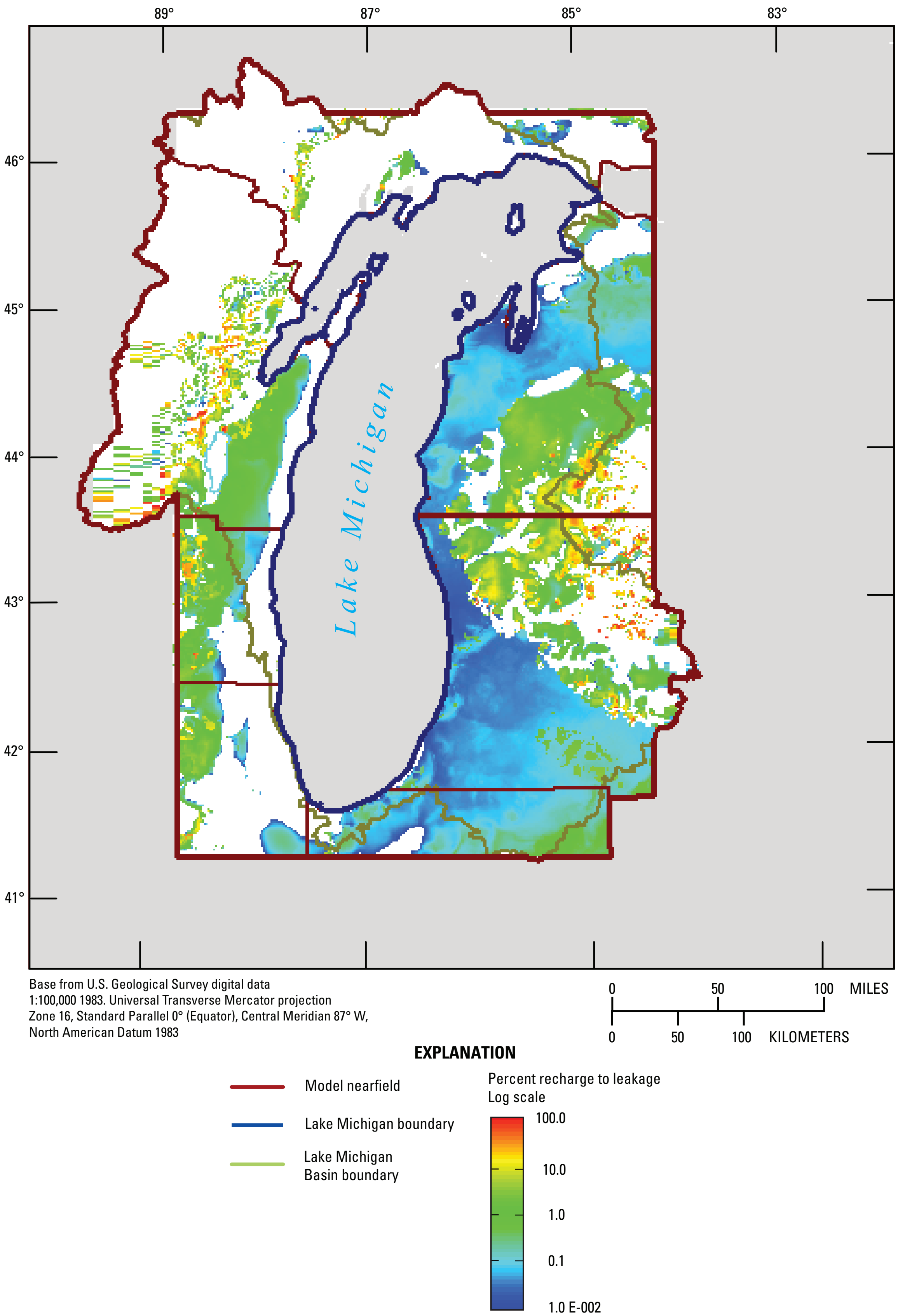

Figure 62*A*. Simulated downward leakage to uppermost aquifer system in deep part of flow system as percent of recharge: Predevelopment. (White areas represent zones of upward flow. The area of Lake Michigan is excluded because the underlying sediment does not receive groundwater recharge.)

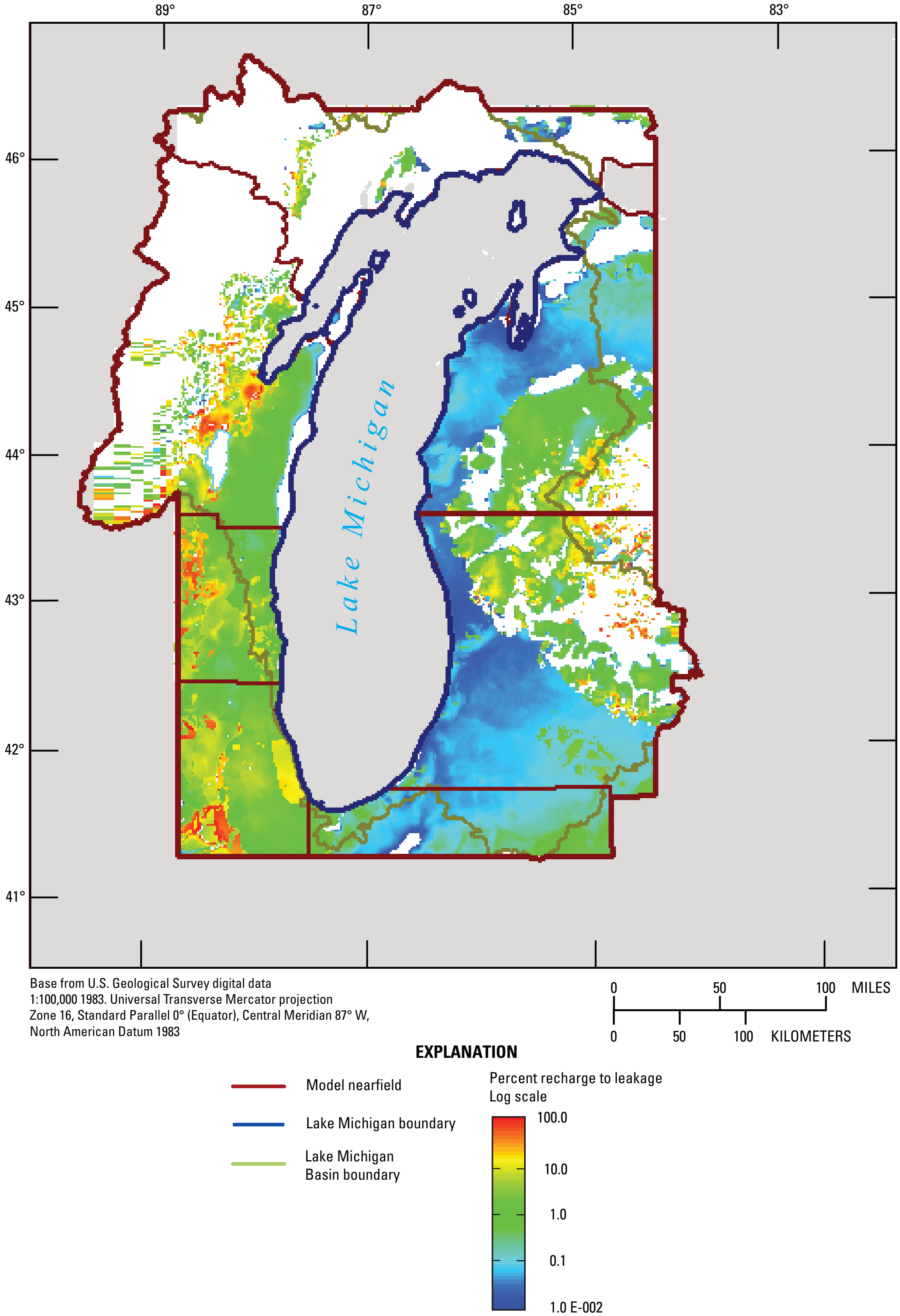

Figure 62*B*. Simulated downward leakage to uppermost aquifer system in deep part of flow system as percent of recharge: 2005. (White areas represent zones of upward flow. The area of Lake Michigan is excluded because the underlying sediment does not receive groundwater recharge.)

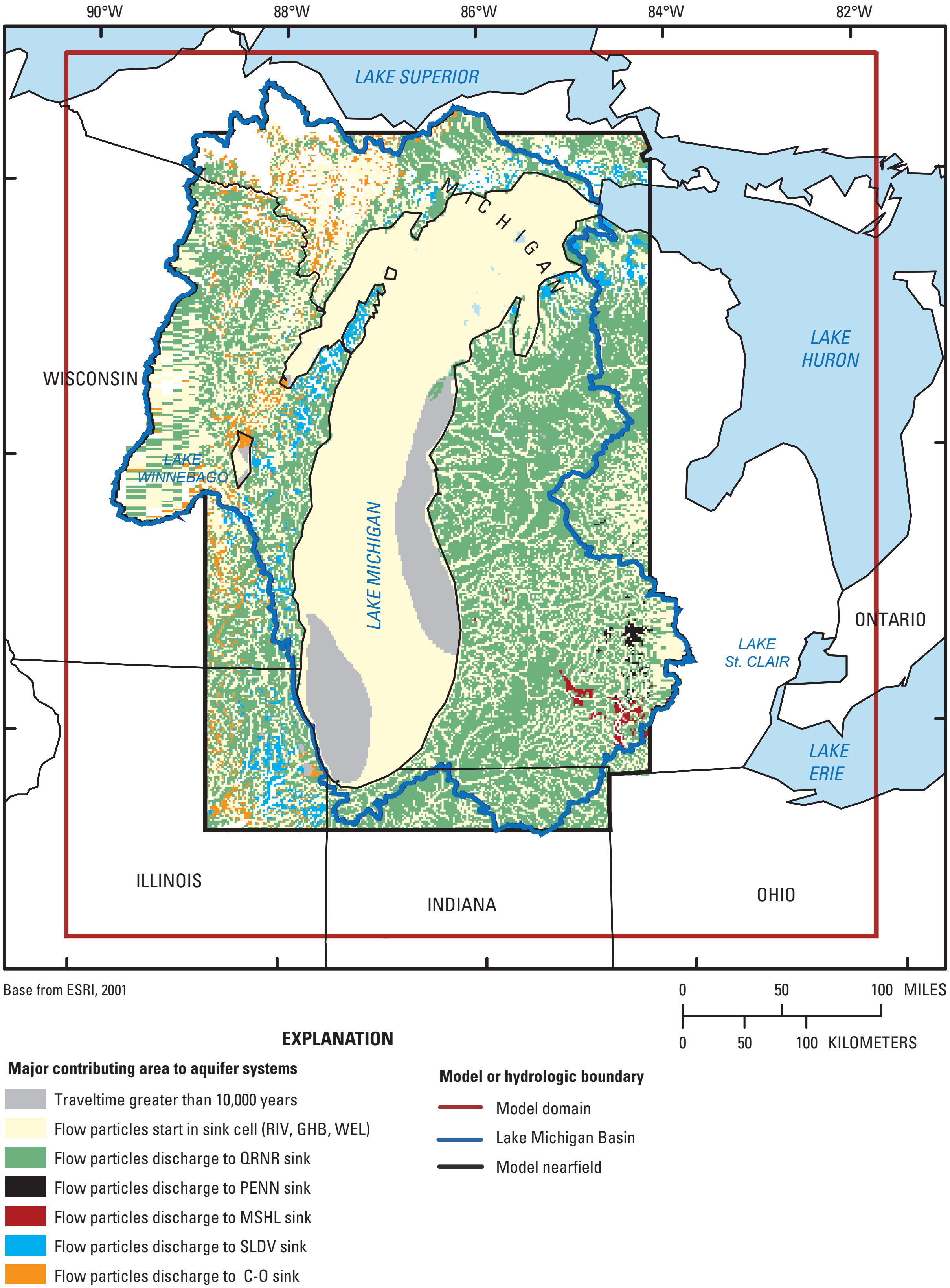

Figure 63*A*. Simulated contributing areas to aquifer-system sinks in 2005.

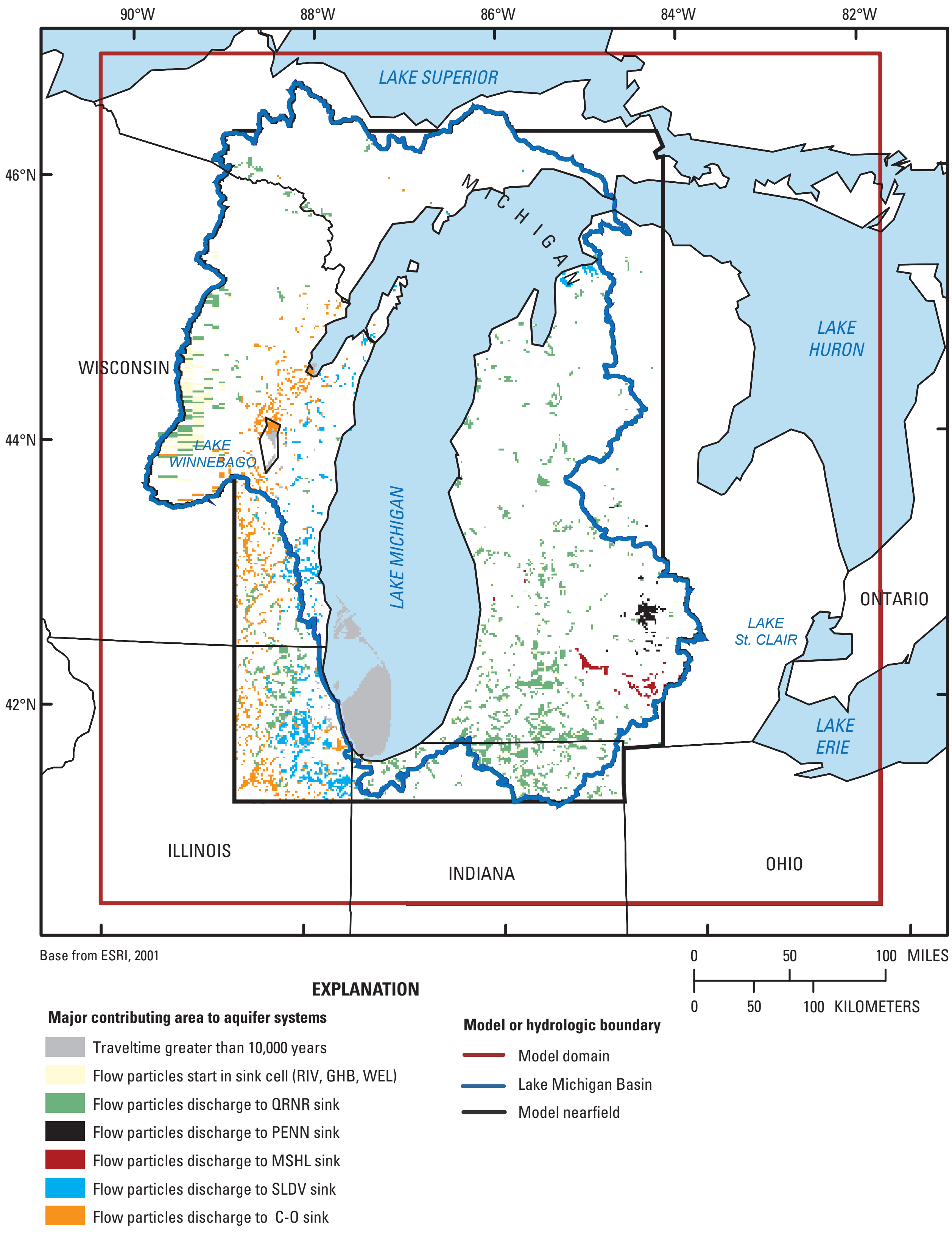

Figure 63*B*. Simulated contributing areas to pumping wells in 2005.

The simulated traveltimes to wells for 1991–2005 fixed conditions vary considerably by aquifer system. Not surprisingly, the median traveltime from the water table to pumping wells increases with the depth of the aquifer system. Circulation of recharge at the water table to wells in the QRNR and PENN systems is typically on the order of 20–30 years. It increases to a median traveltime of 60−70 years for MSHL and SLDV system wells, and then increases sharply to close to 600 years for the C-O system wells (table 15). However, the large variability around the median traveltime simulated by the model also must be recognized. Wells in all aquifer systems can withdraw relatively old water. The 95th percentile for simulated traveltimes (table 15) implies that much of the water withdrawn by C-O wells is much more than 1,000 years old. Noble gas data in conjunction with stable isotopes and ^{14}C ages of groundwater samples collected from C-O pumping wells in southeastern Wisconsin support the finding that some of the water discharged by wells is very old, dating as far back as just after the most recent glaciation, 8,000 or 9,000 years ago (Klump and others, 2008).

Table 15. Time of travel to pumping wells, by aquifer system.

[Traveltimes correspond to 1990–2005 flow conditions. Values correspond to the confined model, SLMB-C. All traveltime statistics are in years]

Aquifer system	Traveltime statistic			
	Average	Median	5th quantile	95th quantile
QRNR	59.3	21.6	2.1	235.7
PENN	174.5	24.2	9.8	389.6
MSHL	135.0	61.8	2.5	459.2
SLDV	110.4	69.7	19.1	311.3
C-O	1,361.1	577.2	44.6	5,804.5

Pumping in the Lake Michigan Basin and adjacent areas has had a profound effect on flow directions and rates, often completely transforming the natural flow pattern and substituting wells for surface-water features as regional sinks. It is instructive in this regard to contrast predevelopment flow directions and rates with 2005 conditions in the vicinity of the important pumping center in northeastern Illinois (fig. 64). Before the onset of high-capacity pumping, groundwater flow—both inland and under Lake Michigan—tended toward the lake at rates typically between 1.0 E−3 and 1.0 E−5 ft/d (fig. 64*A*). The groundwater basin in the bedrock extended far to the west of the Lake Michigan Basin topographic divide. With pumping, flow directions under the lake reversed: rather than acting as a regional sink, the lake is simulated to lose water to the groundwater system, whereas deep flow rates even in saline areas were to some extent increased (fig. 64*B*). In support of the finding that pumping has changed the flow regime in saline areas, an examination of archived data for deep bedrock aquifers in northeastern Illinois shows that, in some locations, dissolved solids in well discharge are increasing (Kelly and Meyer, 2005).

It is important to qualify the sense in which Lake Michigan is a source of water to wells under developed conditions. Although simulated gradients under the lake are reversed, the rate of flow is extremely slow, and, as shown by the gray area in figure 63*B*, pumping would have to be maintained at 2005 levels for thousands of years before any water drawn from Lake Michigan would emerge as well discharge. Although not a direct source of water to wells, parts of the lake do contribute some flow (very small in magnitude at any given location, as evidenced by the very low flow rates registered below the lake in fig. 64*B*), which replenishes water moving under the influence of reversed gradients into the areas of drawdown around pumping centers.

The ultimate sources of water pumped from wells can be quantified by comparing the relative magnitudes of sources and sinks in the simulated groundwater budget under natural conditions (without pumping) and under pumped conditions. The effect of variable recharge on the water budget can be isolated by constructing a version of the calibrated model that contains variable recharge but no pumping. The water budgets computed with this special model version can then be subtracted from the same terms from the calibrated model that contains pumping. The residuals represent the effect of pumping *alone* on the sources and sinks in the model.

For convenience, the sources of water to wells can be combined into four quantities derived from the water budget:

- Reduction in base flow to inland surface-water features combined with induced flow out of inland surface-water features to groundwater.
- Reduction in net direct discharge to Lake Michigan (reduction in direct discharge to the lake plus increased induced flow or out of the lake to groundwater).
- Lateral flow into the area of interest.
- Net release from storage.

The compilation of sources through time for the Lake Michigan Basin shows the dominant role of inland surface water as a source of water to wells pumping within the basin (table 16). The relative contribution of inland surface water increases from 86 percent of all sources for the 1940–50 period to 91 percent for the 1975–80 period, and to 94 percent for the 2001–5 period. Part of this change can be attributed to the relative shift of pumping from deep to shallow wells over time (see table 9). Shallow wells tend to draw more directly from nearby surface-water features, whereas deep wells tend to induce more lateral flow into the area of interest and, at least initially, cause rapid water-level declines that remove water from storage. The drop in the storage contribution after 1980 is attributable to reduced withdrawals in some major pumping centers resulting from a shift to a Lake Michigan water supply and from declining industrial water use.

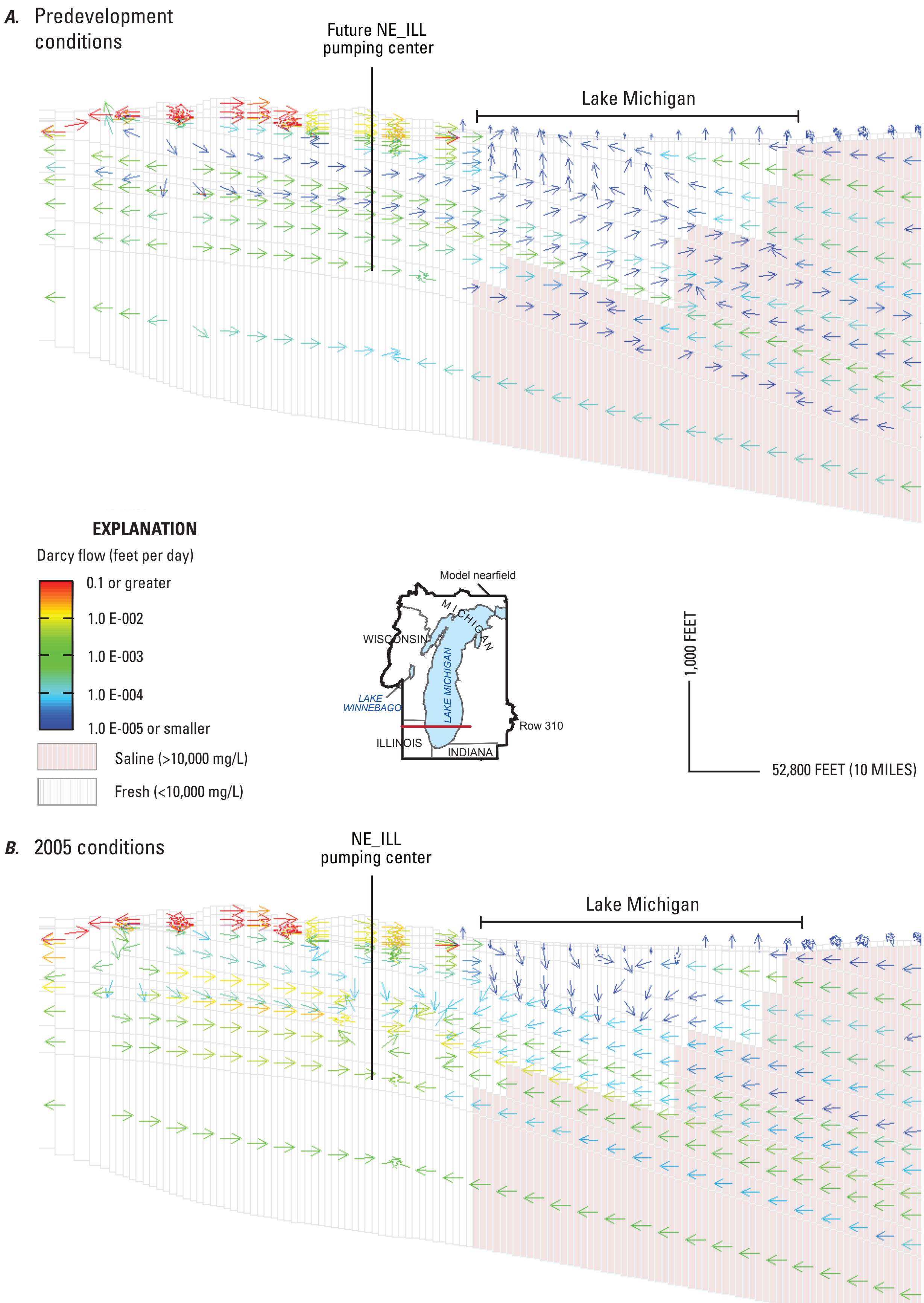

Figure 64. Simulated flow direction and magnitude along west/east cross section in NE_ILL: *A*, Predevelopment. *B*, 2005.

Table 16. Sources of water to pumping wells within Lake Michigan Basin.

[Because recharge changes between stress periods, one cannot simply use the change in direct discharge to Lake Michigan simulated by the model over time to isolate the effect of changes in pumping on flows. Instead, the effect of pumping is calculated by comparing a simulation *without* pumping to a simulation *with* pumping, and computing the difference in flows. Values correspond to the confined model, SLMB-C; Mgal/d, million gallons per day; ---, not applicable]

Stress period	Date	Source to wells from reduced base flow *to* or induced outflow *from* inland surface water (Mgal/d)	Source to wells from reduced discharge *to* or induced outflow *from* Lake Michigan (Mgal/d)	Source to wells from change in lateral flow across Lake Michigan Basin boundary[1] (Mgal/d)	Source to wells from net storage release (Mgal/d)	Total sources to wells (Mgal/d)	Well withdrawals (net of injection) (Mgal/d)	Percent discrepancy due to numerical error
1	Predevelopment	0	0	0	0	0	0	---
2	Oct. 1864–Oct. 1900	7.83	.04	−1.09	1.32	8.10	8.41	−3.58
3	Oct. 1900–Oct. 1920	17.31	.62	−3.27	5.53	20.20	19.97	1.17
4	Oct. 1920–Oct. 1940	48.32	2.53	−3.37	8.25	55.73	55.38	.63
5	Oct. 1940–Oct. 1950	102.41	4.62	−1.67	13.93	119.29	118.82	.40
6	Oct. 1950–Oct. 1960	168.18	6.80	−1.80	14.60	187.78	187.29	.26
7	Oct. 1960–Oct. 1970	250.41	7.23	−1.76	16.96	272.84	272.29	.20
8	Oct. 1970–Oct. 1975	292.42	8.08	−5.88	23.45	318.07	317.54	.17
9	Oct. 1975–Oct. 1980	336.62	9.21	−8.67	31.72	368.87	368.19	.18
10	Oct. 1980–Oct. 1985	393.08	10.18	−9.78	31.04	424.52	423.60	.22
11	Oct. 1985–Oct. 1990	404.88	11.19	−.70	20.83	436.19	435.77	.10
12	Oct. 1990–Oct. 2000	530.10	16.31	7.91	19.78	574.11	576.00	−.33
13	Oct. 2000–Oct. 2005	534.27	16.46	6.90	9.76	567.38	569.52	−.37

[1]Negative values indicate flow out of Lake Michigan Basin to wells in adjacent basins (for example, Mississippi River or Lake Huron Basins).

The relative contribution of sources of water to wells varies not only as a function of time but also as a function of the part of the Lake Michigan Basin under consideration. It is useful to contrast the sources for shallow wells and deep wells by subregion for 2005 conditions. For shallow wells in all subregions, the dominant source of water is diverted or induced flow from streams and inland lakes (fig. 65*A*). For deep wells below confining units, especially in NLP_MI, SE_WI, and NE_ILL, other sources are more important (fig. 65*B*).

The term in the water budget that reflects the effect of pumping on inland surface water can be subdivided into several components:

- Reduction of base flow to streams (“Stream Out”).
- Reduction of base flow to water bodies (“Inland Lake Out”).
- Increase in induced flow out of streams (“Stream In”).[30]

Note that the terms, “Stream Out,” “Inland Lake Out,” and “Stream In” quantify sources of water to wells derived from surface-water features. Through time the most important individual source of water to wells in the Lake Michigan Basin is the reduction of base flow to streams. In 1950, 1980, and 2005, it has accounted according to the SLMB-C model for 60 percent or more of all the sources of water to pumping wells (fig. 66*A–C*). In the Lake Michigan Basin the chief effect of pumping is to reduce base flow to streams. However, it is also important to realize that temporal variations in recharge (see fig. 30) can cause overall base flow to increase despite increased pumping or, alternatively, to decrease more than pumping alone would provoke.

The analysis of the sources of water to wells indicates that, on balance, pumping causes lateral flow to exit the Lake Michigan Basin and flow toward wells in neighboring drainage basins for part of the postdevelopment period (resulting in negative “Outside Basin” terms in fig. 66*A*, *B*). This outflow is caused almost entirely by deep pumping in areas of SE_WI and NE_ILL, which are to the west of the Lake Michigan Basin. The dynamics of the system can be illustrated by comparing the source terms for the *Lake Michigan Basin* to the source terms for the *model nearfield* (fig. 67), which includes, but extends beyond, the basin. The lateral flow source component is inward (positive) to the model nearfield (owing to the effect of pumping centers within the nearfield but west of the Lake Michigan Basin). Moreover, the nearfield net storage contribution is larger than that for the Lake Michigan Basin. For the 1976–80 stress period, for example, the nearfield storage component amounts to 17 percent of the source of water to wells (fig. 67*B*) as opposed to only 9 percent for the Lake Michigan Basin (fig. 66*B*). This comparison shows the sensitivity of the source-of-water-to-wells analysis to the specific area referenced and points to the difference between basins defined by surface-water divides as opposed to those defined by groundwater divides. This finding is discussed further in the next subsection.

6.5 Regional Groundwater Divides

Particle tracking applied to the input and output of the calibrated LMB model can also be used to delineate the configuration of the regional Lake Michigan groundwater basin. For the objectives of this study, the extent of the regional basin is defined by the location of *divides* between areas where water discharges to sinks within the Lake Michigan Basin (that is, to inland surface water or to pumping wells within the drainage area of Lake Michigan, or to Lake Michigan itself) and areas where it discharges to sinks in surrounding basins (those, for example, within the Lake Superior, Lake Huron, Lake Erie, or Mississippi River drainages). It is important to show how the extent of the groundwater basin bounded by its regional divides varies as a function of

- the depth below the water table and
- the absence or presence of pumping.

The influence of depth is shown by mapping the extent of the Lake Michigan groundwater basin for model layers in distinct aquifer systems. The influence of pumping is shown by mapping its extent for predevelopment and for 1991–2005 conditions. Only freshwater areas are mapped to emphasize the availability of subsurface water for human use within and outside of the Lake Michigan Basin.

For all cases analyzed, it is important to contrast (1) the boundary of the regional Lake Michigan groundwater basin separating it from surrounding groundwater basins with (2) the boundary of the Lake Michigan drainage basin separating it from surrounding surface-water drainages. Whereas the outline of surface-water drainage basins is determined by land-surface *topography*, the outline of the groundwater basins is determined by the land surface over which recharge circulates to regional *groundwater sinks*, including deep pumping centers.

[30] As mentioned previously, water bodies such as lakes and wetlands are effectively treated as drains in the LMB model setup and are not permitted to lose water to the groundwater system.

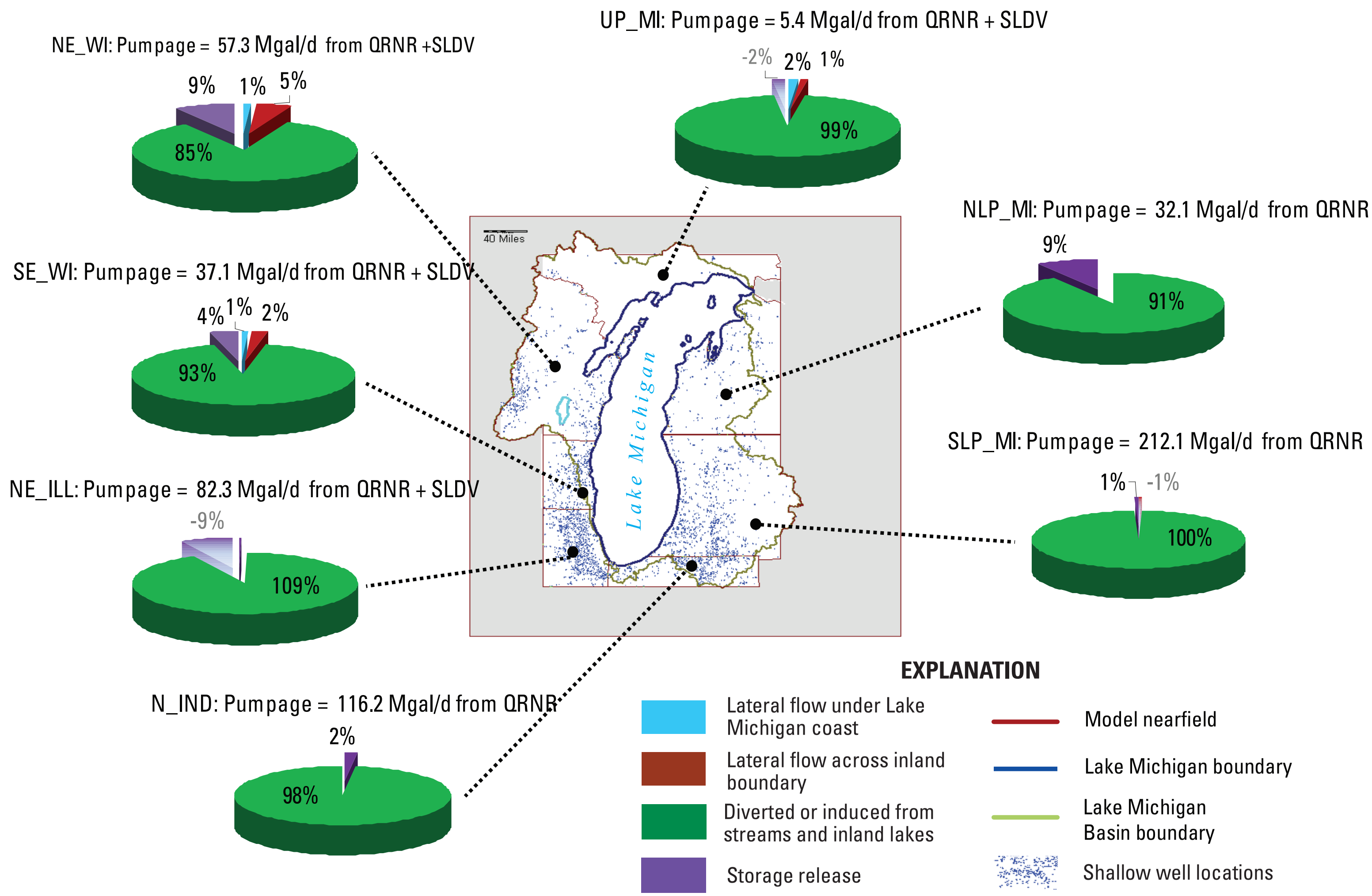

Figure 65A. Sources of water to wells by subregion in 2005: Shallow part of flow system. (Negative values (in shadow) indicate storage gain or lateral flow out of subregion. Lateral flow toward wells is distinguished as a source by whether it moves under the Lake Michigan shoreline into a subregion or whether it moves across an inland boundary into a subregion.)

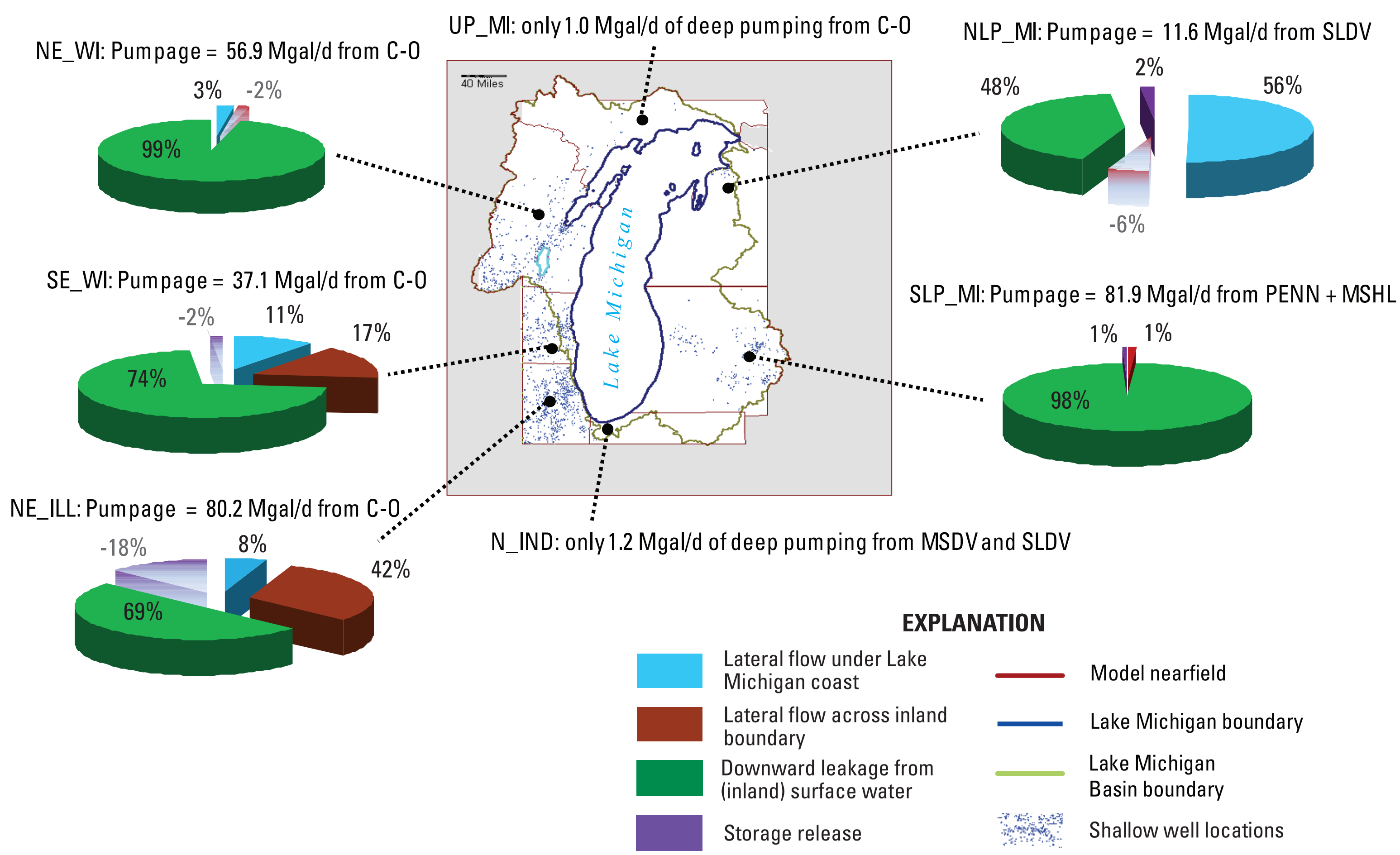

Figure 65*B*. Sources of water to wells by subregion in 2005: Deep part of flow system. (Negative values (in shadow) indicate storage gain or lateral flow out of subregion. Lateral flow toward wells is distinguished as a source by whether it moves under the Lake Michigan shoreline into a subregion or whether it moves across an inland boundary into a subregion.)

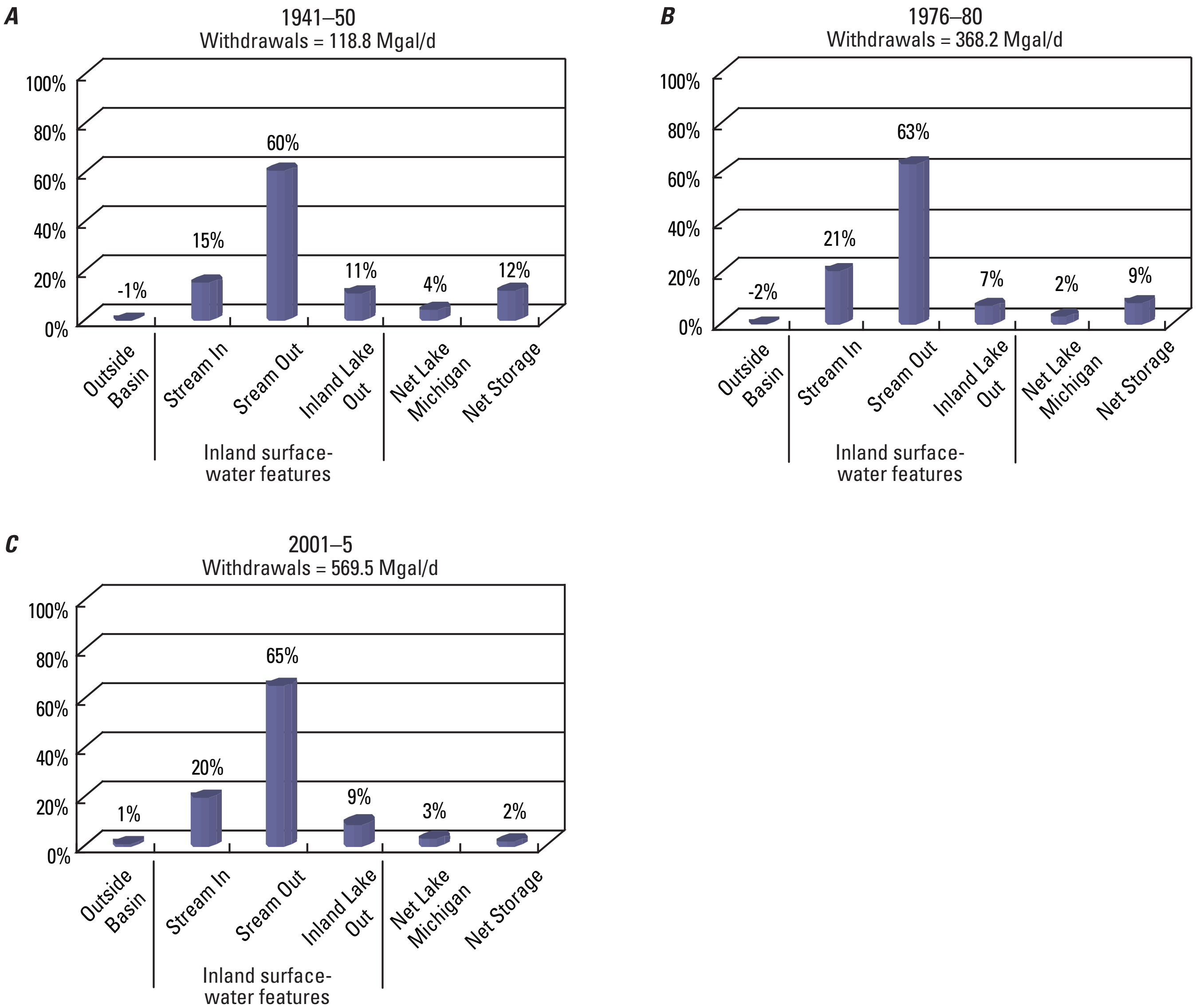

Figure 66. Sources of water to wells for Lake Michigan Basin: *A*, 1941–50. *B*, 1976–80. *C*, 2001–5. (**Outside Basin** is inflow from neighboring surface-water basins toward wells; when negative, the term represents a loss to pumping outside the Lake Michigan Basin. **Stream In** is induced flow from streams toward wells; **Stream Out** is diverted base flow from streams toward wells. **Inland Lake Out** is diverted base flow from inland lakes toward wells. **Total Lake Michigan** is diverted discharge to the lake plus induced flow from the lake toward wells. **Net Storage** is storage release around pumping wells minus storage gain around deactivated wells or injection wells.)

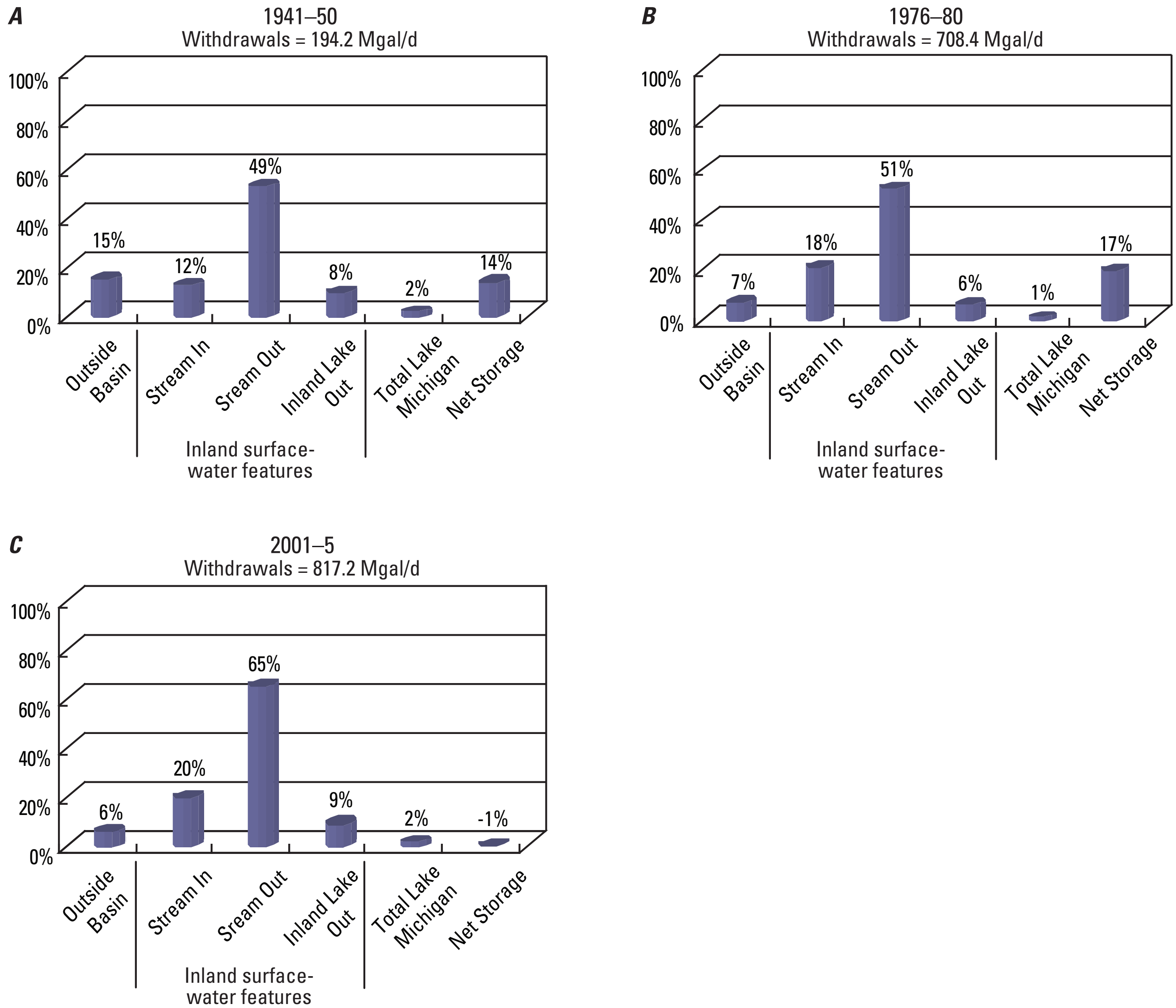

Figure 67. Sources of water to wells for model nearfield: *A*, 1941–50. *B*, 1976–80. *C*, 2001–5. (**Outside Basin** is inflow from neighboring surface-water basins toward wells; when negative, the term represents a loss to pumping outside the Lake Michigan Basin. **Stream In** is induced flow from streams toward wells; **Stream Out** is diverted base flow from streams toward wells. **Inland Lake Out** is diverted base flow from inland lakes toward wells. **Total Lake Michigan** is diverted discharge to the lake plus induced flow from the lake toward wells. **Net Storage** is storage release around pumping wells minus storage gain around deactivated wells or injection wells.)

The extent of the Lake Michigan groundwater basin simulated by the SLMB-C model for *predevelopment* conditions closely matches the extent of the Lake Michigan drainage basin for layers representative of the QRNR, PENN, and MSHL aquifer systems (figs. 68*A*–*C*). The maps indicate that groundwater flowing through these aquifer systems discharges to surface-water features within the surface-water basin. The predevelopment divides, which identify groundwater flow in the SLDV and C-O aquifer systems that discharges to surface-water features within the Lake Michigan drainage basin, do not coincide with the drainage boundaries (figs. 68*D*, *E*). The differences for the SLDV aquifer system are most marked in northern Indiana, where groundwater circulating through the dolomite in areas south of the Lake Michigan drainage area ultimately discharges to surface-water sinks to the north within the Lake Michigan drainage area. The differences for the C-O aquifer system (represented by a map of the groundwater basin in the IRGA unit, fig. 68*E*) are most marked in SE_WI and NE_ILL, where the groundwater-basin divides bulge westward into parts of the neighboring drainage basin. For both these deep aquifer systems, the lateral enlargement of the Lake Michigan groundwater-basin area at the expense of surrounding groundwater basins is fairly sizable, exceeding 20 mi.

The configuration of regional groundwater divides is more complicated after 1864 once high-capacity wells perturb the flow system. Two sets of sinks—surface-water features and pumping wells— compete for groundwater. Wells in the Lake Michigan Basin can draw water from surrounding surface-water basins, and clearly the opposite also can occur. For this reason it is useful to map the extent of the groundwater basin by means of four distinct colors that delineate areas which contribute groundwater to

- surface-water features within the Lake Michigan Basin,
- pumping wells within the Lake Michigan Basin,
- surface-water features outside the Lake Michigan Basin, and
- pumping wells outside the Lake Michigan Basin.

The combination of the first two areas constitutes the Lake Michigan groundwater basin under postdevelopment conditions. The postdevelopment period is represented by flow rates and directions simulated for the 1991–2005 model stress periods.

According to model results, pumping does not cause transfers from one regional surface-water drainage basin to another in the PENN and MSHL aquifer systems (figs. 69*B*, *C*). The groundwater-basin maps distinguish areas where flow discharges to surface water (light blue) from areas where it discharges to shallow or deep pumping wells (dark blue). For the uppermost QRNR system, cross-basin transfers occur in NE_ILL because shallow and deep wells outside of the Lake Michigan Basin are close to a drainage boundary that is almost coincident with the lakeshore (fig. 69*A*). The areas (mapped orange) under Lake Michigan contribute water to pumping wells in the Mississippi Basin. Elsewhere, areas contributing QRNR groundwater to surface-water sinks cover most of the model domain for both the Lake Michigan and surrounding drainage basins, but there are large stretches where flow generally terminates at pumping wells (for example, in NE_WI, in a zone of intensive irrigation on both sides of the boundary between the Lake Michigan and Mississippi River Basins).

For the SLDV aquifer system the contrast between groundwater divides under predevelopment conditions (fig. 68*D*) and postdevelopment conditions (fig. 69*D*) simulated by the model is particularly noticeable for the southern part of Lake Michigan. Pumping reversed the direction of much of the flow through the Silurian and Devonian units that originally discharged to the lake. Some of that flow moves from under Lake Michigan to wells in NE_ILL located in the Mississippi River drainage. The effects are even more dramatic for units in the C-O aquifer system (compare figs. 68*E* and 69*E*). The groundwater circulating under all NE_ILL and adjacent areas of Lake Michigan discharges under 1991–2005 conditions to pumping wells west of the Lake Michigan Basin. The strength of the NE_ILL deep pumping center is evident in the shift of postdevelopment groundwater divides. In SE_WI, a shift is also evident, again at the expense of the size of the Lake Michigan groundwater basin. Pumping wells in the Mississippi Basin discharge deep groundwater flow that discharged toward Lake Michigan under predevelopment conditions. The cross-basin transfers are complicated along the drainage boundaries in this area; maps for other aquifers in the C-O system (STPT, MTSM) show slightly different divides than the ones mapped for the IRGA. The simulated divide between the Lake Michigan and Mississippi River groundwater basins can vary in location by several miles depending on the C-O unit selected. Finally, it is worth noting the large effect that deep pumping has had on the location of C-O groundwater divides in parts of NE_WI.

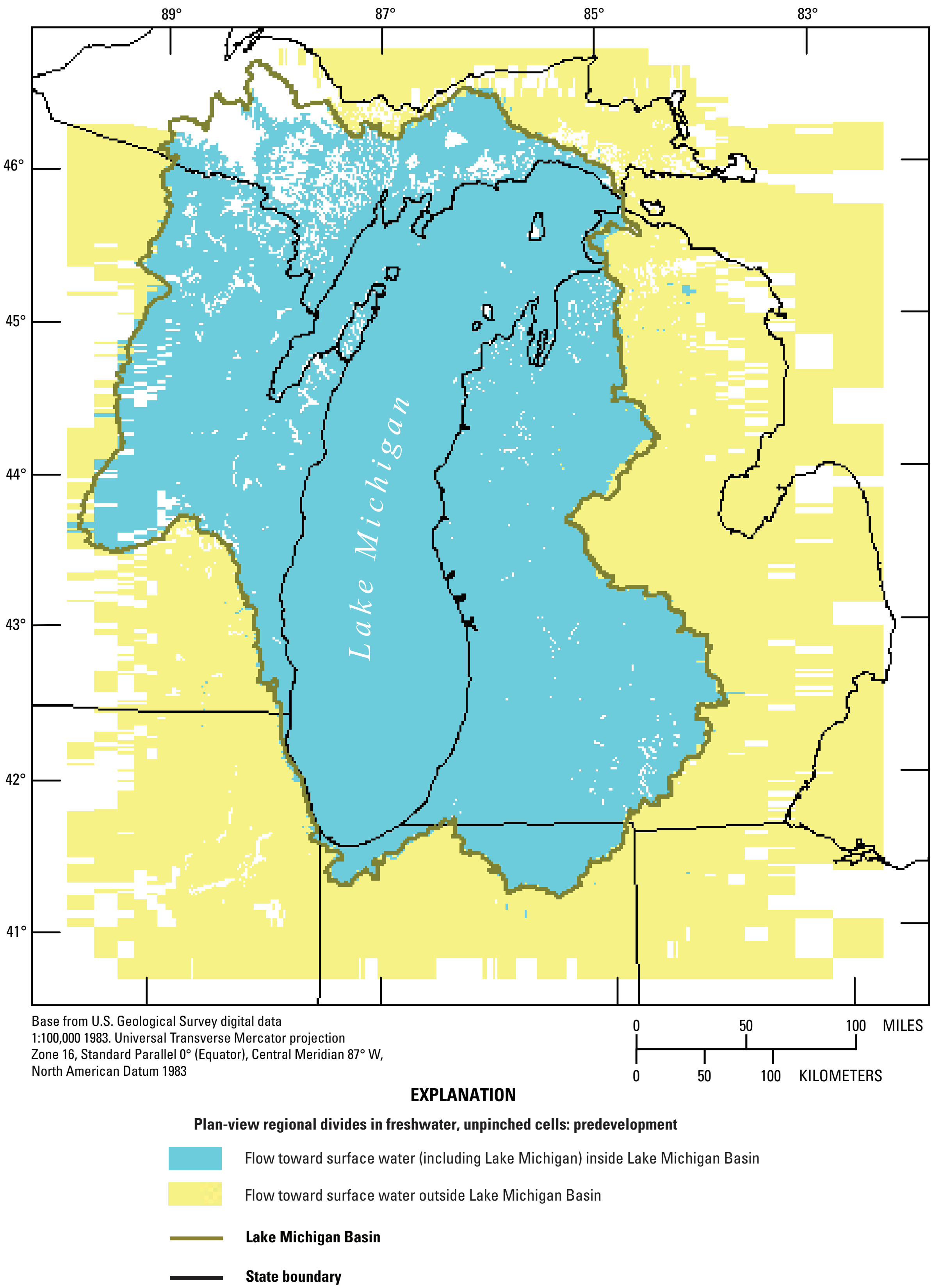

Figure 68*A*. Simulated groundwater basins, by aquifer system, for predevelopment conditions: QRNR (layer 1).

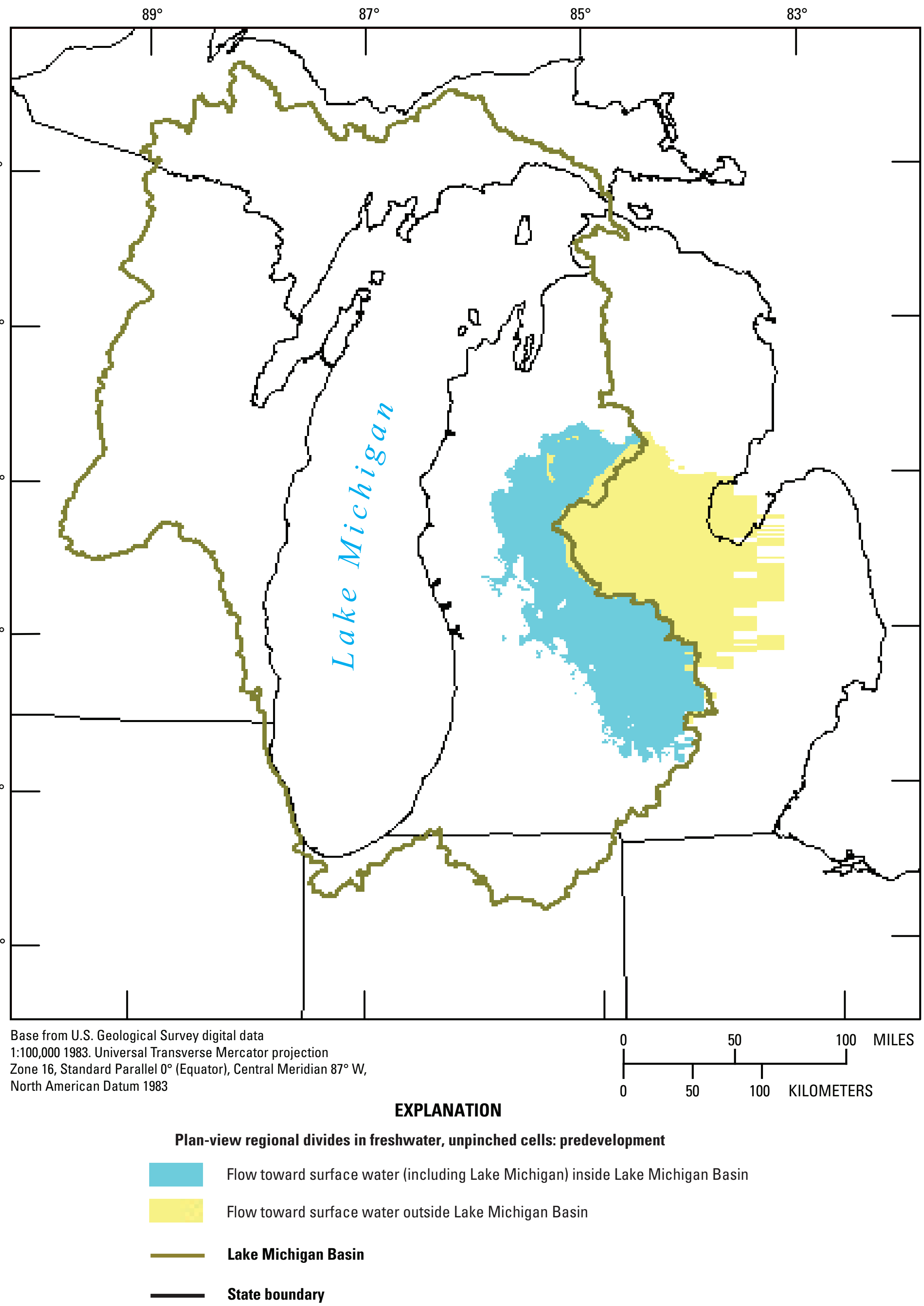

Figure 68*B*. Simulated groundwater basins, by aquifer system, for predevelopment conditions: PENN (layer 5).

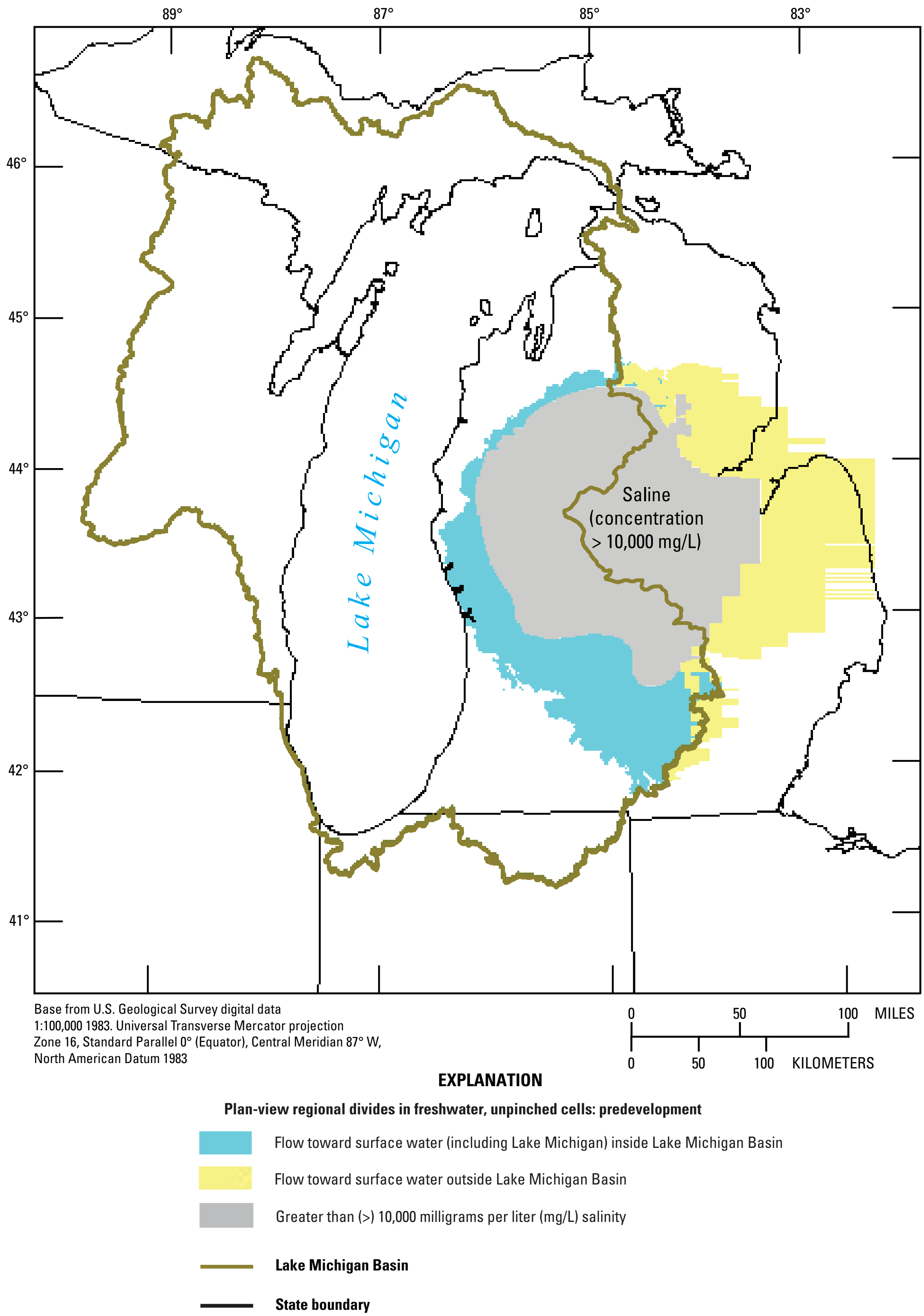

Figure 68*C*. Simulated groundwater basins, by aquifer system, for predevelopment conditions: MSHL (layer 8).

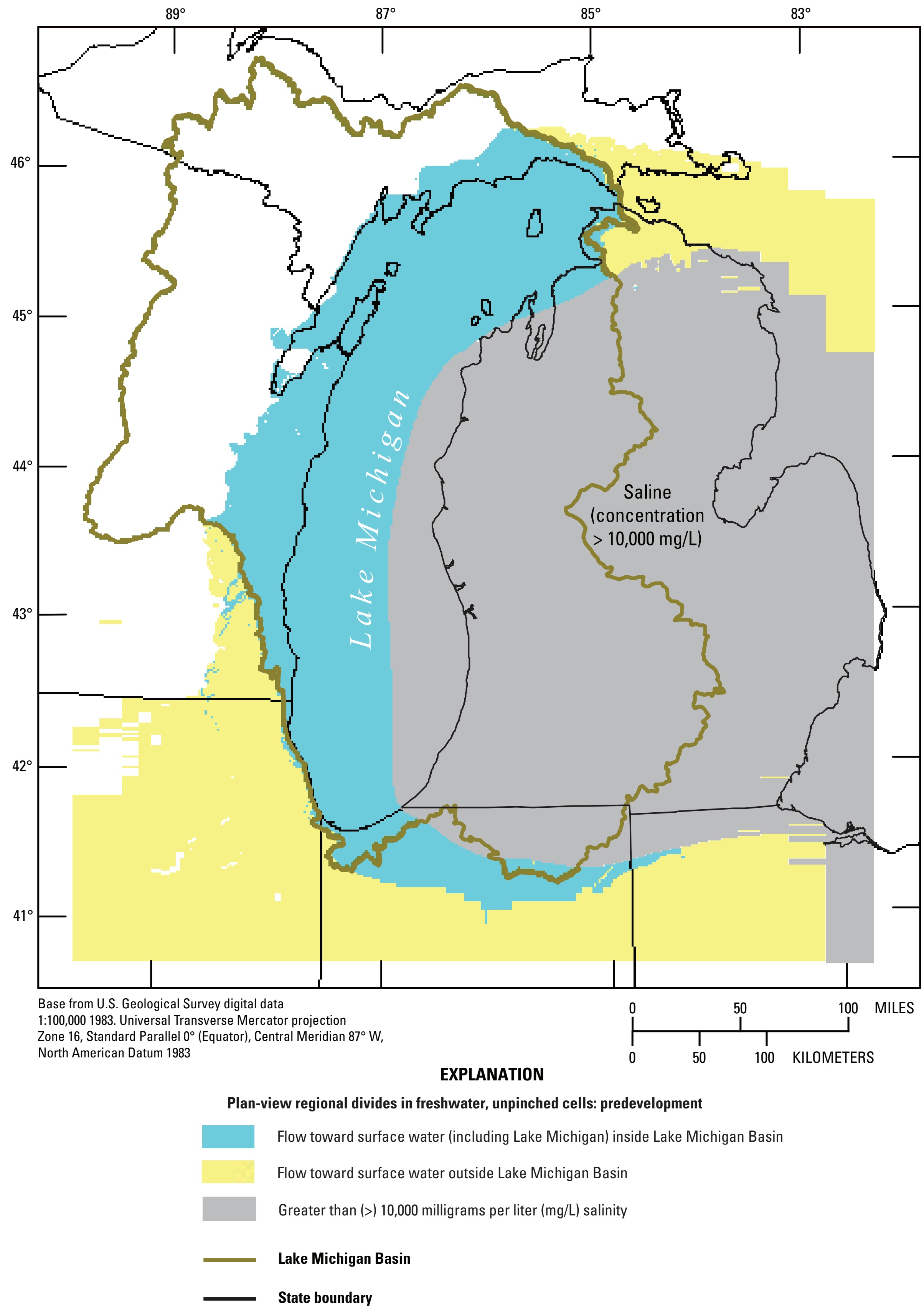

Figure 68*D*. Simulated groundwater basins, by aquifer system, for predevelopment conditions: SLDV (layer 10).

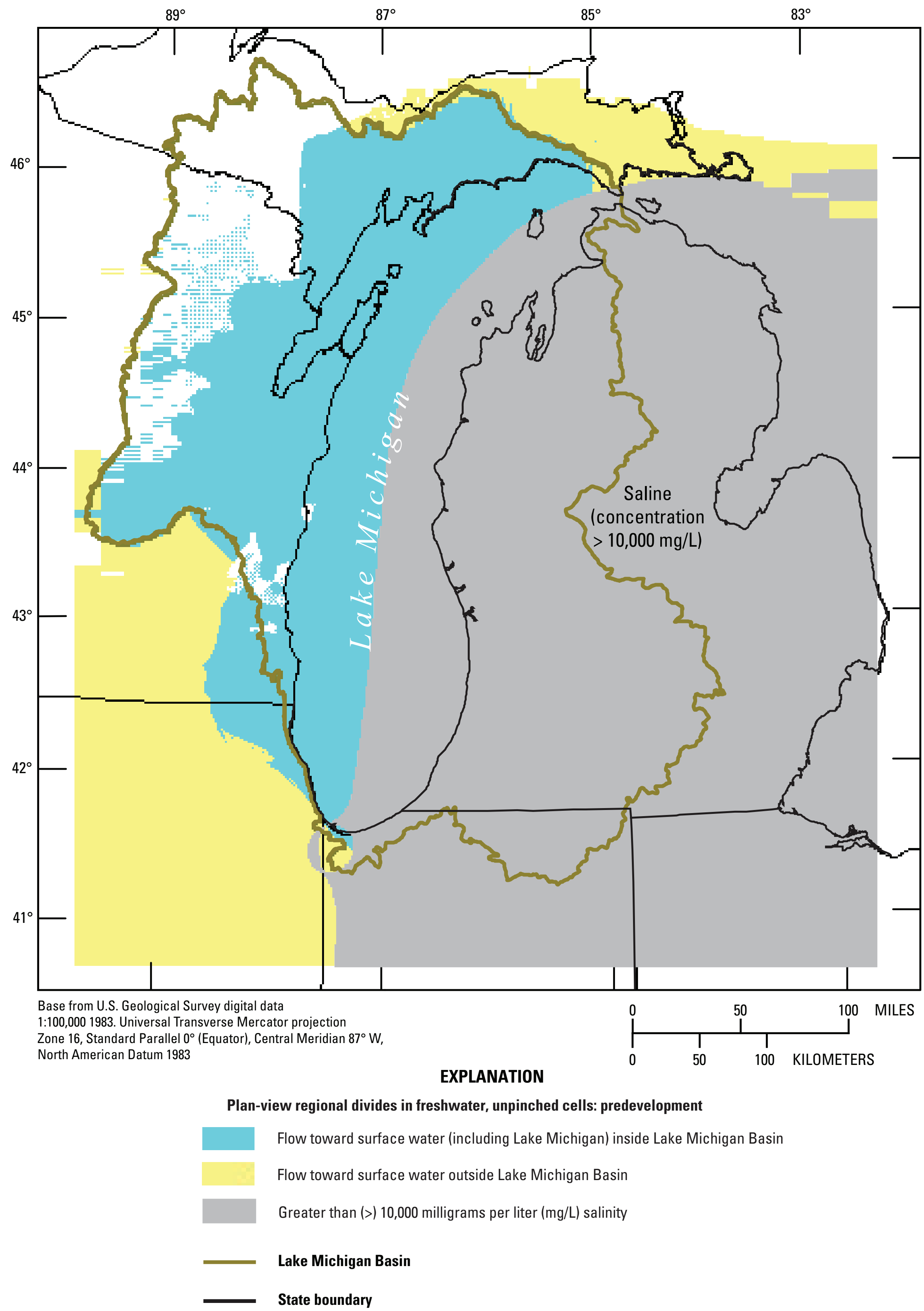

Figure 68*E*. Simulated groundwater basins, by aquifer system, for predevelopment conditions: C-O (layer 17).

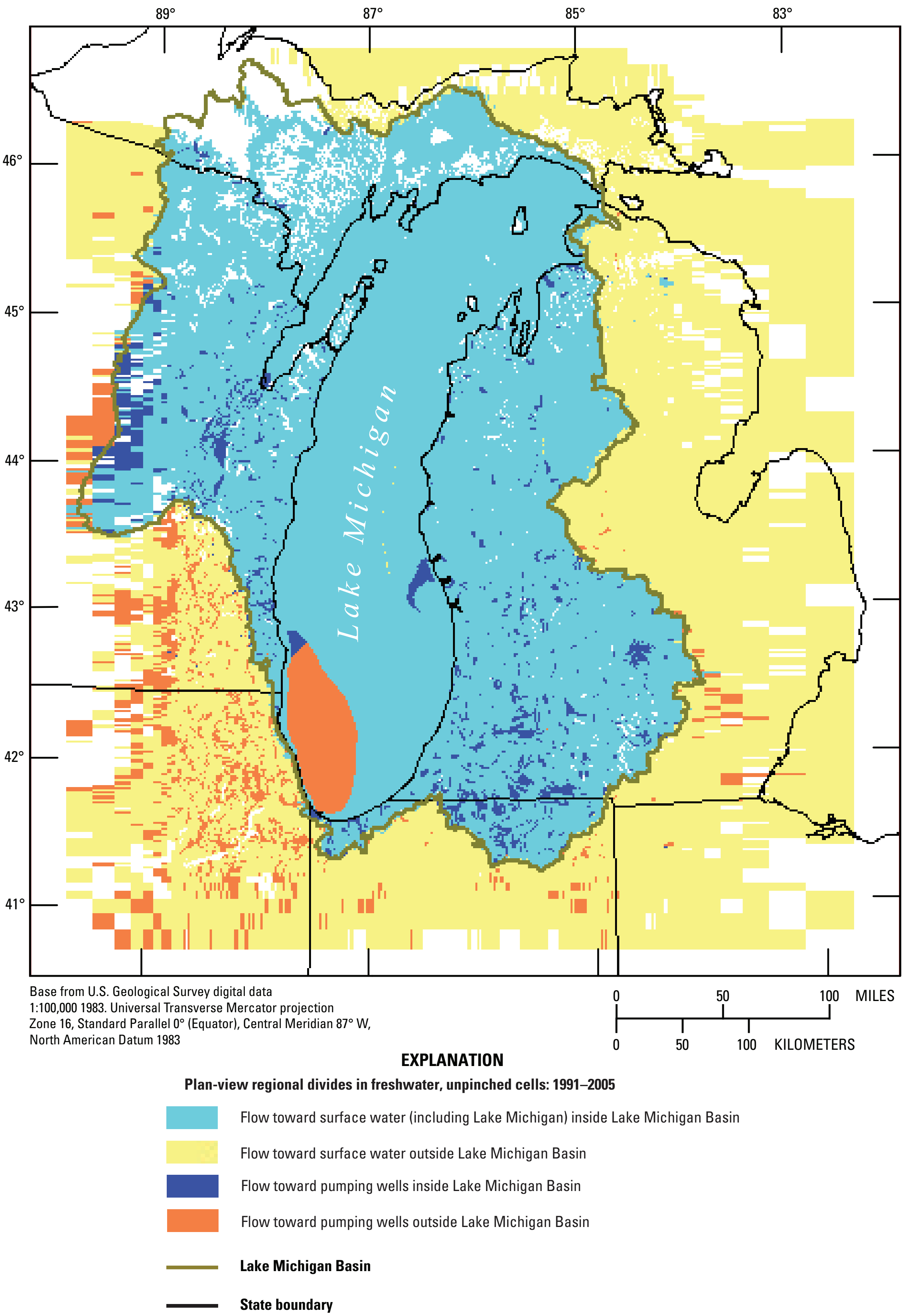

Figure 69*A*. Simulated groundwater basins, by aquifer system, for 1991–2005 conditions: QRNR (layer 1).

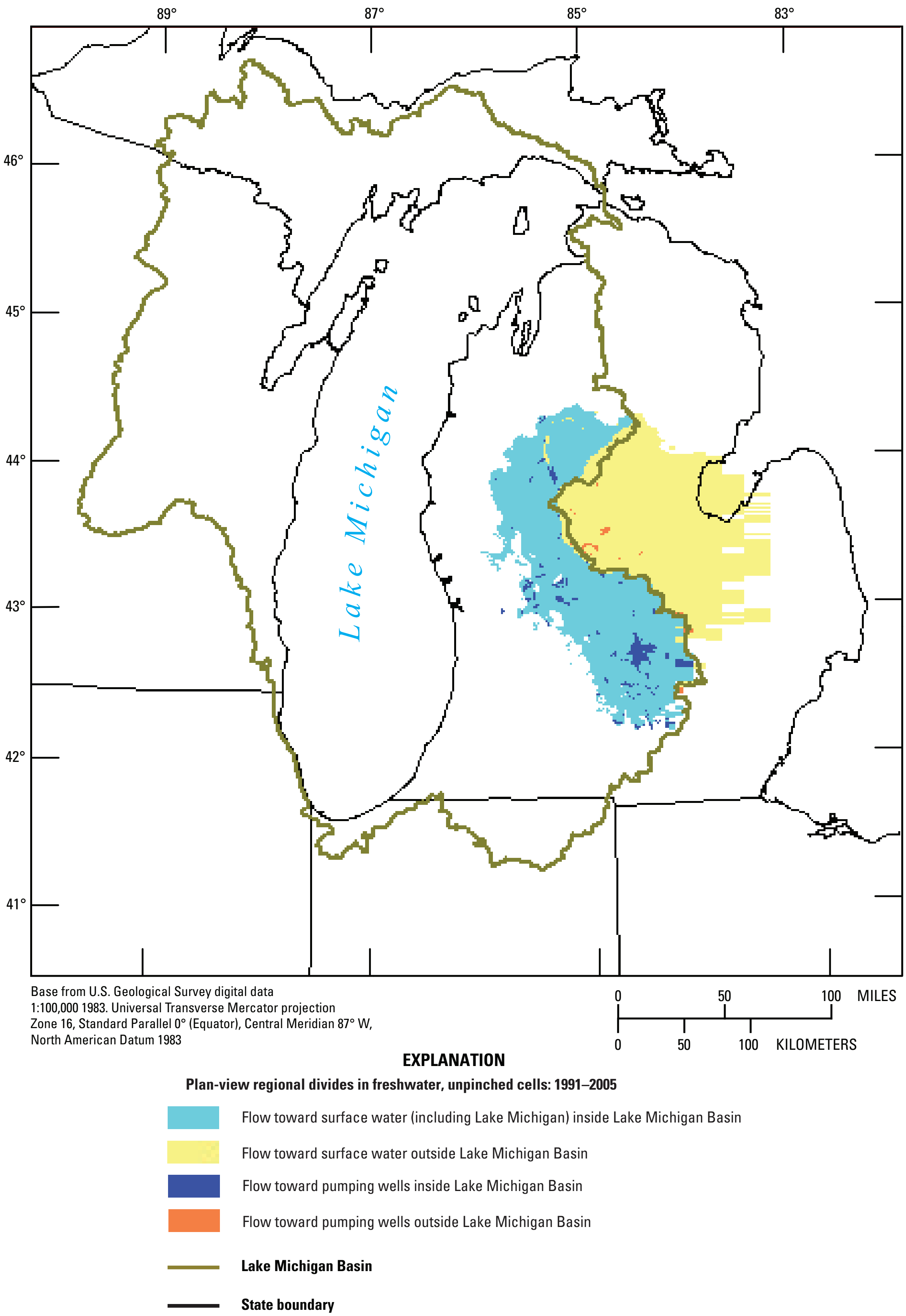

Figure 69*B*. Simulated groundwater basins, by aquifer system, for 1991–2005 conditions: PENN (layer 5).

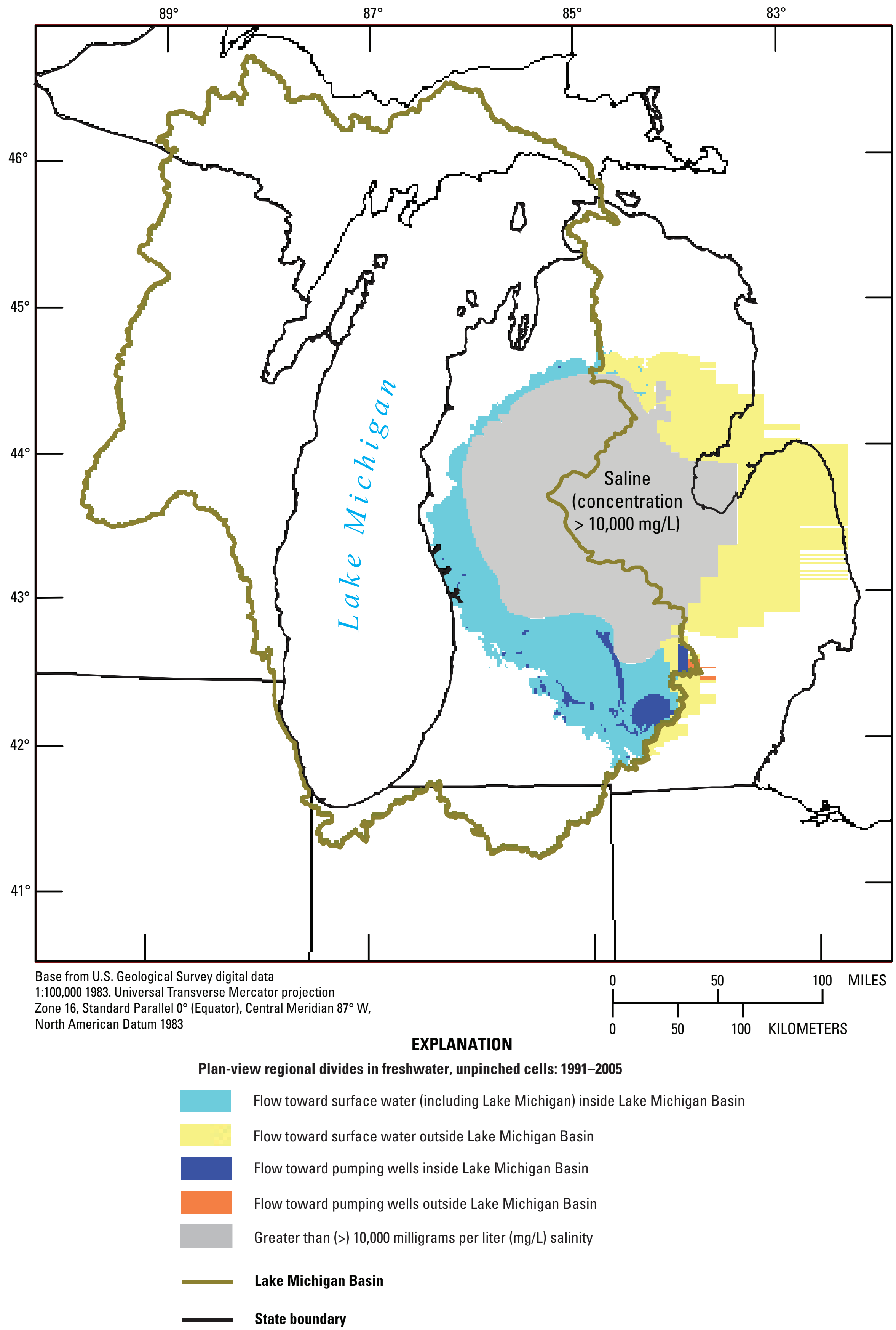

Figure 69*C*. Simulated groundwater basins, by aquifer system, for 1991–2005 conditions: MSHL (layer 8).

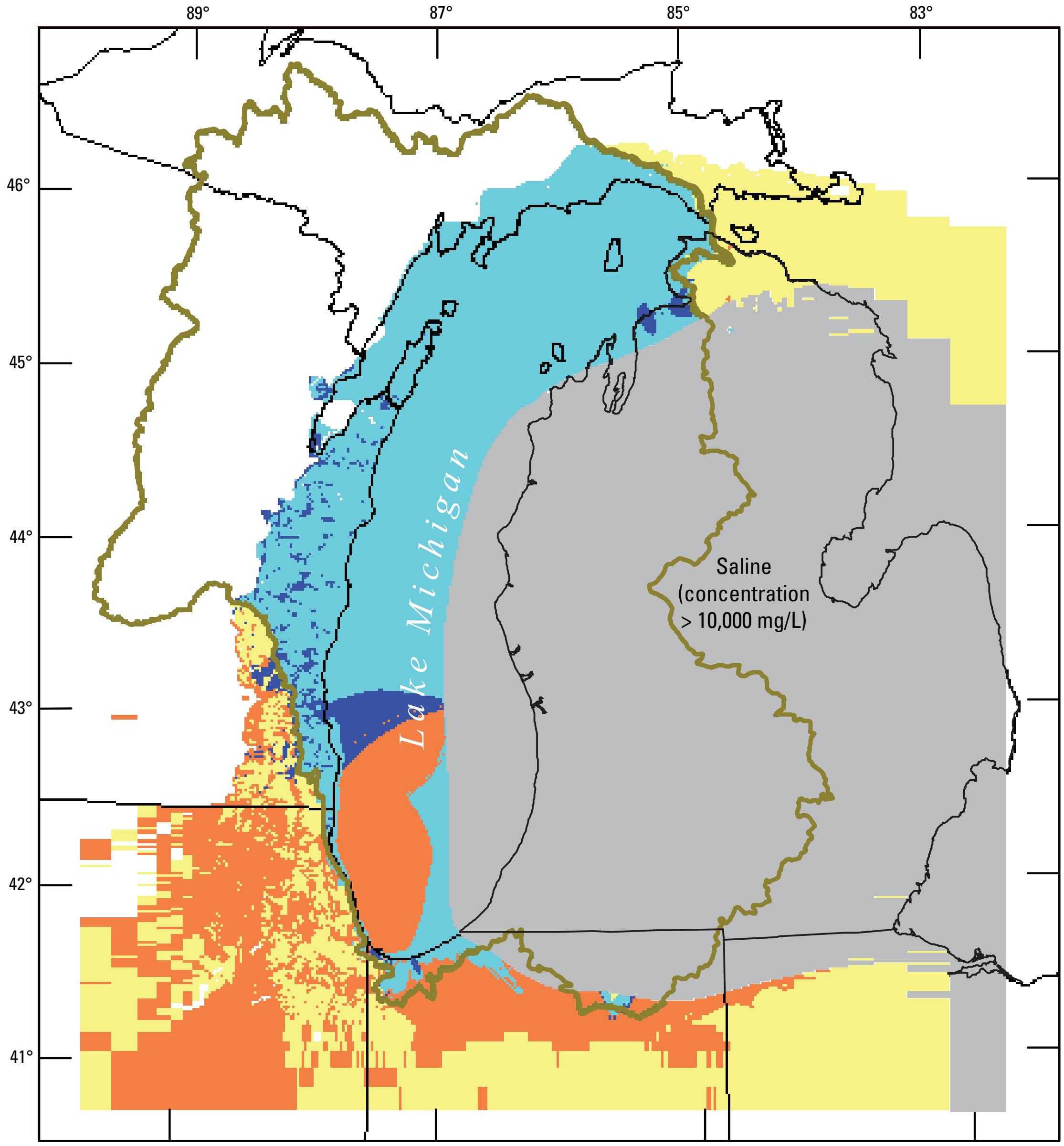

Base from U.S. Geological Survey digital data
1:100,000 1983. Universal Transverse Mercator projection
Zone 16, Standard Parallel 0° (Equator), Central Meridian 87° W,
North American Datum 1983

0 50 100 MILES
0 50 100 KILOMETERS

EXPLANATION

Plan-view regional divides in freshwater, unpinched cells: 1991–2005

Flow toward surface water (including Lake Michigan) inside Lake Michigan Basin

Flow toward surface water outside Lake Michigan Basin

Flow toward pumping wells inside Lake Michigan Basin

Flow toward pumping wells outside Lake Michigan Basin

Greater than (>) 10,000 milligrams per liter (mg/L) salinity

Lake Michigan Basin

State boundary

Figure 69*D*. Simulated groundwater basins, by aquifer system, for 1991–2005 conditions: SLDV (layer 10).

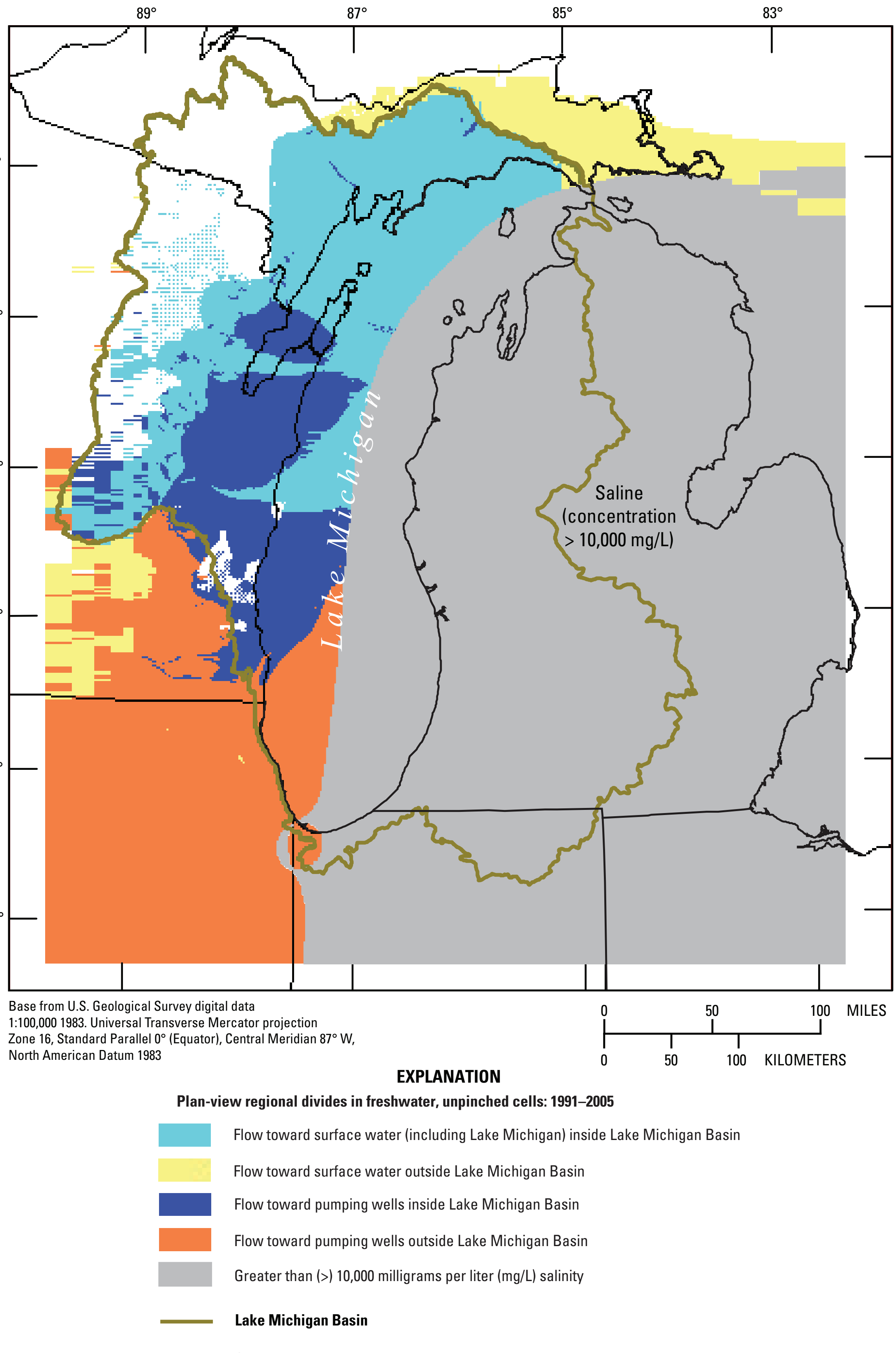

Figure 69*E*. Simulated groundwater basins, by aquifer system, for 1991–2005 conditions: C-O (layer 17).